arXiv:1606.09281v1 [cs.CV] 29 Jun 2016

Multiphase Segmentation For Simultaneously Homogeneous and Textural Images

Duy Hoang Thai *† and Lucas Mentch*

July 1, 2016

Abstract

Segmentation remains an important problem in image processing. For homogeneous (piecewise smooth) images, a number of important models have been developed and refined over the past several decades. However, these models often fail when applied to the substantially larger class of natural images that simultaneously contain regions of both texture and homogeneity. This work introduces a bi-level constrained minimization model for simultaneous multiphase segmentation of images containing both homogeneous and textural regions. We develop novel norms defined in different functional Banach spaces for the segmentation which results in a non-convex minimization. Finally, we develop a generalized notion of segmentation delving into approximation theory and demonstrating that a more refined decomposition of these images results in multiple meaningful components. Both theoretical results and demonstrations on natural images are provided.

Keywords: Image Decomposition, Variational Calculus, Image Denoising, Feature Extraction, Image Segmentation

1 Introduction

Image segmentation remains at the forefront of issues in computer vision and image processing and an abundance of approaches have been developed to solve a wide range of problems; see, for example, [1, 2]. The goal of image segmentation is to decompose the image domain into a montage of meaningful components. This has lead to breakthroughs in a number of research areas such as medical imaging [3], astronomical imaging [4], and biometric recognition [5, 6, 7].

*Statistical and Applied Mathematical Science Institute (SAMSI), USA.
†Corresponding Author: Email: dhthai@samsi.info

Segmentation methods can be broadly characterized by the class of target images for which they are intended, either homogeneous (piecewise smooth) or textural. Many such methods have been suggested, including approaches based on the intensity of pixels [8, 9, 10] and others based on curve evolution[11, 12, 13, 14]. For homogeneous images in particular, the classical approach to segmentation is based on active contours [15]. Given an image f on a bounded domain $\Omega \subset \mathbb{R}^2$, contours are driven to object boundaries by internal and external forces in the functional

$$\inf_{C(s)} \left\{ \alpha \int_0^1 \left|C'(s)\right|^2 ds + \beta \int_0^1 \left|C''(s)\right| ds - \lambda \int_0^1 \left|\nabla f(C(s))\right|^2 ds \right\} \tag{1}$$

with a curve $C(s) : [0,1] \to \mathbb{R}^2$ and positive parameters $\alpha\,, \beta$ and λ.

Under the classical model $f(\boldsymbol{x}) = u(\boldsymbol{x}) + \epsilon(\boldsymbol{x})$ with $\boldsymbol{x} \in \Omega$, Mumford and Shah [16] proposed a solution by minimizing the energy functional

$$\inf_{u,C} \left\{ \int_\Omega \big(f(\boldsymbol{x}) - u(\boldsymbol{x})\big)^2 d\boldsymbol{x} \;+\; \nu \int_{\Omega\setminus C} \left|\nabla u(\boldsymbol{x})\right|^2 d\boldsymbol{x} + \mu|C| \right\}. \tag{2}$$

However, this piecewise smooth Mumford-Shah model is NP-hard due to the Hausdorff 1-dimensional measure $\mathcal{H}^1(\mathbb{R}^2)$. A simplified version for image segmentation when f is assumed to be piecewise constant can be written as

$$\inf_{[c_n]_{n=1}^N, [\Omega_n]_{n=1}^N} \left\{ \sum_{n=1}^N \int_\Omega \big(f(\boldsymbol{x}) - c_n\big)^2 \mathbf{1}_{\Omega_n}(\boldsymbol{x}) d\boldsymbol{x} \;+\; \frac{\mu}{2} \sum_{n=1}^N \int_\Omega \left|\nabla \mathbf{1}_{\Omega_n}(\boldsymbol{x})\right| d\boldsymbol{x} \right\}. \tag{3}$$

which closely resembles the Potts model [17] developed decades earlier. Rudin et al. [18] proposed an alternative, more computationally efficient version of the model in (2) that preserves sharp edges in the restored image. These advantages led to numerous extensions including examination in different functional spaces, [19, 20, 21, 22, 23, 24], versions involving higher-order derivatives [25, 26, 27, 28], mean curvature [29], Euler's elastica [30, 31], total variation of the first and second order derivatives [32], and higher-order PDEs for diffusion solved by directional operator splitting schemes [33]. Various techniques have been proposed for solving the convex optimization including Chambolle's projection [34], the splitting Bregman method [35], and iterative shrinkage/thresholding (IST) algorithms [36, 37, 38]. In 2010, Wu et al. [39] proved the equivalence between the augmented Lagrangian method (ALM), dual methods, and the splitting Bregman method.

Letting $p_n(\boldsymbol{x})$ denote the indicator function $\mathbf{1}_{\Omega_n}(\boldsymbol{x})$ with $\boldsymbol{x} \in \Omega$, (3) can be rewritten as the non-convex constrained minimization

$$\min_{\vec{c},\vec{p}} \left\{ \frac{\mu}{2} \sum_{n=1}^N \|\nabla p_n\|_{L_1} + \sum_{n=1}^N \Big\langle (f - c_n)^2 \,, p_n \Big\rangle_{L_2} \text{ s.t.} \sum_{n=1}^N p_n(\boldsymbol{x}) = 1 \,, p_n(\boldsymbol{x}) \in \{0,1\} \right\} \tag{4}$$

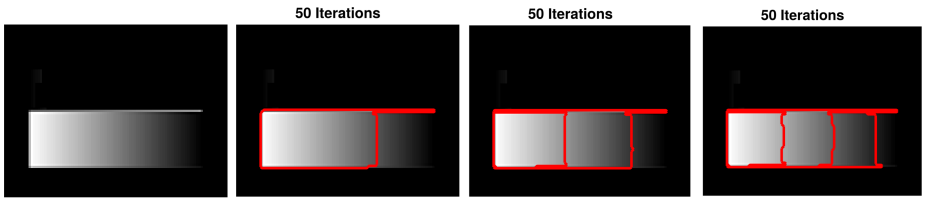

(a) Original image (b) 2 Phases (c) 3 Phases (d) 4 Phases

Figure 1: The original image (a) is segmented by [42] with two phase (b), three phase (c) and four phase segmentation (with the same notation for parameters $n = 4\,, s = 0.001\,, \delta = 0.1$). Using multiple phases allows us to recover portions of the image with different illumination (gradient change).

where $\vec{c} = [c_n]_{n=1}^{N}\,, \vec{p} = [p_n]_{n=1}^{N}$. Note that when $N = 2$, this becomes the celebrated Chan and Vese model [11]. Brown et al. [40, 41] provide a convex relaxation of (4) by relaxing the binary set to $p_n(\boldsymbol{x}) \in [0, 1]$ and Bae et al. [42] solve this relaxed version via a smoothed primal-dual method; see [43, 44, 45, 46] for details. The advantage of the multiphase segmentation is illustrated in Figure 1 using the smoothed primal-dual method in [42] to recover an object under a spectrum of illumination.

Texture segmentation and analysis remains a challenging problem due to its oscillatory nature. Proposed methods include those based on texture descriptors [47, 48], histogram metrics [49], and finding other meaningful features in an observed image for classification [50]. Among the most popular approaches is the vector-valued Chan-Vese model for texture segmentation with a Gabor filter [51] whose convex relaxed version is defined in [40, 52]. This can be seen as a generalized version of the two-phase piecewise constant Mumford and Shah model for a vector valued image $\vec{f} = \left[f_m\right]_{m=1}^{M}$ and constant vector $\vec{c}_1 = \left[c_{1m}\right]_{m=1}^{M}, \vec{c}_2 = \left[c_{2m}\right]_{m=1}^{M}$. The resulting minimization becomes convex by relaxing the binary constraint to $p(\boldsymbol{x}) \in [0\,, 1]$ [40].

Though these techniques have seen much success in their respective domains, many natural images like fingerprints and stem cell imaging contain both homogeneous and textural regions and it is important to define a technique to capture the entirety of this information. The Mumford-Shah model fails in this larger class of images due to the absence of measurement for texture; see Figure 2 for such an example where textural regions appear in each phase.

In this work, we provide a method for multiphase segmentation of images that simultaneously contain regions of both homogeneity and texture. An attempt at this kind of segmentation was provided in [53] but importantly, our work here can be viewed as a decomposition of the original image which approximates the image in functional space instead of using harmonic analysis. This approach to the inverse problem allows us to obtain a piecewise constant component as well

(a) Original image (b) Phase 1 (c) Phase 2 (d) Phase 3

Figure 2: The original image (a) containing both texture and homogeneity is segmented into three phases by the Mumford and Shah (MS) model with $\sigma = 0, N = 3, s = 0.005, \xi = 0.001, \lambda = 10^{-3}, \tau = 0.1, \text{Iteration} = 20$. Note that both homogeneous and textural information appear in all three phases (b)-(d).

as sparse directional information; Figure 3 shows a preview of results obtained using the bilevel SHT method outlined in Section 4.

Following [7, 23, 54, 55, 56], we adopt the idea of the discrete directional G_S-norm to measure texture in several directions and the dual of a generalized Besov space in the curvelet domain $\mathcal{C}$ [55, 57, 58, 59, 60] to measure the residual. This approach is particularly useful for many natural images such as fingerprints in which texture appears in many directions and can easily be adapted for the shearlet, contourlet, steerable wavelet or 2D empirical transforms [61, 62, 63, 64]. Because of the curvelet transform, the residual can be either independent or correlated and need not follow a Gaussian distribution. Since our minimization involves the G_S-norm, we propose two alternative methods based on the two primary approaches to handling the G_S-norm: a multiphase SHT method based on the approach of Aujol and Chambolle [54] and a bilevel SHT method based on the approach of Vese and Osher [23].

The remainder of this paper is organized as follows. In Section 2, we define some preliminary notation and investigate a simple model where only two-phase segmentation is considered and the homogeneous portion is assumed to be piecewise constant. In Section 3 we generalize this set-up both to multiphase segmentation and also to the case where homogeneous regions are considered piecewise-smooth. In Section 4 we introduce a bilevel minimization scheme to more efficiently solve the minimization induced by the multiphase piecewise smooth context. Finally, we apply the methodology to a number of representative images and compare to related approaches in Section 5. For readability, mathematical details and proofs are provided in the Appendix.

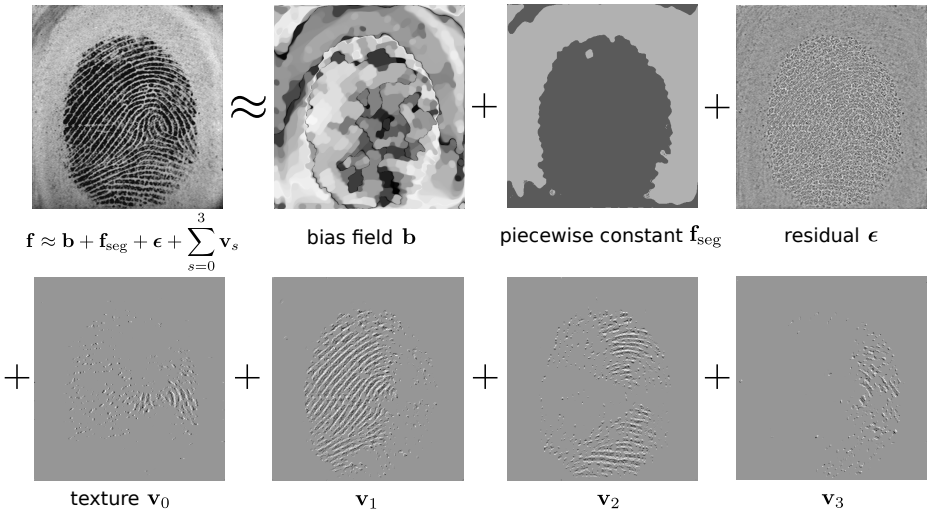

Figure 3: Image representation of a fingerprint decomposed according to the bilevel SHT method described in Section 4. The directional texture is shown in the bottom row.

2 Preliminaries and Simplified Models

We begin by establishing some background notation and definitions. Let X be the Euclidean space with dimension given by the size of the lattice $\Omega = \big\{\boldsymbol{k} = [k_1\,, k_2] \in [0\,, d_1 - 1] \times [0\,, d_2 - 1] \subset \mathbb{Z}^2\big\}$. On the bounded domain Ω, we denote the coordinates of the Fourier transform as $\boldsymbol{\omega} = [\omega_1\,, \omega_2] \in [-\pi\,, \pi]^2$ and the coordinates of the Z transform (the discrete version of the Fourier transform) as $\boldsymbol{z} = \big[z_1\,, z_2\big] = \big[e^{j\omega_1}\,, e^{j\omega_2}\big]$. Denote the discrete Fourier transform pair as

$$f[\boldsymbol{k}] \;\overset{\mathcal{F}}{\longleftrightarrow}\; \mathcal{F}\big\{f[\boldsymbol{k}]\big\}(e^{j\boldsymbol{\omega}}) = F(e^{j\boldsymbol{\omega}}) = \sum_{\boldsymbol{k}\in\Omega} f[\boldsymbol{k}] e^{-j\langle \boldsymbol{k}\,, \boldsymbol{\omega}\rangle_{\ell_2}}\,.$$

Given the discrete function $\mathbf{f} = \big[f[\boldsymbol{k}]\big]_{\boldsymbol{k}\in\Omega} \in X$, a vector $\vec{\mathbf{g}} = [\mathbf{g}_l]_{l=0}^{L-1} \in X^L$ and the direction $l = 0, \ldots, L-1$, we make a few preliminary definitions. The **directional forward/backward difference operators** are given, in matrix notation, by

$$\partial_l^+ \mathbf{f} = \sin\left(\frac{\pi l}{L}\right) \mathbf{D_1 f} + \cos\left(\frac{\pi l}{L}\right) \mathbf{f D_2^{\mathrm{T}}} \qquad \overset{\mathcal{F}}{\longleftrightarrow} \quad \Big[\sin\left(\frac{\pi l}{L}\right)(z_1 - 1) + \cos\left(\frac{\pi l}{L}\right)(z_2 - 1)\Big] F(\boldsymbol{z})$$

$$\partial_l^- \mathbf{f} = -\Big[\sin\left(\frac{\pi l}{L}\right) \mathbf{D_1^{\mathrm{T}} f} + \cos\left(\frac{\pi l}{L}\right) \mathbf{f D_2}\Big] \quad \overset{\mathcal{F}}{\longleftrightarrow} \quad -\Big[\sin\left(\frac{\pi l}{L}\right)(z_1^{-1} - 1) + \cos\left(\frac{\pi l}{L}\right)(z_2^{-1} - 1)\Big] F(\boldsymbol{z})$$

with $\partial_l^{\pm}\mathbf{f} = \Big[\partial_l^{\pm} f[\boldsymbol{k}]\Big]_{\boldsymbol{k}\in\Omega}$ and a matrix

$$\mathbf{D_1} = \begin{pmatrix} -1 & 1 & 0 & \dots & 0 \\ 0 & -1 & 1 & \dots & 0 \\ \vdots & \vdots & \vdots & \ddots & \vdots \\ 0 & 0 & 0 & \dots & 1 \\ 1 & 0 & 0 & \dots & -1 \end{pmatrix} \in \mathbb{R}^{d_1 \times d_1},$$

and similarly $\mathbf{D_2} \in \mathbb{R}^{d_2 \times d_2}$.

Given the adjoint operators of the difference operators as $\left(\partial_x^{\pm}\right)^* = -\partial_x^{\mp}$, $\left(\partial_y^{\pm}\right)^* = -\partial_y^{\mp}$, the adjoint operators of their directional version are

$$\left(\partial_l^{\pm}\right)^* = -\Big[\cos\left(\frac{\pi l}{L}\right)\partial_x^{\mp} + \sin\left(\frac{\pi l}{L}\right)\partial_y^{\mp}\Big] = -\partial_l^{\mp},$$

and we can define the **discrete directional gradient** and **divergence** as

$$\nabla_L^{\pm}\mathbf{f} = \Big[\partial_l^{\pm}\mathbf{f}\Big]_{l=0}^{L-1} \qquad \text{and} \qquad \mathrm{div}_L^{\pm}\vec{\mathbf{g}} = \sum_{l=0}^{L-1}\partial_l^{\pm}\mathbf{g}_l$$

respectively. Note that the adjoint operator of $\nabla_L^{\pm}$ is $\left(\nabla_L^{\pm}\right)^* = -\mathrm{div}_L^{\mp}$; that is

$$\Big\langle \nabla_L^{\pm}\mathbf{f}\,, \vec{\mathbf{g}}\Big\rangle_{\ell_2} = -\Big\langle \mathbf{f}\,, \mathrm{div}_L^{\mp}\vec{\mathbf{g}}\Big\rangle_{\ell_2}.$$

Given a vector of matrices $\vec{\mathbf{p}} = \big[\mathbf{p}_l\big]_{l=0}^{L-1} \in X^L$, the derivative of the divergence operator $\mathrm{div}_L^{-}\vec{\mathbf{p}}$ w.r.t. $\mathbf{p}_l$ for $l = 0, \dots, L-1$ is given by

$$\frac{\partial}{\partial \mathbf{p}_l}\Big\{\mathrm{div}_L^{-}\vec{\mathbf{p}}\Big\} = -\frac{\partial}{\partial \mathbf{p}_l}\Big[\sin\left(\frac{\pi l}{L}\right)\mathbf{D_1}^{\mathrm{T}}\mathbf{p}_l + \cos\left(\frac{\pi l}{L}\right)\mathbf{p}_l\mathbf{D_2}\Big] = \Big[-\partial_l^{+}\delta[\boldsymbol{k}]\Big]_{\boldsymbol{k}\in\Omega},$$

where $\delta(\cdot)$ denotes the Dirac delta function. Thus, the derivative of the directional divergence w.r.t. $\vec{\mathbf{p}}$ is

$$\frac{\partial}{\partial \vec{\mathbf{p}}}\Big\{\mathrm{div}_L^{-}\vec{\mathbf{p}}\Big\} = \Big[-\big[\partial_l^{+}\delta[\boldsymbol{k}]\big]_{l=0}^{L-1}\Big]_{\boldsymbol{k}\in\Omega} = \Big[-\nabla_L^{+}\delta[\boldsymbol{k}]\Big]_{\boldsymbol{k}\in\Omega}.$$

Finally, the **discrete directional $\mathbf{G}_S$-norm** [55] is given by

$$\|\mathbf{v}\|_{\mathrm{G}_S} = \inf\Big\{\big\|\|\vec{\mathbf{g}}|\big\|_{\ell_\infty}\,, \mathbf{v} = \mathrm{div}_S^{-}\vec{\mathbf{g}}\,,\ \vec{\mathbf{g}} = \big[\mathbf{g}_s\big]_{s=0}^{S-1} \in X^S\Big\}$$

and the indicator function on a convex set for noise in the curvelet domain $\mathcal{C}$ [55, 57, 58] by

$$A(\nu) = \Big\{\boldsymbol{\epsilon} \in X \ :\ \big\|\mathcal{C}\{\boldsymbol{\epsilon}\}\big\|_{\ell_\infty} \le \nu\Big\} \ \text{ and } \ \mathscr{G}^*(\frac{\boldsymbol{\epsilon}}{\nu}) = \begin{cases} 0\,, & \boldsymbol{\epsilon} \in A(\nu) \\ +\infty\,, & \text{else} \end{cases}.$$

For a more thorough background on the mathematical preliminaries (including the point-wise operators as $\pm, \backslash, \cdot^{\times}, \max, \text{Shrink}, \text{CST}$, etc.), we refer the reader to [6, 7, 55, 65]. We point out that in the remainder of this work, we use boldface to present a matrix, e.g. $\mathbf{u} \in X$, vector with boldface to denote a vector of matrix, e.g. $\vec{\mathbf{p}} = [\mathbf{p}_n]_{n=1}^N \in X^N$, and vector (without boldface) to denote constant vector, e.g. $\vec{c} = [c_n]_{n=1}^N \in \mathbb{R}^N$.

2.1 Two-phase piecewise constant and texture segmentation

We begin by considering the simple discrete model consisting of a two phase piecewise constant image (indicated by indicator function $\mathbf{p}$ and mean values $(c_1, c_2) \in \mathbb{R}_+$) and texture $\mathbf{v}$ corrupted by i.i.d. (or weakly correlated) noise $\boldsymbol{\epsilon}$ as

$$\mathbf{f} = c_1\mathbf{p} + c_2(1-\mathbf{p}) + \mathbf{v} + \boldsymbol{\epsilon}\,.$$

As in [55], we propose the model for this segmentation as

$$\min_{(\mathbf{p},\boldsymbol{\epsilon},c_1,c_2)\in X^2\times\mathbb{R}^2} \left\{ \left\| \nabla_L^+ \mathbf{p} \right\|_{\ell_1} + \mu_1 \|\mathbf{v}\|_{\mathrm{G}_S} + \mu_2 \|\mathbf{v}\|_{\ell_1} + \mathscr{G}^*\left(\frac{\boldsymbol{\epsilon}}{\nu}\right) \right.$$
$$\left. \text{s.t. } \mathbf{f} = c_1\mathbf{p} + c_2(1-\mathbf{p}) + \mathbf{v} + \boldsymbol{\epsilon}\,, p[\boldsymbol{k}] \in \{0,1\}, \forall \boldsymbol{k} \in \Omega \right\}. \quad (5)$$

In order to solve a non-convex minimization (5), we relax a binary set $p[\boldsymbol{k}] \in \{0\,,1\}$ to $[0\,,1]$ and then apply ALM and the alternating directional method of multipliers (ADMM); see proposition 7.1 and Algorithms 5 in Appendix for detailed calculations. Figure 4 illustrates the results of this model. The histogram of the indicator function $\mathbf{p}$ in Figure 4 (d) shows that $\mathbf{p}$ almost converges to $\{0\,,1\}$ after the 100^{th} iteration. One can use a technique in [42] to make $\mathbf{p}$ be exactly a binary setting as a solution of a minimization (5).

3 Multiphase Segmentation SHT

The above models consider only two-phase segmentation in images where the homogeneous region can be considered piecewise constant. We now generalize this to allow for multiphase segmentation and also allow for piecewise-smooth homogeneity.

3.1 Multiphase piecewise smooth and texture segmentation

As before, we assume that a natural image $\mathbf{f}$ contains both texture $\mathbf{v}$ and homogeneous regions $\mathbf{u}$ as well as noise $\boldsymbol{\epsilon}$ so that $\mathbf{f} = \mathbf{u} + \mathbf{v} + \boldsymbol{\epsilon}$. However, we

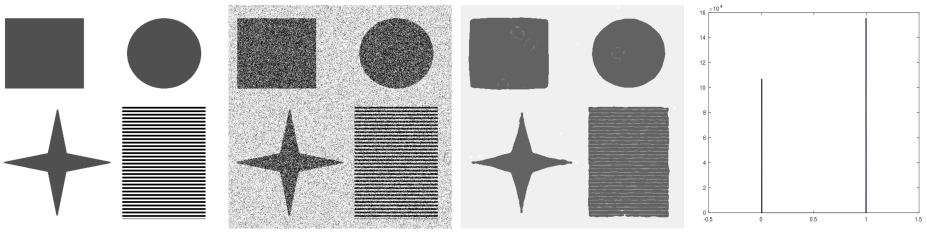

(a) $\mathbf{f}_0$ (b) $\mathbf{f}$ (c) $\mathbf{f}_{\text{seg}}$ (d) Histogram of $\mathbf{p}$

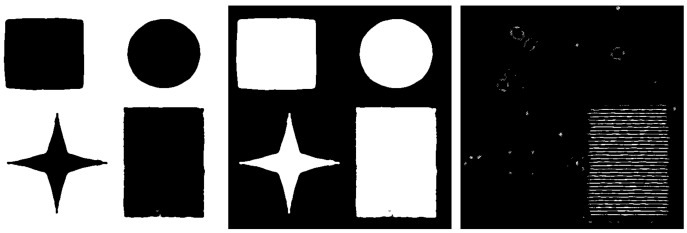

(e) $\mathbf{p}$ (f) $1-\mathbf{p}$ (g) $\mathbf{v}>0$

Figure 4: The original image $\mathbf{f}_0$ is shown in Subfigure (a). Subfigure (b) shows the same image $\mathbf{f}$ with additional i.i.d. noise added from a Gaussian distribution with mean 0 and standard deviation $\sigma = 100$. The segmented version $\mathbf{f}_{\text{seg}} = c_1\mathbf{p}+c_2(1-\mathbf{p})+c_3(v>0)$ of (b) shown in Subfigure (c) is obtained by solving the minimization in (5), see Algorithm 5 in the Appendix with the parameters: $L = 150\,, S = 9\,, c_\delta = 0.1, \theta = 0.9\,, c_{\mu_1} = c_{\mu_2} = 0.03\,, \beta_4 = 0.03\,, \beta_3 = \frac{\theta}{1-\theta}\beta_4\,, \beta_1 = \beta_4\,, \beta_2 = 1.3\beta_3\,, \#\text{iteration} = 100$. The binarized texture $\mathbf{v}$ in (g) shows its sparsity by a minimization of (5) with a percentage of non-zero coefficients in texture $\mathbf{v}$ as $\frac{\#\{\mathbf{v}\neq 0\}}{mn}100\% = 7.75\%$. Figure (e) and (f) are the indicator function and its complement, respectively. The mean values are $c_1 = 240.42\,, c_2 = 98.02$ and we choose $c_3 = 50$.

now further assume that $\mathbf{u}$ consists of both a multiphase (N) piecewise constant (indexed by the indicator function $\vec{\mathbf{p}} = \left[\mathbf{p}_n\right]_{n=1}^N$ and their mean values $\vec{c} = \left[c_n\right]_{n=1}^N$) as well as a bias field $\mathbf{b}$

$$\mathbf{u} = \mathbf{b} + \sum_{n=1}^{N} c_n \mathbf{p}_n\,,$$

to account for the piecewise-smooth component of $\mathbf{f}$. Following [34], we utilize the directional G_S-norm to measure the texture $\mathbf{v}$ and propose a new combined model for multiphase **s**imultaneous **h**omogeneous and **t**exture image segmenta-

tion (the SHT model) as

$$\min_{\left(\vec{c},\vec{\mathbf{p}},\mathbf{u},\mathbf{v},\boldsymbol{\epsilon},\mathbf{b}\right)\in\mathbb{R}^N\times X^{N+4}}\left\{\left\|\nabla_L^+\mathbf{u}\right\|_{\ell_1}+\mu_2\|\mathbf{v}\|_{\ell_1}+\mu_3\sum_{n=1}^N\left\|\nabla_M^+\mathbf{p}_n\right\|_{\ell_1}+\frac{\mu_4}{2}\|\mathbf{b}\|_{\ell_2}^2+\mathscr{G}^*(\frac{\boldsymbol{\epsilon}}{\nu})\right.$$

$$\text{s.t. } \mathbf{f}=\mathbf{u}+\mathbf{v}+\boldsymbol{\epsilon}\,,\|\mathbf{v}\|_{\mathrm{G}_S}\le\mu_1\,,\mathbf{u}=\mathbf{b}+\sum_{n=1}^N c_n\mathbf{p}_n\,,$$

$$\left.\sum_{n=1}^N\mathbf{p}_n=1\,,p_n[\boldsymbol{k}]\in\{0,1\}\,,n=1,\ldots,N\,,\boldsymbol{k}\in\Omega\right\}. \tag{6}$$

Note that in contrast with (5), we no longer assume a piecewise-constant homogeneous region and thus must also take into account the bias term $\mathbf{b}$. Note further that the directional total variation norm (DTV-norm) $\left\|\nabla_L^+\cdot\right\|_{\ell_1}$ and G_S-norm are a dual pair if $L=S$; see Lemma 7.0.1 for details. Finally, observe that as with the ROF model in [18], the process of smoothing the homogeneous areas while preserving the edge information is controlled by the DTV-norm for $\mathbf{u}$.

Solution to the Multiphase SHT Model

In a similar fashion to [42], the minimization in (6) can be solved by a smoothed primal-dual model for the $\vec{\mathbf{p}}$-problem rather than by the Fourier approach used in the two-phase piecewise-constant model in (5). The remainder of this section provides a sketch of the proposed algorithm; for details and proofs, see Propositions 7.2, 7.3, 7.4 in the Appendix.

Define the indicator function on a convex set for the G_S-norm as

$$\mathrm{G}_S(\mu_1)=\left\{\mathbf{v}\in X\,,\vec{\mathbf{g}}\in X^S\ :\ \|\mathbf{v}\|_{\mathrm{G}_S}=\|\vec{\mathbf{g}}\|_{\ell_\infty}\le\mu_1\right\}$$

$$\text{and } J_S^*\left(\frac{\mathbf{v}}{\mu_1}\right)=\begin{cases}0\,, & \mathbf{v}\in\mathrm{G}_S(\mu_1)\\ +\infty\,, & \text{otherwise}\end{cases}.$$

By applying ALM to the equality constraint $\mathbf{f}=\mathbf{u}+\mathbf{v}+\boldsymbol{\epsilon}$ and relaxing the binary setting $p_n[\boldsymbol{k}]\in\{0,1\}$ to the convex set $p_n[\boldsymbol{k}]\in[0,1]$, the nonconvex minimization in (6) becomes convex as

$$\min_{(\vec{c},\vec{\mathbf{p}},\mathbf{u},\mathbf{v},\boldsymbol{\epsilon})\in\mathbb{R}^N\times X^{N+3}}\left\{\mathcal{L}\big(\vec{c},\vec{\mathbf{p}},\mathbf{u},\mathbf{v},\boldsymbol{\epsilon};\boldsymbol{\lambda}\big)\ \text{s.t. }\ \sum_{n=1}^N\mathbf{p}_n=1\,,p_n[\boldsymbol{k}]>0\,,n=1,\ldots,N\,,\boldsymbol{k}\in\Omega\right\} \tag{7}$$

with

$$\mathcal{L}(\cdot;\cdot) = \left\|\nabla_L^+ \mathbf{u}\right\|_{\ell_1} + \mu_2\|\mathbf{v}\|_{\ell_1} + \mu_3 \sum_{n=1}^{N} \left\|\nabla_M^+ \mathbf{p}_n\right\|_{\ell_1} + \frac{\mu_4}{2}\left\|\mathbf{u} - \sum_{n=1}^{N} c_n \mathbf{p}_n\right\|_{\ell_2}^2 + J_S^*(\frac{\mathbf{v}}{\mu_1}) + \mathscr{G}^*(\frac{\boldsymbol{\epsilon}}{\nu})$$

$$+ \frac{\beta}{2}\left\|\mathbf{f} - \mathbf{u} - \mathbf{v} - \boldsymbol{\epsilon} + \frac{\boldsymbol{\lambda}}{\beta}\right\|_{\ell_2}^2 .$$

Due to the multi-variable minimization, we apply ADMM to (7) whose minimizer is numerically computed through iteration t with updated Lagrange multiplier

$$\left(\vec{c}^{(t)}, \vec{\mathbf{p}}^{(t)}, \mathbf{u}^{(t)}, \mathbf{v}^{(t)}, \boldsymbol{\epsilon}^{(t)}\right) = \operatorname{argmin} \mathcal{L}\left(\vec{c}, \vec{\mathbf{p}}, \mathbf{u}, \mathbf{v}, \boldsymbol{\epsilon}\,;\ \boldsymbol{\lambda}^{(t-1)}\right). \tag{8}$$

Given the initialization $\mathbf{u}^{(0)} = \mathbf{f}\,, \vec{\mathbf{p}}^{(0)} = \mathbf{v}^{(0)} = \boldsymbol{\epsilon}^{(0)} = \boldsymbol{\lambda}^{(0)} = \mathbf{0}$ and $c_n = (n-1)\lfloor \frac{255}{N} \rfloor$ for $n = 1, \ldots, N$, we solve the following five subproblems before updating the Lagrange multiplier.

The u-problem: Fix $\vec{c}, \vec{\mathbf{p}}, \mathbf{v}, \boldsymbol{\epsilon}$ and solve

$$\min_{\mathbf{u}\in X} \left\{ \left\|\nabla_L^+ \mathbf{u}\right\|_{\ell_1} \ + \ \frac{\mu_4 + \beta}{2}\|\mathbf{u} - \mathbf{h}\|_{\ell_2}^2 \right\} \tag{9}$$

where $\mathbf{h} = \frac{\mu_4}{\mu_4+\beta}\sum_{n=1}^{N} c_n \mathbf{p}_n + \frac{\beta}{\mu_4+\beta}\left[\mathbf{f} - \mathbf{v} - \boldsymbol{\epsilon} + \frac{\boldsymbol{\lambda}}{\beta}\right]$.

From Proposition 7.2 and the numerical solver in (8), a primal solution of the DTV-ℓ_2 (9) at iteration t is given by

$$\mathbf{u}^{(t)} = \mathbf{h} - \frac{1}{\mu_4 + \beta}\operatorname{div}_L^- \vec{\mathbf{r}}^{(t)}$$

with dual variable

$$\vec{\mathbf{r}}^{(t)} = \frac{\vec{\mathbf{r}}^{(t-1)} + \tau\nabla_L^+\left[\operatorname{div}_L^- \vec{\mathbf{r}}^{(t-1)} - (\mu_4+\beta)\mathbf{h}\right]}{1 + \tau\left|\nabla_L^+\left[\operatorname{div}_L^- \vec{\mathbf{r}}^{(t-1)} - (\mu_4+\beta)\mathbf{h}\right]\right|}.$$

The v-problem: Fix $\vec{c}, \vec{\mathbf{p}}, \mathbf{u}, \boldsymbol{\epsilon}$, denote $\mathbf{h}_{\mathrm{v}} = \mathbf{f} - \mathbf{u} - \boldsymbol{\epsilon} + \frac{\boldsymbol{\lambda}}{\beta}$ and solve

$$\min_{\mathbf{v}\in X} \left\{ J_S^*\left(\frac{\mathbf{v}}{\mu_1}\right) + \|\mathbf{v}\|_{\ell_1} + \frac{1}{2}\frac{\beta}{\mu_2}\|\mathbf{v} - \mathbf{h}_{\mathrm{v}}\|_{\ell_2}^2 \right\}. \tag{10}$$

To simplify the problem, we apply Proposition 7.3 with a quadratic penalty ($\boldsymbol{\lambda_1} = 0$). The primal solution of the directional $\mathrm{G}_S - \ell_1$ model (10) at iteration

t is updated as

$$v^{(t)} = \text{Shrink}\left(\frac{\frac{\beta}{\mu_2}}{\alpha+\frac{\beta}{\mu_2}}\mathbf{h}_{\text{v}} + \frac{\alpha\mu_1}{\alpha+\frac{\beta}{\mu_2}}\text{div}_S^-\vec{\mathbf{g}}^{(t)}\,,\ \frac{1}{\alpha+\frac{\beta}{\mu_2}}\right),$$

with dual variable

$$\vec{\mathbf{g}}^{(t)} = \frac{\vec{\mathbf{g}}^{(t-1)} + \tau\nabla_S^+\left[\alpha\mu_1\text{div}_S^-\vec{\mathbf{g}}^{(t-1)} - \alpha\mathbf{v}^{(t-1)}\right]}{1+\tau\left|\nabla_S^+\left[\alpha\mu_1\text{div}_S^-\vec{\mathbf{g}}^{(t-1)} - \alpha\mathbf{v}^{(t-1)}\right]\right|}.$$

The $\boldsymbol{\epsilon}$-problem: Fix $\vec{c}, \vec{\mathbf{p}}, \mathbf{u}, \mathbf{v}$ and solve

$$\min_{\boldsymbol{\epsilon}\in X}\left\{\mathscr{G}^*\left(\frac{\boldsymbol{\epsilon}}{\nu}\right) + \frac{\beta}{2}\left\|\boldsymbol{\epsilon} - \left[\mathbf{f}-\mathbf{u}-\mathbf{v}+\frac{\boldsymbol{\lambda}}{\beta}\right]\right\|_{\ell_2}^2\right\}. \tag{11}$$

In a similar fashion to [55], the solution of (11) is given by

$$\boldsymbol{\epsilon}^* = \left[\mathbf{f}-\mathbf{u}-\mathbf{v}+\frac{\boldsymbol{\lambda}}{\beta}\right] - \text{CST}\left(\left[\mathbf{f}-\mathbf{u}-\mathbf{v}+\frac{\boldsymbol{\lambda}}{\beta}\right], \nu\right).$$

The $\vec{c} = \left[c_n\right]_{n=1}^N$-problem: Fix $\vec{\mathbf{p}}, \mathbf{u}, \mathbf{v}, \boldsymbol{\epsilon}$ and solve

$$\min_{\vec{c}\in\mathbb{R}^N}\left\{\left\|\mathbf{u} - \sum_{n=1}^N c_n\mathbf{p}_n\right\|_{\ell_2}^2\right\}. \tag{12}$$

Due to its separability, the solution of (12) is given by

$$c_n = \frac{\sum_{\boldsymbol{k}\in\Omega} u[\boldsymbol{k}]p_n[\boldsymbol{k}]}{\sum_{\boldsymbol{k}\in\Omega} p_n[\boldsymbol{k}]},\ n = 1,\ldots,N.$$

The $\vec{\mathbf{p}} = \left[\mathbf{p}_n\right]_{n=1}^N$-problem: Fix $\vec{c}, \mathbf{u}, \mathbf{v}, \boldsymbol{\epsilon}$ and solve

$$\min_{\vec{\mathbf{p}}\in X^N}\left\{\mu_3\sum_{n=1}^N\left\|\nabla_M^+\mathbf{p}_n\right\|_{\ell_1} + \frac{\mu_4}{2}\left\|\mathbf{u} - \sum_{n=1}^N c_n\mathbf{p}_n\right\|_{\ell_2}^2\right.$$
$$\left.\text{s.t.}\ \sum_{n=1}^N \mathbf{p}_n = 1, p_n[\boldsymbol{k}]\in\{0,1\}, n = 1,\ldots,N, \boldsymbol{k}\in\Omega\right\}. \tag{13}$$

From Proposition 7.4 with a smooth primal-dual model and Chambolle's projection, the primal solution of (13) at iteration t (for $n = 1, \ldots, N$) is

$$\mathbf{p}_n = \frac{\exp\left\{-\frac{1}{\xi}\left[\mathrm{div}_M^- \vec{\mathbf{q}}_n + \frac{\mu_4}{2\mu_3}\big(\mathbf{u} - c_n\big)^{.2}\right]\right\}}{\sum_{i=1}^{N} \exp\left\{-\frac{1}{\xi}\left[\mathrm{div}_M^- \vec{\mathbf{q}}_i + \frac{\mu_4}{2\mu_3}\big(\mathbf{u} - c_i\big)^{.2}\right]\right\}}$$

$$= \frac{\exp\left\{-\frac{1}{\xi}\Big[-\sum_{m=0}^{M-1}\Big[\sin(\frac{\pi m}{M})\mathbf{D_1}^{\mathrm{T}}\mathbf{q}_{nm} + \cos(\frac{\pi m}{M})\mathbf{q}_{nm}\mathbf{D_2}\Big] + \frac{\mu_4}{2\mu_3}\big(\mathbf{u} - c_n\big)^{.2}\Big]\right\}}{\sum_{i=1}^{N} \exp\left\{-\frac{1}{\xi}\Big[-\sum_{m=0}^{M-1}\Big[\sin(\frac{\pi m}{M})\mathbf{D_1}^{\mathrm{T}}\mathbf{q}_{im} + \cos(\frac{\pi m}{M})\mathbf{q}_{im}\mathbf{D_2}\Big] + \frac{\mu_4}{2\mu_3}\big(\mathbf{u} - c_i\big)^{.2}\Big]\right\}},$$

with dual variable

$$\vec{\mathbf{q}}_n^{(t)} = \frac{\vec{\mathbf{q}}_n^{(t-1)} + \tau\nabla_M^+ \mathbf{p}_n^{(t)}}{1 + \tau\left|\nabla_M^+ \mathbf{p}_n^{(t)}\right|} \in X^M$$

$$\Leftrightarrow\ \mathbf{q}_{nm}^{(t)} = \frac{\mathbf{q}_{nm}^{(t-1)} + \tau\left[\sin(\frac{\pi m}{M})\mathbf{D_1}\mathbf{p}_n^{(t)} + \cos(\frac{\pi m}{M})\mathbf{p}_n^{(t)}\mathbf{D_2}^{\mathrm{T}}\right]}{1 + \tau\left[\sum_{m=0}^{M-1}\big[\sin(\frac{\pi m}{M})\mathbf{D_1}\mathbf{p}_n^{(t)} + \cos(\frac{\pi m}{M})\mathbf{p}_n^{(t)}\mathbf{D_2}^{\mathrm{T}}\big]^{.2}\right]^{.\frac{1}{2}}},\ m = 0, \ldots, M-1\,.$$

Finally, we update the Lagrange multiplier as

$$\boldsymbol{\lambda}^{(t+1)} = \boldsymbol{\lambda}^{(t)} + \beta\big(\mathbf{f} - \mathbf{u} - \mathbf{v} - \boldsymbol{\epsilon}\big)\,.$$

This solution is summarized in Algorithm 1. Figures 5 and 6 depict the segmented results without noise and with independent Gaussian noise, respectively. In both cases, our proposed method provides good segmented results, though some large-scale texture (e.g. the books shown in the upper left-hand corner) still remains in the piecewise constant images; see Figures 5 (f) and 6 (f). This is likely due to the minimizer obtained by the primal-dual method with Chambolle's projection [34] and since there is no shrinkage to produce sparse signals in some transform domains. Similar to (5), one can use the technique in [42] to obtain a binary setting of $\mathbf{p}$. As in [7, 55], the convergence of the algorithm is defined by a relative error on the log scale

$$\mathrm{Err}_{\mathbf{u}}(t) = \log\frac{\left\|\mathbf{u}^{(t)} - \mathbf{u}^{(t-1)}\right\|_{\ell_2}}{\left\|\mathbf{u}^{(t-1)}\right\|_{\ell_2}},\ t = 1, 2, \ldots \tag{14}$$

Algorithm 1 The SHT model

Initialization: $\mathbf{u}^{(0)} = \mathbf{f}\,, \mathbf{v}^{(0)} = \boldsymbol{\epsilon}^{(0)} = \vec{\mathbf{r}}^{(0)} = \vec{\mathbf{g}}^{(0)} = \vec{\mathbf{p}}^{(0)} = \vec{\mathbf{q}}^{(0)} = \mathbf{0}\,,\ c_n^{(0)} = (n-1)\lfloor\frac{255}{N}\rfloor\,, n = 1, \ldots, N.$

for $t = 1\,, \ldots\,, T$ **do**

I. Compute $\left(\vec{c}, \vec{\mathbf{r}}, \mathbf{u}, \vec{\mathbf{g}}, \mathbf{v}, \boldsymbol{\epsilon}, \vec{\mathbf{p}}, \vec{\mathbf{q}}\right) \in \mathbb{R}^N \times X^{L+S+N+NM+3}$**:**

1. $\mathbf{h}^{(t)} = \dfrac{\mu_4}{\mu_4+\beta}\displaystyle\sum_{n=1}^{N} c_n^{(t-1)}\mathbf{p}_n^{(t-1)} + \dfrac{\beta}{\mu_4+\beta}\Big[\mathbf{f} - \mathbf{v}^{(t-1)} - \boldsymbol{\epsilon}^{(t-1)} + \dfrac{\boldsymbol{\lambda}^{(t-1)}}{\beta}\Big]$

2. $\vec{\mathbf{r}}^{(t)} = \dfrac{\vec{\mathbf{r}}^{(t-1)} + \tau\nabla_L^+\Big[\mathrm{div}_L^-\vec{\mathbf{r}}^{(t-1)} - (\mu_4+\beta)\mathbf{h}^{(t)}\Big]}{1 + \tau\Big|\nabla_L^+\Big[\mathrm{div}_L^-\vec{\mathbf{r}}^{(t-1)} - (\mu_4+\beta)\mathbf{h}^{(t)}\Big]\Big|}$

3. $\mathbf{u}^{(t)} = \mathbf{h}^{(t)} - \dfrac{1}{\mu_4+\beta}\mathrm{div}_L^-\vec{\mathbf{r}}^{(t)}$

4. $\vec{\mathbf{g}}^{(t)} = \dfrac{\vec{\mathbf{g}}^{(t-1)} + \tau\nabla_S^+\Big[\alpha\mu_1\mathrm{div}_S^-\vec{\mathbf{g}}^{(t-1)} - \boldsymbol{\lambda}^{(t-1)} - \alpha\mathbf{v}^{(t)}\Big]}{1 + \tau\Big|\nabla_S^+\Big[\alpha\mu_1\mathrm{div}_S^-\vec{\mathbf{g}}^{(t-1)} - \boldsymbol{\lambda}^{(t-1)} - \alpha\mathbf{v}^{(t)}\Big]\Big|}$

5. $\mathbf{v}^{(t)} = \mathrm{Shrink}\Big(\underbrace{\dfrac{\frac{\beta}{\mu_2}}{\alpha+\frac{\beta}{\mu_2}}\big[\mathbf{f} - \mathbf{u}^{(t)} - \boldsymbol{\epsilon}^{(t-1)} + \dfrac{\boldsymbol{\lambda}^{(t-1)}}{\beta}\big] + \dfrac{\alpha\mu_1}{\alpha+\frac{\beta}{\mu_2}}\mathrm{div}_S^-\vec{\mathbf{g}}^{(t)}}_{:=\mathcal{T}_{\mathbf{v}}}, \dfrac{1}{\alpha+\frac{\beta}{\mu_2}}\Big)\,,$

$$\mu_2 = \frac{\beta c_{\mu_2}\max_{\boldsymbol{k}\in\Omega}\big|\mathcal{T}_v[\boldsymbol{k}]\big|}{1 - \alpha c_{\mu_2}\max_{\boldsymbol{k}\in\Omega}\big|\mathcal{T}_v[\boldsymbol{k}]\big|}$$

6. $\boldsymbol{\epsilon}^{(t)} = \Big[\mathbf{f} - \mathbf{u}^{(t)} - \mathbf{v}^{(t)} + \dfrac{\boldsymbol{\lambda}^{(t-1)}}{\beta}\Big] - \mathrm{CST}\left(\Big[\mathbf{f} - \mathbf{u}^{(t)} - \mathbf{v}^{(t)} + \dfrac{\boldsymbol{\lambda}^{(t-1)}}{\beta}\Big], \nu\right)$

7. $\mathbf{p}_n^{(t)} = \dfrac{\exp\Big\{-\dfrac{1}{\xi}\Big[\mathrm{div}_M^-\vec{\mathbf{q}}_n^{(t-1)} + \dfrac{\mu_4}{2\mu_3}\big(\mathbf{u}^{(t)} - c_n^{(t-1)}\big)^{\cdot 2}\Big]\Big\}}{\displaystyle\sum_{i=1}^{N}\exp\Big\{-\dfrac{1}{\xi}\Big[\mathrm{div}_M^-\vec{\mathbf{q}}_i^{(t-1)} + \dfrac{\mu_4}{2\mu_3}\big(\mathbf{u}^{(t)} - c_i^{(t-1)}\big)^{\cdot 2}\Big]\Big\}}\,,\ n = 1, \ldots, N$

8. $\vec{\mathbf{q}}_n^{(t)} = \dfrac{\vec{\mathbf{q}}_n^{(t-1)} + \tau\nabla_M^+\mathbf{p}_n^{(t)}}{1 + \tau\Big|\nabla_M^+\mathbf{p}_n^{(t)}\Big|}\,,\ n = 1, \ldots, N$

9. $c_n^{(t)} = \dfrac{\displaystyle\sum_{\boldsymbol{k}\in\Omega} u^{(t)}[\boldsymbol{k}]p_n^{(t)}[\boldsymbol{k}]}{\displaystyle\sum_{\boldsymbol{k}\in\Omega} p_n^{(t)}[\boldsymbol{k}]}\,,\ n = 1, \ldots, N$

II. Update $\boldsymbol{\lambda} \in X$**:**

$$\boldsymbol{\lambda}^{(t)} = \boldsymbol{\lambda}^{(t-1)} + \beta\Big(\mathbf{f} - \mathbf{u}^{(t)} - \mathbf{v}^{(t)} - \boldsymbol{\epsilon}^{(t)}\Big)$$

end for

(a) $\mathbf{f}_0$ (b) $\mathbf{u} = \mathbf{b} + \mathbf{f}_{\text{seg}}$ (c) Contours of $\mathbf{u}$ (d) $\text{Err}_{\mathbf{u}}(t)$

(e) $\mathbf{b}$ (f) $\mathbf{f}_{\text{seg}} = \sum_{n=1}^{N} c_n \mathbf{p}_n$ (g) $\boldsymbol{\epsilon} + 150$ (h) $\mathbf{v} + 150$

(i) $\mathbf{p}_1$ (j) $\mathbf{p}_2$ (k) $\mathbf{p}_3$ (l) $\mathbf{v}_{\text{bin}} = \mathbf{v} > 0$

Figure 5: The original image $\mathbf{f}$ (a) is decomposed into a bias field $\mathbf{b}$ (e), a piecewise constant image $\mathbf{f}_{\text{seg}}$ (f), small scale objects (residual) $\boldsymbol{\epsilon}$ (g), and sparse texture $\mathbf{v}$ (h) with binarized verion $\mathbf{v}_{\text{bin}}$ in (l). A piecewise smooth image $\mathbf{u}$ (b) is obtained by a summation of $\mathbf{b}$ (e) and $\mathbf{f}_{\text{seg}}$ (f). Subfigure (c) shows segmented contours superimposed on $\mathbf{u}$. The relative error of $\mathbf{u}$ is shown in (d). The indicator functions for phases 1, 2, and 3 are shown in Subfigures i, j, and k, respectively. The parameters are $\nu = 10, N = 3, L = S = M = 2, \tau = 0.1, \xi = 0.001, \alpha = \mu_1 = \mu_2 = \mu_3 = 0.1, c_{\mu_1} = 0.14, \mu_4 = 0.01, \beta = 0.04, \#\text{iteration} = 10000$. The mean square error of the original image $\mathbf{f}$ and a reconstructed image $\mathbf{f}_{\text{re}} = \mathbf{b} + \mathbf{f}_{\text{seg}} + \mathbf{v} + \boldsymbol{\epsilon}$ is $\text{MSE} = 9.02 \times 10^{-5}$.

4 The Bilevel-SHT Model

We now propose an alternative to the multiphase SHT model. As above, we assume that an image $\mathbf{f}$ is composed of a homogeneous region (consisting of a bias field $\mathbf{b}$ and piecewise-constant with mean values $\vec{c}$ and indicator functions

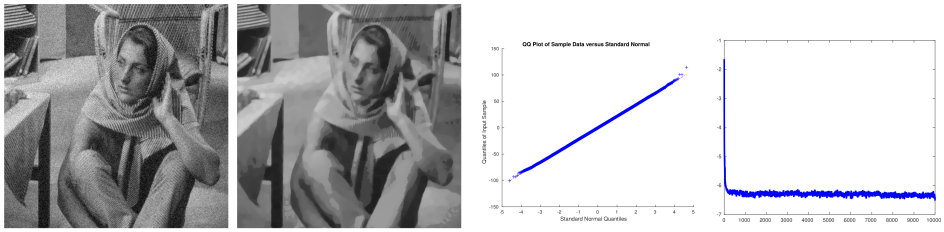

(a) $\mathbf{f}$ (b) $\mathbf{u} = \mathbf{b} + \mathbf{f}_{\text{seg}}$ (c) QQ plot of $\boldsymbol{\epsilon}$ (d) $\text{Err}_{\mathbf{u}}(t)$

(e) $\mathbf{b}$ (f) $\mathbf{f}_{\text{seg}} = \sum_{n=1}^{N} c_n \mathbf{p}_n$ (g) $\boldsymbol{\epsilon} + 150$ (h) $\mathbf{v} + 150$

(i) $\mathbf{p}_1$ (j) $\mathbf{p}_2$ (k) $\mathbf{p}_3$ (l) $\mathbf{v}_{\text{bin}} = \mathbf{v} > 0$

Figure 6: Original image $\mathbf{f}$ with added i.i.d. noise from $\mathcal{N}(0\,, 20^2)$ is shown in (a). With the addition of noise, we choose $\nu = 16$ with the remaining parameters set similar to those in Figure 5. The QQplot in (c) for noise $\boldsymbol{\epsilon}$ in (g) shows that $\nu = 16$ can separate most of the noise and some texture information. The MSE is 7.47×10^{-5}. Note that increasing L will not make $\mathbf{u}$ (b) smoother due to the lack of a sparsity constraint in Chambolle's projection. The algorithm still performs well with sparse texture $\mathbf{v}$ as illustrated in (l).

$\vec{\mathbf{p}}$) as well as texture $\mathbf{v}$ and residual $\boldsymbol{\epsilon}$, but we now consider a bilevel scheme for decomposing the image into these base components. Specifically, we consider the decomposition and segmentation as separate levels:

- **Level 1:** Image decomposition

$$\mathbf{f} = \mathbf{u} + \mathbf{v} + \boldsymbol{\epsilon}$$

- **Level 2:** Multiphase piecewise-smooth image segmentation

$$\mathbf{u} = \mathbf{b} + \sum_{n=1}^{N} c_n \mathbf{p}_n \,, \;\; \sum_{n=1}^{N} \mathbf{p}_n = 1 \,, \;\; p_n[\boldsymbol{k}] \in \{0,1\} \,, \;\; n = 1, \ldots, N \,, \;\; \boldsymbol{k} \in \Omega \,.$$

The bilevel minimization scheme for simultaneously homogeneous and textural (SHT) image segmentation is defined as

$$\min_{\left(\vec{c}\,,\vec{\mathbf{p}}\,,\mathbf{b}\right) \in \mathbb{R}^N \times X^{N+1}} \left\{ \min_{(\mathbf{u},\mathbf{v},\boldsymbol{\epsilon}) \in X^3} \left\{ \mathcal{I}_1\big(\mathbf{u},\mathbf{v},\boldsymbol{\epsilon}\big) \text{ s.t. } \mathbf{f} = \mathbf{u} + \mathbf{v} + \boldsymbol{\epsilon} \right\} + \mathcal{I}_2\big(\vec{\mathbf{p}},\mathbf{b}\big) \text{ s.t. } \mathcal{S}\big(\vec{c},\vec{\mathbf{p}},\mathbf{b};\mathbf{u}\big) \right\} \tag{15}$$

with set $\mathcal{S}$

$$\mathcal{S}\big(\vec{c}\,,\vec{\mathbf{p}}\,,\mathbf{b}\,;\mathbf{u}\big) = \left\{ \mathbf{u} = \mathbf{b} + \sum_{n=1}^{N} c_n \mathbf{p}_n \,, \;\; \sum_{n=1}^{N} \mathbf{p}_n = 1 \,, \;\; p_n[\boldsymbol{k}] \in \{0,1\} \,, \;\; n = 1, \ldots, N \,, \;\; \boldsymbol{k} \in \Omega \right\}$$

and energy functions

$$\mathcal{I}_1(\mathbf{u},\mathbf{v},\boldsymbol{\epsilon}) \;=\; \left\| \nabla_L^+ \mathbf{u} \right\|_{\ell_1} + \mu_1 \|\mathbf{v}\|_{\mathrm{G}_S} + \mu_2 \|\mathbf{v}\|_{\ell_1} + \mathscr{G}^* \left(\frac{\boldsymbol{\epsilon}}{\nu} \right) \quad \text{and}$$

$$\mathcal{I}_2\big(\vec{\mathbf{p}}\,,\mathbf{b}\big) \;=\; \sum_{n=1}^{N} \left\| \nabla_M^+ \mathbf{p}_n \right\|_{\ell_1} + \frac{\mu_3}{2} \|\mathbf{b}\|_{\ell_2}^2 \,.$$

Similar to the above multiphase SHT model, this bilevel-SHT model also measures a bias field $\mathbf{b}$ via ℓ_2 distance as data fidelity term in the regularization. In contrast with [45, 46], we enforce the constraint for the smoothness in $\mathbf{u}$ with $\left\| \nabla_L^+ \mathbf{u} \right\|_{\ell_1}$.

4.1 Solution of the bilevel-SHT model

We now describe a numerical algorithm to obtain the solution of the bilevel-SHT model (15):

- **Level 1: D**irectional **G**lobal **T**hree-**p**art **D**ecomposition (DG3PD)

$$(\mathbf{u}^*,\mathbf{v}^*,\boldsymbol{\epsilon}^*) \;=\; \underset{(\mathbf{u},\mathbf{v},\boldsymbol{\epsilon}) \in X^3}{\operatorname{argmin}} \left\{ \mathcal{I}_1\big(\mathbf{u},\mathbf{v},\boldsymbol{\epsilon}\big) \text{ s.t. } \mathbf{f} = \mathbf{u} + \mathbf{v} + \boldsymbol{\epsilon} \right\} \tag{16}$$

- **Level 2: S**imultaneously **H**omogeneous and **T**exture **M**ultiphase **S**egmentation (SHTMS)

$$\left(\vec{c}^{\,*}\,,\vec{\mathbf{p}}^{\,*}\,,\mathbf{b}^*\right) \;=\; \underset{\left(\vec{c}\,,\vec{\mathbf{p}}\,,\mathbf{b}\right) \in \mathbb{R}^N \times X^{N+1}}{\operatorname{argmin}} \left\{ \mathcal{I}_2\big(\vec{\mathbf{p}},\mathbf{b}\big) \text{ s.t. } \mathcal{S}\big(\vec{c}\,,\vec{\mathbf{p}}\,,\mathbf{b}\,;\mathbf{u}^*\big) \right\} \tag{17}$$

As alluded to above, we first decompose the original image $\mathbf{f}$ into piecewise-smooth, texture, and residual components $\mathbf{u}$, $\mathbf{v}$, and $\boldsymbol{\epsilon}$. We then segment the piecewise-smooth image $\mathbf{u}$ into multiphase (N) piecewise-constant images and a bias field $\mathbf{b}$. Sparse (or segmented) texture $\mathbf{v}$ is measured by $\|\mathbf{v}\|_{\ell_1}$ and $\|\mathbf{v}\|_{\mathrm{G}_S}$ and we note that G_S is a generalized version of the Banach space G in the discrete setting [54, 55, 66]. Note also that though we assume the original image $\mathbf{f}$ contains both texture and homogeneous areas, only the homogeneous areas are segmented by level 2.

4.1.1 Solution of Level 1 - DG3PD

The solution of the convex minimization in (16) is defined in [55, Algorithm 1] and [7] and is solved by introducing new variables and applying ALM and ADMM. In an effort to make this paper self-contained, the kernel of the DG3PD method is provided in Algorithm 3.

Note that DG3PD approximates $\|\vec{\mathbf{g}}\|_{\ell_\infty}$ in the G_S-norm by $\|\vec{\mathbf{g}}\|_{\ell_1}$; see [23] for details. This approximation in ℓ_1-norm enforces sparsity of $\vec{\mathbf{g}}$ (in our case, the texture $\mathbf{v}$).

4.1.2 Solution of Level 2 - SHTMS

Note that since the bias field is defined as

$$\mathbf{b} = \mathbf{u} - \sum_{n=1}^{N} c_n \mathbf{p}_n$$

with the binary set $p_n[\boldsymbol{k}] \in \{0\,,1\}$, we can rewrite the ℓ_2-norm and recast the non-convex minimization in (17) as

$$\min_{(\vec{c},\vec{\mathbf{p}})\in\mathbb{R}^N\times X^N} \left\{ \sum_{n=1}^{N} \left\| \nabla_M^+ \mathbf{p}_n \right\|_{\ell_1} + \frac{\mu_3}{2} \sum_{n=1}^{N} \left\langle \left(\mathbf{u} - c_n\right)^{.2}, \mathbf{p}_n \right\rangle_{\ell_2}, \right.$$

$$\left. \sum_{n=1}^{N} p_n[\boldsymbol{k}] = 1, p_n[\boldsymbol{k}] \in \{0,1\}, n = 1, \ldots, N, \boldsymbol{k} \in \Omega \right\}. \quad (18)$$

As in [55, 7], a solution of the multivariate minimization (18) can be obtained by alternating between solving the following two subproblems:

a. The $\vec{c} = \left[c_n\right]_{n=1}^{N}$ problem: Fix $\vec{\mathbf{p}}$ and solve

$$\min_{\vec{c}\in\mathbb{R}^N} \left\{ \mathcal{L}(\vec{c}) = \frac{\mu_3}{2} \sum_{n=1}^{N} \left\langle \left(\mathbf{u} - c_n\right)^{.2}, \mathbf{p}_n \right\rangle_{\ell_2} \right\}. \quad (19)$$

Due to its separability, the solution of (19) is given by

$$c_n = \frac{\sum_{\boldsymbol{k}\in\Omega} u[\boldsymbol{k}]p_n[\boldsymbol{k}]}{\sum_{\boldsymbol{k}\in\Omega} p_n[\boldsymbol{k}]}\,,\ n=1,\ldots,N. \tag{20}$$

b. The $\vec{\mathbf{p}} = \big[\mathbf{p}_n\big]_{n=1}^N$ problem: Fix $\vec{c}$ and find $\vec{\mathbf{p}}$.

As in Section 3.1, the nonconvex minimization in (18) w.r.t. $\vec{\mathbf{p}}$ is relaxed and made convex by setting a binary set $p_n[\boldsymbol{k}] \in \{0\,,1\}$ to $[0\,,1]$. Following [42, 46], we apply a smoothed dual formulation by introducing the primal, primal-dual, and dual models:

The primal model: Solve

$$\min_{\vec{\mathbf{p}}\in\mathcal{Q}_+}\left\{\mathcal{L}^{\mathrm{P}}(\vec{\mathbf{p}}) = \sum_{n=1}^N \Big\|\nabla_M^+\mathbf{p}_n\Big\|_{\ell_1} + \frac{\mu_3}{2}\sum_{n=1}^N\Big\langle\big(\mathbf{u}-c_n\big)^{.2},\mathbf{p}_n\Big\rangle_{\ell_2}\right\} \tag{21}$$

over the convex set

$$\mathcal{Q}_+ = \Big\{\big[\mathbf{p}_n\big]_{n=1}^N \in X^N\ :\ \sum_{n=1}^N p_n[\boldsymbol{k}] = 1\,,\ p_n[\boldsymbol{k}]>0\,,\ n=1,\ldots,N\,,\ \boldsymbol{k}\in\Omega\Big\}. \tag{22}$$

The primal-dual model:

Denote a convex set $K_M(1) = \Big\{\vec{\mathbf{q}}_n \in X^M\ :\ \|\vec{\mathbf{q}}_n\|_{\ell_\infty} \le 1\Big\}$ with a dual variable $\vec{\mathbf{q}} = \big[\vec{\mathbf{q}}_n\big]_{n=1}^N = \big[\mathbf{q}_{nm}\big]_{n=[1,N]}^{m=[0,M-1]} \in X^{NM}$ of a primal variable $\vec{\mathbf{p}} = \big[\mathbf{p}_n\big]_{n=1}^N \in X^N$. From Lemma 7.0.1 in the Appendix (for the dual formulation of the directional total variation norm) and the minimax theorem as found in [67, Chapter 6] and [42], the primal-dual model is defined as

$$\max_{\vec{\mathbf{q}}\in\big[K_M(1)\big]^N}\ \min_{\vec{\mathbf{p}}\in\mathcal{Q}_+}\left\{\mathcal{L}^{\mathrm{PD}}(\vec{\mathbf{p}};\vec{\mathbf{q}}) = \sum_{n=1}^N\Big\langle\mathbf{p}_n\,,\frac{\mu_3}{2}\big(\mathbf{u}-c_n\big)^{.2} + \mathrm{div}_M^-\vec{\mathbf{q}}_n\Big\rangle_{\ell_2}\right\}. \tag{23}$$

The smoothed primal-dual model: Solve

$$\max_{\vec{\mathbf{q}}\in\big[K_M(1)\big]^N}\ \underbrace{\min_{\vec{\mathbf{p}}\in\mathcal{Q}_+}\left\{\mathcal{L}^{\mathrm{PD}}_{\xi>0}(\vec{\mathbf{p}};\vec{\mathbf{q}}) = \sum_{n=1}^N\Big\langle\mathbf{p}_n\,,\frac{\mu_3}{2}\big(\mathbf{u}-c_n\big)^{.2} + \mathrm{div}_M^-\vec{\mathbf{q}}_n\Big\rangle_{\ell_2} + \xi\sum_{n=1}^N\Big\langle\mathbf{p}_n\,,\log\mathbf{p}_n\Big\rangle_{\ell_2}\right\}}\,.$$

$$= \mathcal{L}^{\mathrm{D}}_{\xi>0}(\vec{\mathbf{q}}) := -\xi\sum_{\boldsymbol{k}\in\Omega}\log\Big[\sum_{n=1}^N\exp\Big\{-\frac{1}{\xi}\Big[\frac{\mu_3}{2}(u[\boldsymbol{k}]-c_n)^2 + \mathrm{div}_M^-\vec{q}_n[\boldsymbol{k}]\Big]\Big\}\Big] \tag{24}$$

From Proposition 7.5 in the Appendix, the solution of the primal $\vec{\mathbf{p}}$-problem

$$\min_{\vec{\mathbf{p}}\in\mathcal{Q}_+} \mathcal{L}^{\mathrm{PD}}_{\xi>0}(\vec{\mathbf{p}};\vec{\mathbf{q}})$$

is given by (with $n = 1,\ldots,N$)

$$\mathbf{p}^*_n = \frac{\exp\Big[-\frac{1}{\xi}\Big[\frac{\mu_3}{2}\big(\mathbf{u}-c_n\big)^{.2} + \mathrm{div}^-_M\vec{\mathbf{q}}_n\Big]\Big]}{\sum_{i=1}^{N}\exp\Big[-\frac{1}{\xi}\Big[\frac{\mu_3}{2}\big(\mathbf{u}-c_i\big)^{.2} + \mathrm{div}^-_M\vec{\mathbf{q}}_i\Big]\Big]}$$

$$= \frac{\exp\Big[-\frac{1}{\xi}\Big[\frac{\mu_3}{2}\big(\mathbf{u}-c_n\big)^{.2} - \sum_{m=0}^{M-1}\big[\sin\Big(\frac{\pi m}{M}\Big)\mathbf{D}_{\mathbf{1}}^{\mathrm{T}}\mathbf{q}_{nm} + \cos\Big(\frac{\pi m}{M}\Big)\mathbf{q}_{nm}\mathbf{D}_{\mathbf{2}}\big]\Big]\Big]}{\sum_{i=1}^{N}\exp\Big[-\frac{1}{\xi}\Big[\frac{\mu_3}{2}\big(\mathbf{u}-c_i\big)^{.2} - \sum_{m=0}^{M-1}\big[\sin\Big(\frac{\pi m}{M}\Big)\mathbf{D}_{\mathbf{1}}^{\mathrm{T}}\mathbf{q}_{im} + \cos\Big(\frac{\pi m}{M}\Big)\mathbf{q}_{im}\mathbf{D}_{\mathbf{2}}\big]\Big]\Big]}.$$

Due to its separability, we consider the dual $\vec{\mathbf{q}}$-problem

$$\max_{\vec{\mathbf{q}}\in\left[K_M(1)\right]^N} \mathcal{L}^{\mathrm{D}}_{s>0}(\vec{\mathbf{q}}) \tag{25}$$

at $n = 1,\ldots,N$. Given $\vec{\mathbf{q}}_n = \big[\mathbf{q}_{nm}\big]_{m=0}^{M-1}$ and $\nabla^+_M\mathbf{p}_n = \big[\partial^+_m\mathbf{p}_n\big]_{m=0}^{M-1}$, the solution of (25) which is solved by Chambolle's projection [34] at each iteration t is

$$\vec{\mathbf{q}}_n^{(t+1)} = \frac{\vec{\mathbf{q}}_n^{(t)} + \tau\nabla^+_M\mathbf{p}_n^{(t)}}{1+\tau\Big|\nabla^+_M\mathbf{p}_n^{(t)}\Big|}, \quad n = 1,\ldots,N$$

and its element form is (with $m = 0,\ldots,M-1$)

$$\mathbf{q}_{nm}^{(t+1)} = \frac{\mathbf{q}_{nm}^{(t)} + \tau\big[\sin\Big(\frac{\pi m}{M}\Big)\mathbf{D}_{\mathbf{1}}\mathbf{p}_n + \cos\Big(\frac{\pi m}{M}\Big)\mathbf{p}_n\mathbf{D}_{\mathbf{2}}^{\mathrm{T}}\big]}{1+\tau\left[\sum_{m=0}^{M-1}\left[\sin\Big(\frac{\pi m}{M}\Big)\mathbf{D}_{\mathbf{1}}\mathbf{p}_n + \cos\Big(\frac{\pi m}{M}\Big)\mathbf{p}_n\mathbf{D}_{\mathbf{2}}^{\mathrm{T}}\right]^{.2}\right]^{\cdot\frac{1}{2}}}.$$

The numerical solution of the bilevel SHT model is described in Algorithms 2-4. Figure 7 shows the bilevel SHT model applied to the same noisy image as in Figure 6. Note, by comparing the upper left-hand corners of subfigures (l) and (k) of Figures 6 and 7 respectively, that the bilevel SHT model does a better job of fully segmenting the large scale texture from the homogeneous regions. However, these binarized versions also reveal that the bilevel SHT model is slightly oversensitive as some small artifacts are introduced. Finally, in Figure 8 we apply the bilevel SHT model to an image of a galaxy with many stars in the background. Although the stars may constitute small-scale texture, in cases such as these we may set the texture component ($\mathbf{v}$) to 0, thereby treating this fine texture as noise.

Algorithm 2 The Bilevel-SHT model

Denote parameters: $\kappa_{\mathrm{d}} = \Big[L, S, c_{\mu_1}, c_{\mu_2}, \big[\beta_i\big]_{i=1}^{4}, \nu\Big]$ and $\kappa_{\mathrm{s}} = \Big[M, N, \xi, \mu_3, \tau\Big]$

Denote variables:

$$\theta = \Big[\big[\mathbf{r}_l\big]_{l=0}^{L-1}, \big[\mathbf{w}_s\big]_{s=0}^{S-1}, \big[\mathbf{g}_s\big]_{s=0}^{S-1}, \big[\boldsymbol{\lambda}_{\mathbf{1}l}\big]_{l=0}^{L-1}, \big[\boldsymbol{\lambda}_{\mathbf{2}a}\big]_{a=0}^{S-1}, \boldsymbol{\lambda}_{\mathbf{3}}, \boldsymbol{\lambda}_{\mathbf{4}}\Big]$$

Initialization: $\mathbf{u}^{(0)} = \mathbf{f}, \mathbf{v}^{(0)} = \boldsymbol{\epsilon}^{(0)} = \theta^{(0)} = \vec{\mathbf{p}}^{(0)} = \vec{\mathbf{q}}^{(0)} = \mathbf{0}$, $c_n^{(0)} = (n-1)\lfloor\frac{255}{N}\rfloor, n = 1, \ldots, N.$

for $t_1 = 1, \ldots, T_1$ **do**

Level 1 (Decomposition): $(\mathbf{u}, \mathbf{v}, \boldsymbol{\epsilon}) \in X^3$
for $t_2 = 1, \ldots, T_2$ **do**

$$\Big[\mathbf{u}^{(t_2)}, \mathbf{v}^{(t_2)}, \boldsymbol{\epsilon}^{(t_2)}, \theta^{(t_2)}\Big] = \mathrm{DG3PD}\Big(\mathbf{u}^{(t_2-1)}, \mathbf{v}^{(t_2-1)}, \boldsymbol{\epsilon}^{(t_2-1)}, \theta^{(t_2-1)};\ \mathbf{f}, \kappa_{\mathrm{d}}\Big)$$

end for

Level 2 (Multiphase Segmentation of u): $(\vec{c}, \vec{\mathbf{p}}, \vec{\mathbf{q}}) \in \mathbb{R}^N \times X^{N+NM}$

$$\Big[\vec{c}^{(t_1)}, \vec{\mathbf{p}}^{(t_1)}, \vec{\mathbf{q}}^{(t_1)}\Big] = \mathrm{SHTMS}\Big(\vec{c}^{(t_1-1)}, \vec{\mathbf{p}}^{(t_1-1)}, \vec{\mathbf{q}}^{(t_1-1)};\ \mathbf{u}^{(T_2)}, \kappa_{\mathrm{s}}\Big)$$

end for

Global minimizer of (15):

$\mathbf{u}^* = \mathbf{u}^{T_1T_2}, \mathbf{v}^* = \mathbf{v}^{T_1T_2}, \boldsymbol{\epsilon}^* = \boldsymbol{\epsilon}^{T_1T_2}, \vec{\mathbf{q}}^* = \vec{\mathbf{q}}^{T_1}, \vec{c}^* = \vec{c}^{T_1}$, and

$$\mathbf{p}_h^* = \begin{cases} 1, & h = \underset{1\le n\le N}{\operatorname{argmin}} \Big\{ \underbrace{-\sum_{m=0}^{M-1} \big[\sin\Big(\frac{\pi m}{M}\Big)\mathbf{D}_{\mathbf{1}}^{\mathrm{T}}\mathbf{q}_{nm}^* + \cos\Big(\frac{\pi m}{M}\Big)\mathbf{q}_{nm}^*\mathbf{D}_{\mathbf{2}}\big]}_{=\mathrm{div}_M^- \vec{\mathbf{q}}_n^*} + \frac{\beta_5}{2}\big(\mathbf{u}^* - c_n^*\big)^{\cdot 2} \Big\} \\ 0, & \text{else} \end{cases}, h = 1, \ldots, N$$

Algorithm 3 Level 1: The Discrete DG3PD Model [55]

$$\Big[\mathbf{u}^{(\mathrm{new})}\,,\mathbf{v}^{(\mathrm{new})}\,,\boldsymbol{\epsilon}^{(\mathrm{new})}\,,\theta^{(\mathrm{new})}\Big]=\mathrm{DG3PD}\Big(\mathbf{u}^{(\mathrm{old})}\,,\mathbf{v}^{(\mathrm{old})}\,,\boldsymbol{\epsilon}^{(\mathrm{old})}\,,\theta^{(\mathrm{old})}\,;\;\mathbf{f}\,,\kappa_{\mathrm{d}}\Big)$$

1. Compute $\Big(\big[\mathbf{r}_b^{(t)}\big]_{b=0}^{L-1}\,,\big[\mathbf{w}_a^{(t)}\big]_{a=0}^{S-1}\,,\big[\mathbf{g}_a^{(t)}\big]_{a=0}^{S-1}\,,\mathbf{v}^{(t)}\,,\mathbf{u}^{(t)}\,,\boldsymbol{\epsilon}^{(t)}\Big)\in X^{L+2S+3}$:

$$\mathbf{r}_b^{(t)}\;=\;\mathrm{Shrink}\Big(\sin\Big(\frac{\pi b}{L}\Big)\mathbf{D_1}\mathbf{u}^{(t-1)}+\cos\Big(\frac{\pi b}{L}\Big)\mathbf{u}^{(t-1)}\mathbf{D_2}^{\mathrm{T}}-\frac{\boldsymbol{\lambda}_{\mathbf{1}b}^{(t-1)}}{\beta_1}\,,\frac{1}{\beta_1}\Big)\,,\;b=0\,,\ldots\,,L-1$$

$$\mathbf{w}_a^{(t)}\;=\;\mathrm{Shrink}\Big(\mathbf{t}_{\mathbf{w}_a}\;:=\;\mathbf{g}_a^{(t-1)}-\frac{\boldsymbol{\lambda}_{\mathbf{2}a}^{(t-1)}}{\beta_2}\,,\frac{\mu_1}{\beta_2}\Big)\,,\qquad a=0\,,\ldots\,,S-1$$

$$\mathbf{g}_a^{(t)}\;=\;\mathrm{Re}\Big[\mathcal{F}^{-1}\Big\{\mathcal{A}^{(t)}(\boldsymbol{z})\cdot\mathcal{B}^{(t)}(\boldsymbol{z})\Big\}\Big][\boldsymbol{k}]\Big|_{\boldsymbol{k}\in\Omega}\,,\;a=0\,,\ldots\,,S-1$$

$$\begin{aligned}\mathbf{v}^{(t)}=\mathrm{Shrink}\Big(\mathbf{t}_{\mathbf{v}}\;:=\;&\frac{\beta_3}{\beta_3+\beta_4}\Big(\sum_{s=0}^{S-1}\Big[\sin\Big(\frac{\pi s}{S}\Big)\mathbf{D_1}\mathbf{g}_s^{(t)}+\cos\Big(\frac{\pi s}{S}\Big)\mathbf{g}_s^{(t)}\mathbf{D_2}^{\mathrm{T}}\Big]-\frac{\boldsymbol{\lambda}_{\mathbf{3}}^{(t-1)}}{\beta_3}\Big)\\&+\frac{\beta_4}{\beta_3+\beta_4}\Big(\mathbf{f}-\mathbf{u}^{(t-1)}-\boldsymbol{\epsilon}^{(t-1)}+\frac{\boldsymbol{\lambda}_{\mathbf{4}}^{(t-1)}}{\beta_4}\Big)\,,\;\frac{\mu_2}{\beta_3+\beta_4}\Big)\end{aligned}$$

$$\mathbf{u}^{(t)}\;=\;\mathrm{Re}\Big[\mathcal{F}^{-1}\Big\{\mathcal{X}^{(t)}(\boldsymbol{z})\cdot\mathcal{Y}^{(t)}(\boldsymbol{z})\Big\}\Big][\boldsymbol{k}]\Big|_{\boldsymbol{k}\in\Omega}$$

$$\boldsymbol{\epsilon}^{(t)}\;=\;\Big(\mathbf{f}-\mathbf{u}^{(t)}-\mathbf{v}^{(t)}+\frac{\boldsymbol{\lambda}_{\mathbf{4}}^{(t-1)}}{\beta_4}\Big)\;-\;\mathrm{CST}\,\Big(\mathbf{f}-\mathbf{u}^{(t)}-\mathbf{v}^{(t)}+\frac{\boldsymbol{\lambda}_{\mathbf{4}}^{(t-1)}}{\beta_4}\,,\nu\Big)$$

2. Update $\Big(\big[\boldsymbol{\lambda}_{\mathbf{1}b}^{(t)}\big]_{b=0}^{L-1}\,,\big[\boldsymbol{\lambda}_{\mathbf{2}a}^{(t)}\big]_{a=0}^{S-1}\,,\boldsymbol{\lambda}_{\mathbf{3}}^{(t)}\,,\boldsymbol{\lambda}_{\mathbf{4}}^{(t)}\Big)\in X^{L+S+2}$:

$$\boldsymbol{\lambda}_{\mathbf{1}b}^{(t)}\;=\;\boldsymbol{\lambda}_{\mathbf{1}b}^{(t-1)}\;+\;\gamma\beta_1\Big(\mathbf{r}_b^{(t)}-\sin\Big(\frac{\pi b}{L}\Big)\mathbf{D_1}\mathbf{u}^{(t)}-\cos\Big(\frac{\pi b}{L}\Big)\mathbf{u}^{(t)}\mathbf{D_2}^{\mathrm{T}}\Big)\,,\quad b=0\,,\ldots\,,L-1$$

$$\boldsymbol{\lambda}_{\mathbf{2}a}^{(t)}\;=\;\boldsymbol{\lambda}_{\mathbf{2}a}^{(t-1)}\;+\;\gamma\beta_2\Big(\mathbf{w}_a^{(t)}-\mathbf{g}_a^{(t)}\Big)\,,\quad a=0\,,\ldots\,,S-1$$

$$\boldsymbol{\lambda}_{\mathbf{3}}^{(t)}\;=\;\boldsymbol{\lambda}_{\mathbf{3}}^{(t-1)}\;+\;\gamma\beta_3\Big(\mathbf{v}^{(t)}-\sum_{s=0}^{S-1}\big[\sin\Big(\frac{\pi s}{S}\Big)\mathbf{D_1}\mathbf{g}_s^{(t)}+\cos\Big(\frac{\pi s}{S}\Big)\mathbf{g}_s^{(t)}\mathbf{D_2}^{\mathrm{T}}\big]\Big)$$

$$\boldsymbol{\lambda}_{\mathbf{4}}^{(t)}\;=\;\boldsymbol{\lambda}_{\mathbf{4}}^{(t-1)}\;+\;\gamma\beta_4\big(\mathbf{f}-\mathbf{u}^{(t)}-\mathbf{v}^{(t)}-\boldsymbol{\epsilon}^{(t)}\big)$$

(continued Algorithm 3)

$$\mathcal{A}(\boldsymbol{z}) \;=\; \left[\beta_2\mathbf{1_{mn}} + \beta_3\left|\sin\left(\frac{\pi a}{S}\right)(z_1-1) + \cos\left(\frac{\pi a}{S}\right)(z_2-1)\right|^2\right]^{-1},$$

$$\mathcal{B}(\boldsymbol{z}) \;=\; \beta_2\Big[W_a(\boldsymbol{z}) + \frac{\Lambda_{2a}(\boldsymbol{z})}{\beta_2}\Big] \;+\; \beta_3\Big[\sin\left(\frac{\pi a}{S}\right)(z_1^{-1}-1) + \cos\left(\frac{\pi a}{S}\right)(z_2^{-1}-1)\Big]\times$$

$$\Big[V(\boldsymbol{z}) - \sum_{s=[0\,,S-1]\setminus\{a\}}\Big[\sin\left(\frac{\pi s}{S}\right)(z_1-1) + \cos\left(\frac{\pi s}{S}\right)(z_2-1)\Big]G_s(\boldsymbol{z}) + \frac{\Lambda_3(\boldsymbol{z})}{\beta_3}\Big],$$

$$\mathcal{X}(\boldsymbol{z}) = \left[\beta_4\mathbf{1_{mn}} + \beta_1\sum_{l=0}^{L-1}\left|\sin\left(\frac{\pi l}{L}\right)(z_1-1) + \cos\left(\frac{\pi l}{L}\right)(z_2-1)\right|^2\right]^{-1},$$

$$\mathcal{Y}(\boldsymbol{z}) = \beta_4\Big[F(\boldsymbol{z}) - V(\boldsymbol{z}) - \mathcal{E}(\boldsymbol{z}) + \frac{\Lambda_4(\boldsymbol{z})}{\beta_4}\Big] + \beta_1\sum_{l=0}^{L-1}\Big[\sin\left(\frac{\pi l}{L}\right)(z_1^{-1}-1) + \cos\left(\frac{\pi l}{L}\right)(z_2^{-1}-1)\Big]\Big[R_l(\boldsymbol{z}) + \frac{\Lambda_{1l}(\boldsymbol{z})}{\beta_1}\Big].$$

Choice of Parameters

$\mu_1 = c_{\mu_1}\beta_2 \cdot \max\limits_{\boldsymbol{k}\in\Omega}\left(\left|t_{\mathbf{w}_a}[\boldsymbol{k}]\right|\right)$, $\mu_2 = c_{\mu_2}(\beta_3+\beta_4)\cdot\max\limits_{\boldsymbol{k}\in\Omega}\left(\left|t_{\mathbf{v}}[\boldsymbol{k}]\right|\right)$ and $\beta_2 = c_{\beta_2}\beta_3\,, \beta_3 = \dfrac{\theta}{1-\theta}\beta_4\,, \beta_1 = c_{\beta_1}\beta_4$.

Algorithm 4 Level 2: The SHTMS

$$\Big[\vec{c}^{\,(t+1)}\,, \vec{\mathbf{p}}^{\,(t+1)}\,, \vec{\mathbf{q}}^{\,(t+1)}\Big] = \mathrm{SHTMS}\Big(\vec{c}^{\,(t)}\,, \vec{\mathbf{p}}^{\,(t)}\,, \vec{\mathbf{q}}^{\,(t)}\,;\; \mathbf{u}\,, \kappa_{\mathrm{s}}\Big)$$

Compute $\left(\vec{c}\,, \vec{\mathbf{p}}\,, \vec{\mathbf{q}}\right) \in \mathbb{R}^N \times X^{N+NM}$:

$$c_n^{(t+1)} = \frac{\sum\limits_{\boldsymbol{k}\in\Omega} u[\boldsymbol{k}]p_n^{(t)}[\boldsymbol{k}]}{\sum\limits_{\boldsymbol{k}\in\Omega} p_n^{(t)}[\boldsymbol{k}]}\,,\; n = 1, \ldots, N$$

$$\mathbf{p}_n^{(t+1)} = \frac{\exp\Big[-\frac{1}{\xi}\Big[-\sum\limits_{m=0}^{M-1}\big[\sin\left(\frac{\pi m}{M}\right)\mathbf{D_1^{\mathrm{T}}}\mathbf{q}_{nm}^{(t)} + \cos\left(\frac{\pi m}{M}\right)\mathbf{q}_{nm}^{(t)}\mathbf{D_2}\big] + \frac{\mu_3}{2}\big(\mathbf{u} - c_n^{(t+1)}\big)^{\cdot 2}\Big]\Big]}{\sum\limits_{i=1}^{N}\exp\Big[-\frac{1}{\xi}\Big[-\sum\limits_{m=0}^{M-1}\big[\sin\left(\frac{\pi m}{M}\right)\mathbf{D_1^{\mathrm{T}}}\mathbf{q}_{im}^{(t)} + \cos\left(\frac{\pi m}{M}\right)\mathbf{q}_{im}^{(t)}\mathbf{D_2}\big] + \frac{\mu_3}{2}\big(\mathbf{u} - c_i^{(t+1)}\big)^{\cdot 2}\Big]\Big]}\,,\; n = 1, \ldots, N$$

$$\mathbf{q}_{nm}^{(t+1)} = \frac{\mathbf{q}_{nm}^{(t)} + \tau\big[\sin\left(\frac{\pi m}{M}\right)\mathbf{D_1}\mathbf{p}_n^{(t+1)} + \cos\left(\frac{\pi m}{M}\right)\mathbf{p}_n^{(t+1)}\mathbf{D_2^{\mathrm{T}}}\big]}{1 + \tau\Big[\sum\limits_{m=0}^{M-1}\big[\sin\left(\frac{\pi m}{M}\right)\mathbf{D_1}\mathbf{p}_n^{(t+1)} + \cos\left(\frac{\pi m}{M}\right)\mathbf{p}_n^{(t+1)}\mathbf{D_2^{\mathrm{T}}}\big]^{\cdot 2}\Big]^{\cdot\frac{1}{2}}}\,,\quad n = 1, \ldots, N\,,\; m = 0, \ldots, M-1$$

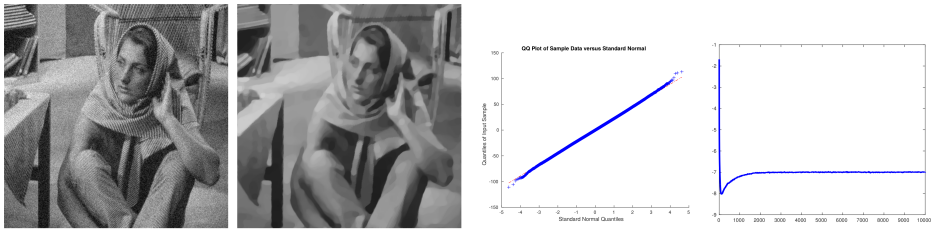

(a) $\mathbf{f}$ (b) $\mathbf{u} = \mathbf{b} + \mathbf{f}_{\text{seg}}$ (c) QQ plot of $\boldsymbol{\epsilon}$ (d) $\text{Err}_{\mathbf{u}}(t)$

(e) $\mathbf{b}$ (f) $\mathbf{f}_{\text{seg}} = \sum_{n=1}^{N} c_n \mathbf{p}_n$ (g) $\boldsymbol{\epsilon} + 150$ (h) $\mathbf{v} + 150$

(i) $\mathbf{p}_1$ (j) $\mathbf{p}_2$ (k) $\mathbf{p}_3$ (l) $\mathbf{v}_{\text{bin}} = \mathbf{v} > 0$

Figure 7: The bilevel SHT model applied to the noise image in Figure 6 with parameters $\sigma = 20\,, L = S = 9\,, c_{\mu_1} = c_{\mu_2} = 0.03\,, \theta = 0.9\,, c_1 = 1, c_2 = 1.3\,, \beta_4 = 0.04\,, \beta_3 = \frac{\theta}{1-\theta}\beta_4\,, \beta_1 = c_{\beta_1}\beta_4\,, \beta_2 = c_{\beta_2}\beta_3\,, \nu = 16\,, M = 2\,, N = 3\,, \xi = 0.001\,, \tau = 0.1\,, \beta_5 = 100\,, T_1 = T_2 = 100$.

5 Comparison with Alternative Approaches

We now apply our approach to several images in order to demonstrate and compare the performance with alternative approaches. The proficiency of and some properties of our models were demonstrated in Figures 5, 6 and 7. Here we focus on more subtle properties and compare our approach with existing methods.

Figure 9 depicts a homogeneous image of an airplane where we compare our bilevel SHT model to the classic Chan-Vese model [11]. The Chan-Vese model is applied in the first two rows and note that for different initial conditions – Subfigures (a) and (e) – that the model produces very different segmentations.

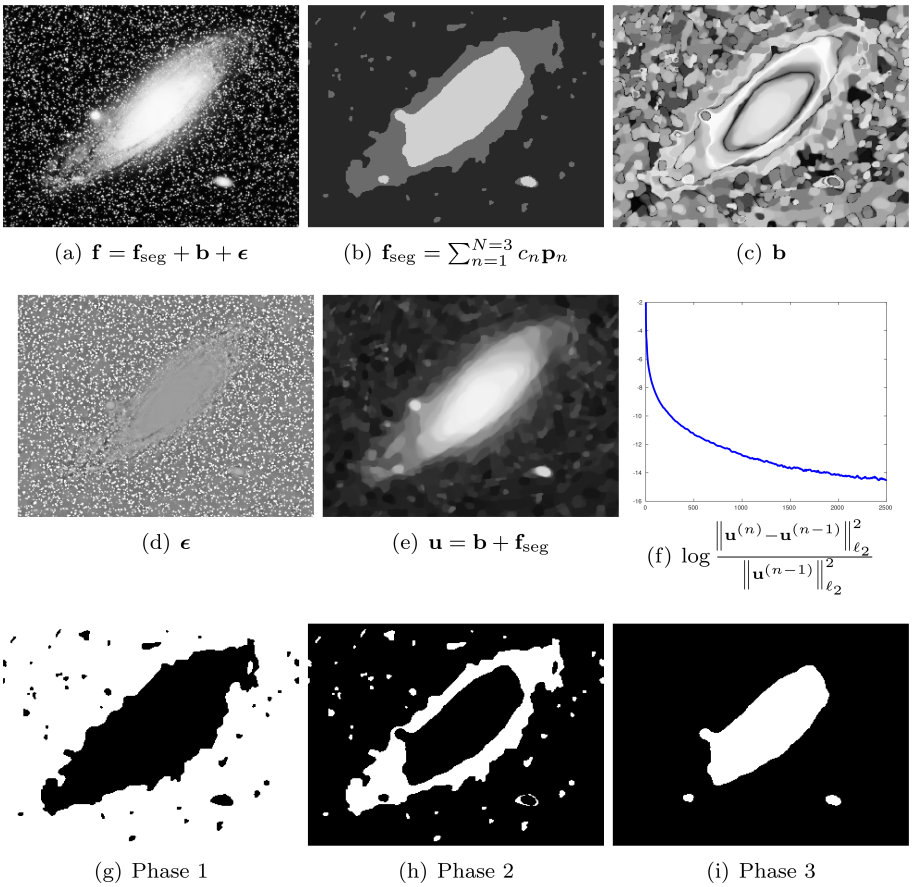

(a) $\mathbf{f} = \mathbf{f}_{\text{seg}} + \mathbf{b} + \boldsymbol{\epsilon}$ (b) $\mathbf{f}_{\text{seg}} = \sum_{n=1}^{N=3} c_n \mathbf{p}_n$ (c) $\mathbf{b}$

(d) $\boldsymbol{\epsilon}$ (e) $\mathbf{u} = \mathbf{b} + \mathbf{f}_{\text{seg}}$ (f) $\log \frac{\left\|\mathbf{u}^{(n)} - \mathbf{u}^{(n-1)}\right\|_{\ell_2}^2}{\left\|\mathbf{u}^{(n-1)}\right\|_{\ell_2}^2}$

(g) Phase 1 (h) Phase 2 (i) Phase 3

Figure 8: The bilevel SHT model applied to the galaxy image with no additional noise added. The background stars represent small-scale texture which can be treated as noise and measured by $\left\|\mathcal{C}\{\boldsymbol{\epsilon}\}\right\|_{\ell_\infty}$. The constant values are $\vec{c} = [40.1\,, 106.81\,, 208.21]$ and MSE $= 3.810^{-7}$. Parameters were chosen as in Figure 7 with the exception of $\nu = 40\,, T_1 = T_2 = 50$.

However, in our bilevel SHT model, we solve a convex minimization and as a result, produce a nearly unique result. The bilevel SHT model is applied in rows three and four with 2 and 3 phases respectively. Note that the 3-phase model is able to segment the sun, sky, and airplane whereas the 2-phase model combines the sky and airplane. Subfigures (k) and (n) show convergence on the log scale, thus implying very fast convergence on the linear scale.

Figure 10 contains (entirely) homogeneous images of a brain and were analyzed in [41]. Subfigure (a) contains the original image with no noise added and in Subfigure (b) we add i.i.d. Gaussian noise with standard deviation 20.

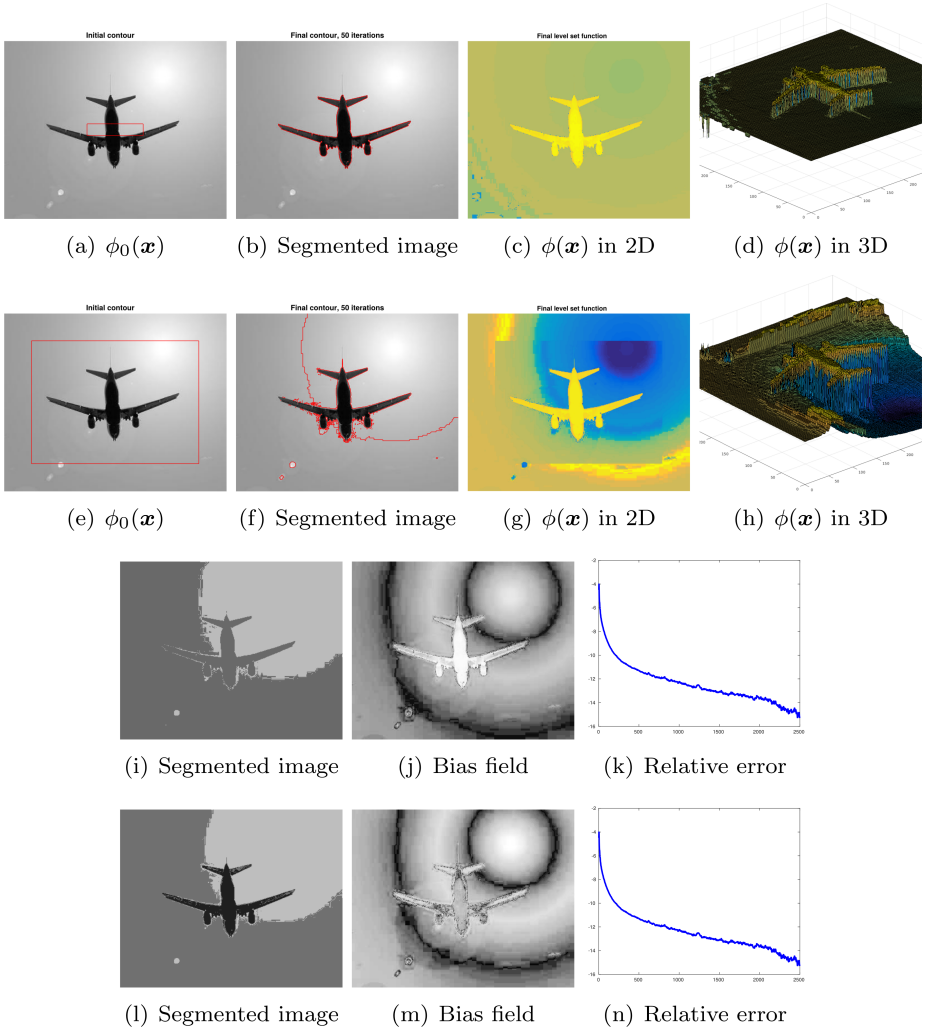

(a) $\phi_0(\boldsymbol{x})$ (b) Segmented image (c) $\phi(\boldsymbol{x})$ in 2D (d) $\phi(\boldsymbol{x})$ in 3D

(e) $\phi_0(\boldsymbol{x})$ (f) Segmented image (g) $\phi(\boldsymbol{x})$ in 2D (h) $\phi(\boldsymbol{x})$ in 3D

(i) Segmented image (j) Bias field (k) Relative error

(l) Segmented image (m) Bias field (n) Relative error

Figure 9: The Chan-Vese model (rows one and two) produces different segmentations for different initializations of the level set function $\phi(\boldsymbol{x})$. The Chan-Vese model parameters were chosen as Iteration $= 50\,, \mu = \lambda_1 = \lambda_2 = \epsilon = 1\,,$ timestep $= 0.1\,, v = 0$. The third and fourth rows show reconstructed images from the 2 and 3-phase bilevel SHT model with $\mathbf{u}_{\text{re}} = \mathbf{b} + \sum_{n=1}^{N} c_n \mathbf{p}_n$. The MSE for $\mathbf{u}_{\text{re}}$ in the 3-phase bilevel SHT model is 3.1510^{-6} and the relative error in Subfigures (k) and (n) is measured by (14). The bilevel model parameters were selected as in Figure 7 with $\nu = 0$ and $T_1 = T_2 = 50$.

The second row (Subfigures (c) - (f)) show the resulting segmented images following the procedures in [42, 52], and the bilevel SHT method with $\nu = 0$ and

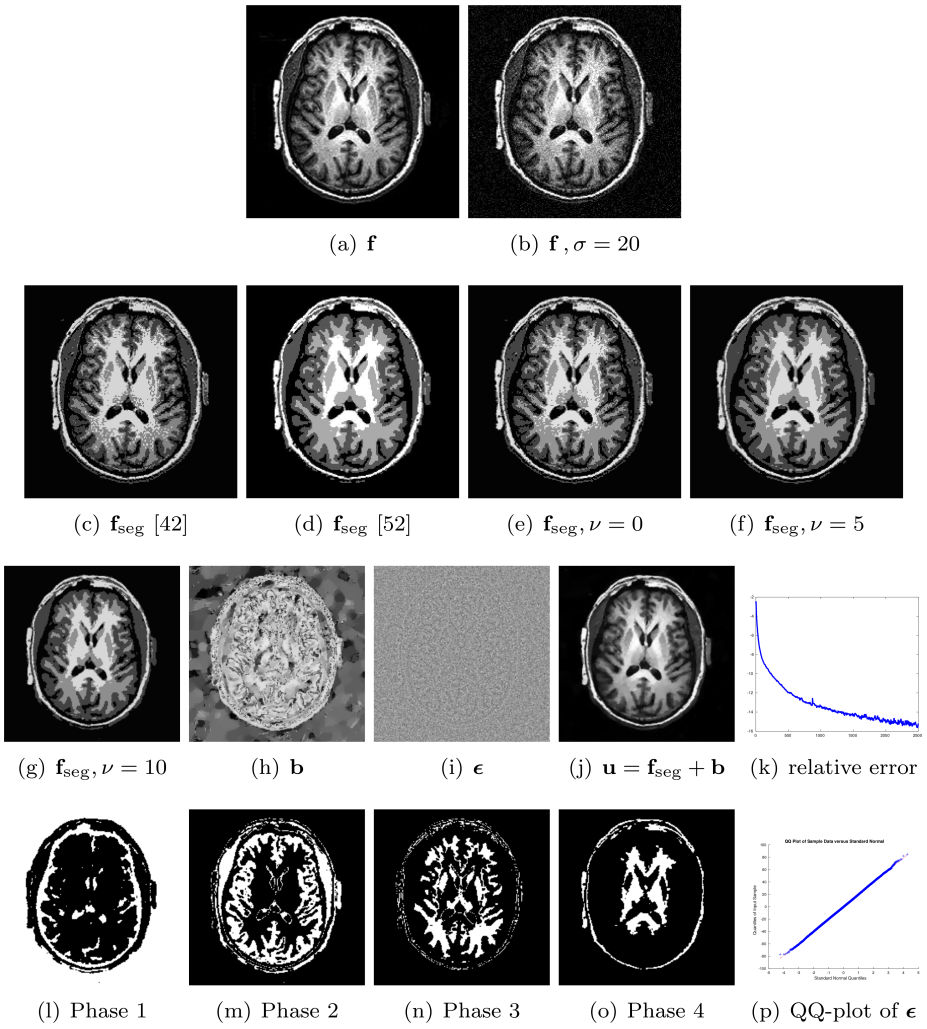

(a) $\mathbf{f}$ (b) $\mathbf{f}\,, \sigma = 20$

(c) $\mathbf{f}_{\text{seg}}$ [42] (d) $\mathbf{f}_{\text{seg}}$ [52] (e) $\mathbf{f}_{\text{seg}}, \nu = 0$ (f) $\mathbf{f}_{\text{seg}}, \nu = 5$

(g) $\mathbf{f}_{\text{seg}}, \nu = 10$ (h) $\mathbf{b}$ (i) $\boldsymbol{\epsilon}$ (j) $\mathbf{u} = \mathbf{f}_{\text{seg}} + \mathbf{b}$ (k) relative error

(l) Phase 1 (m) Phase 2 (n) Phase 3 (o) Phase 4 (p) QQ-plot of $\boldsymbol{\epsilon}$

Figure 10: A comparison with the methods in [42] and [52]. The segmented image in Subfigure (d) is taken from [52]. The results in row two were based on the segmentation of Subfigure (a); those in rows three and four were applied to the noisy version of the image in Subfigure (b). The bilevel model parameters are the same as in Figure 7 with $\nu = 0, 5,$ and 10 as noted in Subfigures (e), (f), and (g), respectively. The relative error of $\mathbf{u}$ is shown in Subfigures (k) and (p).

$\nu = 5$, respectively. We note that Subfigure (d) was taken directly from [52] and Subfigure (c) was programmed by hand. Note that in Subfigure (e) with $\nu = 0$, some small-scale residual still remains but when we increase the threshold to $\nu = 5$ in Subfigure (f), this residual is removed resulting in a smoother

segmented image. Thus, our procedure compares favorably even to other methods that apply only to homogeneous images. Further note that when noise is added (Subfigure (b)), our procedure is able to not only filter out the additional noise from the segmented images – see Subfigures (l) - (o) – but also produces a decomposition with well-separated meaningful components. Note also that by examining Subfigure (p), we see that with $\nu = 10$, almost all of the resulting noise was that which was added (i.e. very little of the information from the original image was classified as noise). As in Figure 10, Subfigure (k) shows convergence on the log scale implying very fast convergence on the linear scale.

Finally, we move on to consider images that contain only a textural region of interest. The images in Figure 11 depict various animals each with well-defined textural markings; the first row of images are taken directly from [49]. We begin by noting that many methods already exist to define a region of texture; see for example the methodology in [49]. Our SHT procedures were not designed for this goal, though extracting such a region is possible with our bilevel SHT model. Row three of Figure 11 shows the texture component of the bilevel SHT decomposition. This texture component was then binarized and a morphological operator applied to obtain the textural boundaries shown in row 2. Rows four and five show the piecewise-smooth and piecewise-constant bilevel SHT components, respectively. Note that our bilevel model, though not designed for this purpose, still does an admirable job of capturing the textural boundary. One advantage to our approach is that instead of only defining this boundary, our procedure also allows one to separate the texture inside from the remainder of the image.

6 Conclusion

This work provides algorithms to simultaneously decompose and segment images containing regions of both texture and homogeneity. This can be seen as an extension of the Mumford and Shah model to a much larger class of natural images. Two approaches are presented corresponding to the two alternative solutions to the G_S-norm for texture $\mathbf{v}$; the multiphase SHT approach based on the G_S-norm solution provided by Aujol and Chambolle [54] and bilevel SHT approach based on the solution of Vese and Osher [23]. In practice we find that the bilevel SHT algorithm is better able to discriminate between the homogeneous and textural regions and thus we focus on this approach in Section 5 and recommend it in practical applications. The likely reason for the superior performance of the bilevel model is that the Vese and Osher [23] approach to solving the G_S-norm utilized in the bilevel SHT model approximates $\|\vec{\mathbf{g}}\|_{\ell_\infty}$ with $\|\vec{\mathbf{g}}\|_{\ell_1}$. This enhances the sparsity of $\vec{\mathbf{g}}$ and though the original image is typically not sparse, it is sparse in some transform domain which is usually measured by ℓ_0-norm (or its relaxed ℓ_1-norm) in function space. One shortcoming of our models is the large number of required parameters and we hope to reduce the size of the parameter set as well as to analyze the convergence of the proposed

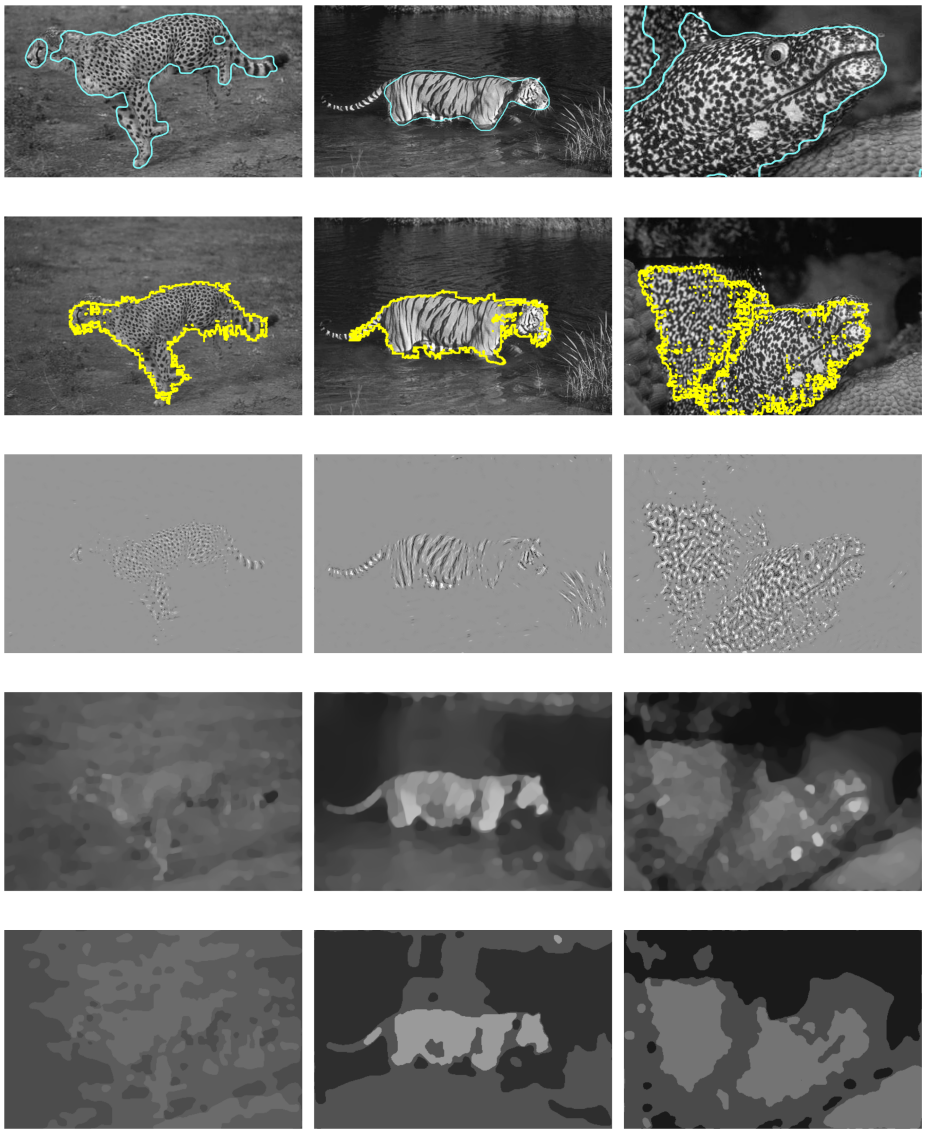

Figure 11: Animal images with textural regions of interest. Row one shows the original images and segmentations taken from [49]. Rows 2 - 5 show the various components of our bilevel SHT model; see main text for details. The bilevel model parameters are the same as in Figure 7 with the following exceptions: $T_2 = 1$ for each of the three images; $L = 40, 40, 12$ and $\nu = 30, 25, 15$ for the images in columns 1, 2, and 3, respectively.

minimization in future work.

Acknowledgements

The authors thank Professors Len Stefanski, David Banks and Ingrid Daubechies for their helpful comments. This material was based upon work partially supported by the National Science Foundation under Grant DMS-1127914 to the Statistical and Applied Mathematical Sciences Institute. Any opinions, findings, and conclusions or recommendations expressed in this material are those of the author(s) and do not necessarily reflect the views of the National Science Foundation.

References

[1] R.C. Gonzalez and R.E. Woods. *Digital Image Processing*. Prentice Hall, Upper Saddle River, NJ, USA, 2002.

[2] R. Szeliski. *Computer Vision: Algorithms and Applications*. Springer, London, United Kingdom, 2011.

[3] A.G. Webb. *Introduction to Biomedical Imaging*. Wiley-IEEE Press, New York, U.S.A., 2003.

[4] J.L. Starck and F. Murtagh, editors. *Astronomical Image and Data Analysis*. Springer, New York, NY, USA, 2006.

[5] A. Jain, A.A. Ross, and K. Nandakumar. *Introduction to Biometrics*. Springer, New York, NY, USA, 2011.

[6] D.H. Thai, S. Huckemann, and C. Gottschlich. Filter design and performance evaluation for fingerprint image segmentation. *PLoS ONE*, 11(5):e0154160, May 2016.

[7] D.H. Thai and C. Gottschlich. Global variational method for fingerprint segmentation by three-part decomposition. *IET Biometrics*, 5(2):120–130, June 2016.

[8] N. Otsu. A threshold selection method from gray-level histograms. *IEEE Transactions on Systems, Man and Cybernetics*, 9(1):62–66, January 1979.

[9] P. Sahoo, C. Wilkins, and J. Yeager. Threshold selection using Renyi's entropy. *Pattern Recognition*, 30(1):71–84, January 1997.

[10] M.P.d. Albuquerque, I.A. Esquef, A.R.G. Mello, and M.P.d. Albuquerque. Image thresholding using Tsallis entropy. *Pattern Recognition Letters*, 25(9):1059–1065, July 2004.

[11] T.F. Chan and L.A. Vese. Active contours without edges. *IEEE Transactions on Image Processing*, 10(2):266–277, February 2001.

[12] X. Bresson, S. Esedoglu, P. Vandergheynst, J.P. Thiran, and S. Osher. Fast global minimization of the active contour/snake model. *Journal of Mathematical Imaging and Vision*, 28(2):151–167, June 2007.

[13] T.F. Chan, S. Esedoglu, and M. Nikolova. Algorithms for finding global minimizers of image segmentation and denoising models. *SIAM J. Appl. Math.*, 66(5):1632–1648, February 2012.

[14] J. Lie, M. Lysaker, and X.C. Tai. A binary level set model and some applications to Mumford-Shah image segmentation. *IEEE Transactions on Image Processing*, 15(5):1171–1181, May 2006.

[15] M. Kass, A. Witkin, and D. Terzopoulos. Snakes: Active contour models. *International Journal of Computer Vision*, 1(4):321–331, January 1988.

[16] D. Mumford and J. Shah. Optimal approximations by piecewise smooth functions and associated variational problems. *Communications on Pure and Applied Mathematics*, 42(5):577–685, July 1989.

[17] R.B. Potts. Some generalized order-disorder transformations. *In Proceedings of the Cambridge Philosophical Society*, 48:106–109, 1952.

[18] L. Rudin, S. Osher, and E. Fatemi. Nonlinear total variation based noise removal algorithms. *Physica D*, 60(1-4):259–268, November 1992.

[19] J.-F. Aujol, G. Gilboa, T. Chan, and S. Osher. Structure-texture image decomposition - modeling, algorithms, and parameter selection. *International Journal of Computer Vision*, 67(1):111–136, April 2006.

[20] J.F. Aujol, G. Aubert, L.B. Feraud, and A. Chambolle. Image decomposition into a bounded variation component and an oscillating component. *Journal of Mathematical Imaging and Vision*, 22(1):71–88, January 2005.

[21] J.F. Aujol and G. Gilboa. Constrained and SNR-based solutions for TV-Hilbert space image denoising. *Journal of Mathematical Imaging and Vision*, 26(1-2):217–237, November 2006.

[22] A. Buades, T.M. Le, J.-M. Morel, and L.A. Vese. Fast cartoon + texture image filters. *IEEE Transactions on Image Processing*, 19(8):1978–1986, August 2010.

[23] L.A. Vese and S. Osher. Modeling textures with total variation minimization and oscillatory patterns in image processing. *Journal of Scientific Computing*, 19(1-3):553–572, December 2003.

[24] G. Aubert and L. Vese. A variational method in image recovery. *SIAM J. Numer. Anal*, 34(5):1948–1979, October 1997.

[25] T. Chan, A. Marquina, and P. Mulet. High-order total variation-based image restoration. *SIAM Journal on Scientific Computing*, 22(2):503–516, July 2000.

[26] M. Lysaker, A. Lundervold, and X.C. Tai. Noise removal using fourth-order partial differential equation with applications to medical magnetic resonance images in space and time. *IEEE Transactions on Image Processing*, 12(12):1579–1590, December 2003.

[27] T. Rahman, X.C. Tai, and S. Osher. A TV-Stokes denoising algorithm. *Lecture Notes in Computer Science*, 4485:473–483, June 2007.

[28] J. Hahn, C. Wu, and X.C. Tai. Augmented Lagrangian method for generalized TV-Stokes model. *Journal of Scientific Computing*, 50(2):235–264, February 2012.

[29] W.Zhu and T. Chan. Image denoising using mean curvature of image surface. *SIAM Journal on Imaging Sciences*, 5(1):1–32, January 2012.

[30] X.C. Tai, J. Hahn, and G.J. Chung. A fast algorithm for Euler's elastica model using augmented Lagrangian method. *SIAM Journal on Imaging Sciences*, 4(1):313–344, February 2011.

[31] W. Zhu, X.C. Tai, and T. Chan. Image segmentation using Euler's elastica as the regularization. *Journal of Scientific Computing*, 57(2):414–438, April 2013.

[32] K. Papafitsoros and C.B. Schönlieb. A combined first and second order variational approach for image reconstruction. *J. Math. Imaging Vis.*, 48(2):308–338, 2014.

[33] L. Calatroni, B. Düring, and C.B. Schönlieb. ADI splitting schemes for a fourth-order nonlinear partial differential equation from image processing. *DCDS Series A*, 34(3):931–957, March 2014.

[34] A. Chambolle. An algorithm for total variation minimization and applications. *Journal of Mathematical Imaging and Vision*, 20(1-2):89–97, January 2004.

[35] T. Goldstein and S. Osher. The split Bregman method for L1-regularized problems. *SIAM Journal on Imaging Sciences*, 2(2):323–343, April 2009.

[36] I. Daubechies, M. Defrise, and C. D. Mol. An iterative thresholding algorithm for linear inverse problems with a sparsity constraint. *Communications on Pure and Applied Mathematics*, 57(11):1413–1457, August 2004.

[37] A. Beck and M. Teboulle. A fast iterative shrinkage-thresholding algorithm for linear inverse problems. *SIAM Journal on Imaging Sciences*, 2(1):183–202, January 2009.

[38] J.B. Dias and M. Figueiredo. A new twist: Two-step iterative shrinkage/thresholding algorithms for image restoration. *IEEE Transactions on Image Processing*, 16(12):2992–3004, December 2007.

[39] C. Wu and X. C. Tai. Augmented Lagrangian method, dual methods, and split Bregman iteration for ROF, vectorial TV, and higher order methods. *SIAM Journal on Imaging Sciences*, 3(3):300–339, July 2010.

[40] E.S. Brown, T.F. Chan, and X. Bresson. A convex relaxation method for a class of vector-valued minimization problems with applications to Mumford-Shah segmentation. *UCLA cam report*, 2010.

[41] E.S. Brown, T.F. Chan, and X. Bresson. Completely convex formulation of the Chan-Vese image segmentation model. *International Journal of Computer Vision*, 98(1):103–121, May 2012.

[42] E. Bae, J. Yuan, and X.C. Tai. Global minimization for continuous multiphase partitioning problems using a dual approach. *International Journal of Computer Vision*, 92(1):112–129, March 2010.

[43] L.L. Wang Y. Gu and X.C. Tai. A direct approach toward global minimization for multiphase labeling and segmentation problems. *IEEE Transactions on Image Processing*, 21(5):2399–2411, May 2012.

[44] E. Bae, J. Lellmann, and X.C. Tai. *Convex Relaxations for a Generalized Chan-Vese Model*, pages 223–236. Springer, Berlin, Germany, 2005.

[45] Y. Gu, L.L. Wang, W. Xiong, J. Cheng, W. Huang, and J. Zhou. Efficient and robust image segmentation with a new piecewise-smooth decomposition model. In *Proc. Int. Conf. IEEE ICIP*, pages 2718–2722, Melbourne, Australia, September 2013.

[46] Y. Gu, W. Xiong, L.L. Wang, J. Cheng, W. Huang, and J. Zhou. A new approach for multiphase piecewise smooth image segmentation. In *Proc. Int. Conf. IEEE ICIP*, pages 4417–4421, Paris, France, October 2014.

[47] C. Sagiv, N.A. Sochen, and Y.Y. Zeevi. Integrated active contours for texture segmentation. *IEEE Transactions on Image Processing*, 15(6):1633–1646, June 2006.

[48] N. Houhou, J.P. Thiran, and X. Bresson. Fast texture segmentation based on semi-local region descriptor and active contour. *Numer. Math. Theor. Meth. Appl.*, 2(4):445–468, November 2009.

[49] K. Ni, X. Bresson, T. Chan, and S. Esedoglu. Local histogram based segmentation using the wasserstein distance. *Int J Comput Vis*, 84(1):97–111, April 2009.

[50] M. Unser. Texture classification and segmentation using wavelet frames. *IEEE Transactions on Image Processing*, 4(11):1549–1560, November 1995.

[51] T.F. Chan, B.Y. Sandberg, and L.A. Vese. Active contours without edges for vector-valued images. *Journal of Visual Communication and Image Representation*, 11(2):130–141, June 2000.

[52] E.S. Brown, T.F. Chan, and X. Bresson. Convex formulation and exact global solutions for multi-phase piecewise constant Mumford-Shah image segmentation. *UCLA cam report*, 2009.

[53] J. Liu, X.C. Tai, H. Huang, and Z. Huan. A fast segmentation method based on constraint optimization and its applications: Intensity inhomogeneity and texture segmentation. *Pattern Recognition*, 44(9):2093–2108, September 2011.

[54] J.-F. Aujol and A. Chambolle. Dual norms and image decomposition models. *International Journal of Computer Vision*, 63(1):85–104, June 2005.

[55] D.H. Thai and C. Gottschlich. Directional global three-part image decomposition. *EURASIP Journal on Image and Video Processing*, 2016(12):1–20, March 2016.

[56] J. Gilles. Multiscale texture separation. *Multiscale Model. Simul.*, 10(4):1409–1427, December 2012.

[57] E. Candès and D. Donoho. New tight frames of curvelets and optimal representations of objects with piecewise singularities. *Communications on Pure and Applied Mathematics*, 57(2):219–266, February 2004.

[58] E. Candès, L. Demanet, D. Donoho, and L. Ying. Fast discrete curvelet transforms. *Multiscale Model. Simul.*, 5(3):861–899, September 2006.

[59] Starck, D.L. Donoho, and E.J. Candès. Astronomical image representation by the curvelet transform. *Astron. Astrophys.*, 398(2):785–800, February 2003.

[60] J. Ma and G. Plonka. The curvelet transform. *IEEE Signal Processing Magazin*, 27(2):118–133, March 2010.

[61] G. Kutyniok and D. Labate, editors. *Shearlets. Multiscale Analysis for Multivariate Data*. Birkhäuser, Boston, MA, USA, 2012.

[62] M.N. Do and M. Vetterli. The contourlet transform: An efficient directional multiresolution image representation. *IEEE Transactions on Image Processing*, 14(12):2091–2106, December 2005.

[63] M. Unser and D. Van De Ville. Wavelet steerability and the higher-order Riesz transform. *IEEE Transactions on Image Processing*, 19(3):636–652, March 2010.

[64] J. Gilles, G. Tran, and S. Osher. 2D Empirical transforms. Wavelets, ridgelets, and curvelet revisited. *SIAM J. Imaging Sci.*, 7(1):157–186, January 2014.

[65] D.H. Thai. *Fourier and Variational Based Approaches for Fingerprint Segmentation*. PhD thesis, University of Goettingen, Goettingen, Germany, January 2015.

[66] Y. Meyer. *Oscillating Patterns in Image Processing and Nonlinear Evolution Equations: The Fifteenth Dean Jacqueline B. Lewis Memorial Lectures*. American Mathematical Society, Boston, MA, USA, 2001.

[67] I. Ekeland and R. T/'eman. *Convex analysis and variational problems*. Society for Industrial and Applied Mathematics, Philadelphia, PA, USA, 1999.

[68] R. T. Rockafellar. *Convex analysis*. Princeton Mathematical Series, No. 28. Princeton University Press, Princeton, N.J., 1970.

7 Appendix

Proposition 7.1. *The numerical solution of the two-phase piecewise constant and texture image segmentation (5) as described in Algorithm 5.*

Proof. This proof follows many of the techniques in [55]. The minimization in (5) can be written as

$$\min_{(\mathbf{p},\boldsymbol{\epsilon},c_1,c_2)\in X^2\times\mathbb{R}^2} \left\{ \sum_{l=0}^{L-1} \left\| \sin\left(\frac{\pi l}{L}\right) \mathbf{D_1 p} + \cos\left(\frac{\pi l}{L}\right) \mathbf{p D_2^{\mathrm{T}}} \right\|_{\ell_1} + \mu_1 \sum_{s=0}^{S-1} \|\mathbf{g}_s\|_{\ell_1} + \mu_2 \|\mathbf{v}\|_{\ell_1} \right.$$

$$\text{s.t. } \left\|\mathcal{C}\{\boldsymbol{\epsilon}\}\right\|_{\ell_\infty} \leq \nu \,, \mathbf{v} = \sum_{s=0}^{S-1} \left[\sin\left(\frac{\pi s}{S}\right) \mathbf{D_1 g}_s + \cos\left(\frac{\pi s}{S}\right) \mathbf{g}_s \mathbf{D_2^{\mathrm{T}}} \right],$$

$$\left. \mathbf{f} = (c_1 + \mathbf{v} + \boldsymbol{\epsilon}) \cdot^{\times} \mathbf{p} + (c_2 + \mathbf{v} + \boldsymbol{\epsilon}) \cdot^{\times} (1 - \mathbf{p}) \,, p[\boldsymbol{k}] \in \{0,1\}, \forall \boldsymbol{k} \in \Omega \right\}. \tag{26}$$

We define a convex set (by relaxing the binary set) and its indicator function as

$$\mathcal{D} = \left\{ \mathbf{p} \in X \ : \ p[\boldsymbol{k}] \in [0,1] \,, \forall \boldsymbol{k} \in \Omega \right\} \ \text{ and } \ H^*(\mathbf{p}) = \begin{cases} 0 \,, & \mathbf{p} \in \mathcal{D} \\ +\infty \,, & \mathbf{p} \notin \mathcal{D} \end{cases}.$$

We introduce two new variables

$$\mathbf{r}_b = \sin\left(\frac{\pi b}{L}\right) \mathbf{D_1 p} + \cos\left(\frac{\pi b}{L}\right) \mathbf{p D_2^{\mathrm{T}}} \,, \quad b = 0, \ldots, L-1$$

and

$$\mathbf{w}_a = \mathbf{g}_a \,, \ a = 0, \ldots, S-1 \,.$$

Given $\vec{\mathbf{g}} = \big[\mathbf{g}_s\big]_{s=0}^{S-1}, \vec{\mathbf{r}} = \big[\mathbf{r}_l\big]_{l=0}^{L-1}, \vec{\mathbf{w}} = \big[\mathbf{w}_s\big]_{s=0}^{S-1}$, the augmented Lagrangian method of (26) is

$$\min_{(c_1,c_2,\mathbf{p},\mathbf{v},\boldsymbol{\epsilon},\vec{\mathbf{g}},\vec{\mathbf{r}},\vec{\mathbf{w}})\in\mathbb{R}^2\times X^{3+L+2S}} \mathcal{L}(\cdot\,;\vec{\boldsymbol{\lambda}}_{\mathbf{1}},\vec{\boldsymbol{\lambda}}_{\mathbf{2}},\boldsymbol{\lambda}_{\mathbf{3}},\boldsymbol{\lambda}_{\mathbf{4}}) \tag{27}$$

with

$$\mathcal{L}(\cdot\,;\cdot) = \sum_{l=0}^{L-1}\|\mathbf{r}_l\|_{\ell_1} + \mu_1\sum_{s=0}^{S-1}\|\mathbf{w}_s\|_{\ell_1} + \mu_2\|\mathbf{v}\|_{\ell_1} + G^*\big(\frac{\boldsymbol{\epsilon}}{\nu}\big) + H^*(\mathbf{p})$$

$$+ \frac{\beta_1}{2}\sum_{l=0}^{L-1}\left\|\mathbf{r}_l - \sin\left(\frac{\pi l}{L}\right)\mathbf{D_1}\mathbf{p} - \cos\left(\frac{\pi l}{L}\right)\mathbf{p}\mathbf{D_2}^{\mathrm{T}} + \frac{\boldsymbol{\lambda}_{\mathbf{1}l}}{\beta_1}\right\|_{\ell_2}^2 + \frac{\beta_2}{2}\sum_{s=0}^{S-1}\left\|\mathbf{w}_s - \mathbf{g}_s + \frac{\boldsymbol{\lambda}_{\mathbf{2}s}}{\beta_2}\right\|_{\ell_2}^2$$

$$+ \frac{\beta_3}{2}\left\|\mathbf{v} - \sum_{s=0}^{S-1}\Big[\sin\left(\frac{\pi s}{S}\right)\mathbf{D_1}\mathbf{g}_s + \cos\left(\frac{\pi s}{S}\right)\mathbf{g}_s\mathbf{D_2}^{\mathrm{T}}\Big] + \frac{\boldsymbol{\lambda}_{\mathbf{3}}}{\beta_3}\right\|_{\ell_2}^2$$

$$+ \underbrace{\frac{\beta_4}{2}\Big\langle\big[\mathbf{f} - c_1 - \mathbf{v} - \boldsymbol{\epsilon} + \frac{\boldsymbol{\lambda}_{\mathbf{4}}}{\beta_4}\big]^{\cdot 2}, \mathbf{p}\Big\rangle_{\ell_2} + \frac{\beta_4}{2}\Big\langle\big[\mathbf{f} - c_2 - \mathbf{v} - \boldsymbol{\epsilon} + \frac{\boldsymbol{\lambda}_{\mathbf{4}}}{\beta_4}\big]^{\cdot 2}, 1-\mathbf{p}\Big\rangle_{\ell_2}}_{\approx \frac{\beta_4}{2}\left\|\mathbf{f} - c_1\mathbf{p} - c_2(1-\mathbf{p}) - \mathbf{v} - \boldsymbol{\epsilon} + \frac{\boldsymbol{\lambda}_{\mathbf{4}}}{\beta_4}\right\|_{\ell_2}^2 \quad \text{(due to the relaxed version of the binary set)}}.$$

We solve (27) by ADMM with the ordering subproblems and then update the Lagrange multipliers at each iteration as

The c_1-problem: Fix $c_2\,, \mathbf{p}\,, \mathbf{v}\,, \boldsymbol{\epsilon}\,, \vec{\mathbf{g}}\,, \vec{\mathbf{r}}\,, \vec{\mathbf{w}}$ and solve

$$\min_{c_1\in\mathbb{R}}\Big\{\mathcal{L}(c_1) = \frac{\beta_4}{2}\sum_{\boldsymbol{k}\in\Omega}\Big[f[\boldsymbol{k}] - c_1 - v[\boldsymbol{k}] - \epsilon[\boldsymbol{k}] + \frac{\lambda_4[\boldsymbol{k}]}{\beta_4}\Big]^2 p[\boldsymbol{k}]\Big\rangle_{\ell_2}\Big\}.$$

The Euler-Lagrange equation is

$$0 = \frac{\partial\mathcal{L}(c_1)}{\partial c_1} = -\beta_4\sum_{\boldsymbol{k}\in\Omega} p[\boldsymbol{k}]\Big[f[\boldsymbol{k}] - c_1 - v[\boldsymbol{k}] - \epsilon[\boldsymbol{k}] + \frac{\lambda_4[\boldsymbol{k}]}{\beta_4}\Big]$$

$$\Leftrightarrow\ c_1 = \frac{\sum_{\boldsymbol{k}\in\Omega}\big[f[\boldsymbol{k}] - v[\boldsymbol{k}] - \epsilon[\boldsymbol{k}] + \frac{\lambda_4[\boldsymbol{k}]}{\beta_4}\big]p[\boldsymbol{k}]}{\sum_{\boldsymbol{k}\in\Omega} p[\boldsymbol{k}]}\,.$$

The c_2-problem: Fix $c_1\,, \mathbf{p}\,, \mathbf{v}\,, \boldsymbol{\epsilon}\,, \vec{\mathbf{g}}\,, \vec{\mathbf{r}}\,, \vec{\mathbf{w}}$ and solve

$$\min_{c_2\in\mathbb{R}}\Big\{\mathcal{L}(c_2) = \frac{\beta_4}{2}\sum_{\boldsymbol{k}\in\Omega}\Big[f[\boldsymbol{k}] - c_2 - v[\boldsymbol{k}] - \epsilon[\boldsymbol{k}] + \frac{\lambda_4[\boldsymbol{k}]}{\beta_4}\Big]^2\Big[1 - p[\boldsymbol{k}]\Big]\Big\}.$$

The Euler-Lagrange equation is

$$0 = \frac{\partial \mathcal{L}(c_2)}{\partial c_2} = -\beta_4 \sum_{\boldsymbol{k}\in\Omega} \Big[f[\boldsymbol{k}] - c_2 - v[\boldsymbol{k}] - \epsilon[\boldsymbol{k}] \frac{\lambda_4[\boldsymbol{k}]}{\beta_4} \Big] \big[1 - p[\boldsymbol{k}]\big]$$

$$\Leftrightarrow \; c_2 = \frac{\sum_{\boldsymbol{k}\in\Omega} \big[f[\boldsymbol{k}] - v[\boldsymbol{k}] - \epsilon[\boldsymbol{k}] + \frac{\lambda_4[\boldsymbol{k}]}{\beta_4} \big] \big[1 - p[\boldsymbol{k}]\big]}{\sum_{\boldsymbol{k}\in\Omega} (1 - p[\boldsymbol{k}])} \,.$$

The $\vec{\mathbf{r}} = \big[\mathbf{r}_l\big]_{l=0}^{L-1}$-problem: Fix $c_1\,, c_2\,, \mathbf{p}\,, \mathbf{v}\,, \boldsymbol{\epsilon}\,, \vec{\mathbf{g}}\,, \vec{\mathbf{w}}$ and solve

$$\min_{\vec{\mathbf{r}}\in X^L} \left\{ \sum_{l=0}^{L-1} \|\mathbf{r}_l\|_{\ell_1} + \frac{\beta_1}{2} \sum_{l=0}^{L-1} \left\| \mathbf{r}_l - \sin\left(\frac{\pi l}{L}\right) \mathbf{D_1 p} - \cos\left(\frac{\pi l}{L}\right) \mathbf{p D_2^{\mathrm{T}}} + \frac{\boldsymbol{\lambda}_{\mathbf{1}l}}{\beta_1} \right\|_{\ell_2}^2 \right\}$$

Due to the separable problems, we consider the problem at $a = 0, \ldots, L-1$

$$\mathbf{r}_a^* = \underset{\mathbf{r}_a\in X}{\operatorname{argmin}} \left\{ \|\mathbf{r}_a\|_{\ell_1} + \frac{\beta_1}{2} \left\| \mathbf{r}_a - \sin\left(\frac{\pi a}{L}\right) \mathbf{D_1 p} - \cos\left(\frac{\pi a}{L}\right) \mathbf{p D_2^{\mathrm{T}}} + \frac{\boldsymbol{\lambda}_{\mathbf{1}a}}{\beta_1} \right\| \right\}$$

$$= \operatorname{Shrink}\Big(\sin\left(\frac{\pi a}{L}\right) \mathbf{D_1 p} + \cos\left(\frac{\pi a}{L}\right) \mathbf{p D_2^{\mathrm{T}}} - \frac{\boldsymbol{\lambda}_{\mathbf{1}a}}{\beta_1}\,, \frac{1}{\beta_1} \Big)\,, \quad a = 0, \ldots, L-1.$$

The $\vec{\mathbf{w}} = \big[\mathbf{w}_s\big]_{s=0}^{S-1}$-problem: Fix $c_1\,, c_2\,, \mathbf{p}\,, \mathbf{v}\,, \boldsymbol{\epsilon}\,, \vec{\mathbf{g}}\,, \vec{\mathbf{r}}$ and solve

$$\min_{\vec{\mathbf{w}}\in X^S} \left\{ \mu_1 \sum_{s=0}^{S-1} \|\mathbf{w}_s\|_{\ell_1} + \frac{\beta_2}{2} \sum_{s=0}^{S-1} \left\| \mathbf{w}_s - \mathbf{g}_s + \frac{\boldsymbol{\lambda}_{\mathbf{2}s}}{\beta_2} \right\|_{\ell_2}^2 \right\}$$

Due to the separable problems, we consider the problem at $a = 0, \ldots, S-1$

$$\mathbf{w}_a^* = \underset{\mathbf{w}_a\in X}{\operatorname{argmin}} \left\{ \mu_1 \|\mathbf{w}_a\|_{\ell_1} + \frac{\beta_2}{2} \left\| \mathbf{w}_a - \mathbf{g}_a + \frac{\boldsymbol{\lambda}_{\mathbf{2}a}}{\beta_2} \right\|_{\ell_2}^2 \right\}$$

$$= \operatorname{Shrink}\Big(\mathbf{g}_a - \frac{\boldsymbol{\lambda}_{\mathbf{2}a}}{\beta_2}\,, \frac{\mu_1}{\beta_2} \Big)\,, a = 0, \ldots, S-1\,.$$

The $\vec{\mathbf{g}} = \big[\mathbf{g}_s\big]_{s=0}^{S-1}$-problem: Fix $c_1\,, c_2\,, \mathbf{p}\,, \mathbf{v}\,, \boldsymbol{\epsilon}\,, \vec{\mathbf{r}}\,, \vec{\mathbf{w}}$ and solve

$$\min_{\vec{\mathbf{g}}\in X^S} \left\{ \frac{\beta_2}{2} \sum_{s=0}^{S-1} \left\| \mathbf{w}_s - \mathbf{g}_s + \frac{\boldsymbol{\lambda}_{\mathbf{2}s}}{\beta_2} \right\|_{\ell_2}^2 + \frac{\beta_3}{2} \left\| \mathbf{v} - \sum_{s=0}^{S-1} \Big[\sin\left(\frac{\pi s}{S}\right) \mathbf{D_1 g}_s + \cos\left(\frac{\pi s}{S}\right) \mathbf{g}_s \mathbf{D_2^{\mathrm{T}}} \Big] + \frac{\boldsymbol{\lambda}_{\mathbf{3}}}{\beta_3} \right\|_{\ell_2}^2 \right\}$$

The solution of its separable problem is

$$\mathbf{g}_a^* = \operatorname{Re}\left[\mathcal{F}^{-1}\Big\{ \frac{\mathcal{B}_a(\boldsymbol{z})}{\mathcal{A}_a(\boldsymbol{z})} \Big\} \right][\boldsymbol{k}]\Big|_{\boldsymbol{k}\in\Omega}, a = 0, \ldots, S-1$$

$$\mathcal{A}_a(\boldsymbol{z}) = \beta_2 + \beta_3 \left| \sin\left(\frac{\pi a}{S}\right)(z_1 - 1) + \cos\left(\frac{\pi a}{S}\right)(z_2 - 1) \right|^2$$

$$\mathcal{B}_a(\boldsymbol{z}) = \beta_2 \Big[W_a(\boldsymbol{z}) + \frac{\Lambda_{2a}(\boldsymbol{z})}{\beta_2} \Big] + \beta_3 \Big[\sin\left(\frac{\pi a}{S}\right)(z_1^{-1} - 1) + \cos\left(\frac{\pi a}{S}\right)(z_2^{-1} - 1) \Big] \times$$

$$\left[V(\boldsymbol{z}) - \sum_{s=[0,S-1]\setminus\{a\}} \left[\sin\left(\frac{\pi s}{S}\right)(z_1 - 1) + \cos\left(\frac{\pi s}{S}\right)(z_2 - 1) \right] G_s(\boldsymbol{z}) + \frac{\Lambda_3(\boldsymbol{z})}{\beta_3} \right]$$

The v-problem: Fix $c_1\,, c_2\,, \mathbf{p}\,, \boldsymbol{\epsilon}\,, \vec{\mathbf{g}}\,, \vec{\mathbf{r}}\,, \vec{\mathbf{w}}$ and solve

$$\min_{\mathbf{v}\in X} \Big\{ \mathcal{L}(\mathbf{v}) = \mu_2 \|\mathbf{v}\|_{\ell_1} + \frac{\beta_3}{2} \left\| \mathbf{v} - \sum_{s=0}^{S-1} \Big[\sin\left(\frac{\pi s}{S}\right) \mathbf{D_1} \mathbf{g}_s + \cos\left(\frac{\pi s}{S}\right) \mathbf{g}_s \mathbf{D_2}^{\mathrm{T}} \Big] + \frac{\boldsymbol{\lambda_3}}{\beta_3} \right\|_{\ell_2}^2$$

$$+ \frac{\beta_4}{2} \Big\langle \big[\mathbf{f} - c_1 - \mathbf{v} - \boldsymbol{\epsilon} + \frac{\boldsymbol{\lambda_4}}{\beta_4} \big]^{\cdot 2}, \mathbf{p} \Big\rangle_{\ell_2} + \frac{\beta_4}{2} \Big\langle \big[\mathbf{f} - c_2 - \mathbf{v} - \boldsymbol{\epsilon} + \frac{\boldsymbol{\lambda_4}}{\beta_4} \big]^{\cdot 2}, 1 - \mathbf{p} \Big\rangle_{\ell_2} \Big\}.$$

The Euler-Lagrange equation (in matrix form) is

$$0 = \frac{\partial \mathcal{L}(\mathbf{v})}{\partial \mathbf{v}} = \mu_2 \frac{\mathbf{v}}{|\mathbf{v}|} + \beta_3 \left[\mathbf{v} - \sum_{s=0}^{S-1} \left[\sin\left(\frac{\pi s}{S}\right) \mathbf{D_1} \mathbf{g}_s + \cos\left(\frac{\pi s}{S}\right) \mathbf{g}_s \mathbf{D_2}^{\mathrm{T}} \right] + \frac{\boldsymbol{\lambda_3}}{\beta_3} \right]$$

$$- \beta_4 \big[\mathbf{f} - c_1 - \mathbf{v} - \boldsymbol{\epsilon} + \frac{\boldsymbol{\lambda_4}}{\beta_4} \big] \cdot^{\times} \mathbf{p} - \beta_4 \big[\mathbf{f} - c_2 - \mathbf{v} - \boldsymbol{\epsilon} + \frac{\boldsymbol{\lambda_4}}{\beta_4} \big] \cdot^{\times} \big[1 - \mathbf{p} \big]$$

$$\Leftrightarrow \ \mathbf{v} = \mathcal{J} - \frac{\mu_2}{\beta_3 + \beta_4} \frac{\mathbf{v}}{|\mathbf{v}|} \ := \ \mathrm{Shrink}\Big(\mathcal{J}\,, \frac{\mu_2}{\beta_3 + \beta_4} \Big)$$

with

$$\mathcal{J} = \frac{\beta_3}{\beta_3 + \beta_4} \left[\sum_{s=0}^{S-1} \left[\sin\left(\frac{\pi s}{S}\right) \mathbf{D_1} \mathbf{g}_s + \cos\left(\frac{\pi s}{S}\right) \mathbf{g}_s \mathbf{D_2}^{\mathrm{T}} \right] - \frac{\boldsymbol{\lambda_3}}{\beta_3} \right] + \frac{\beta_4}{\beta_3 + \beta_4} \big[\mathbf{f} - c_1 - \boldsymbol{\epsilon} + \frac{\boldsymbol{\lambda_4}}{\beta_4} \big] \cdot^{\times} \mathbf{p}$$

$$+ \frac{\beta_4}{\beta_3 + \beta_4} \big[\mathbf{f} - c_2 - \boldsymbol{\epsilon} + \frac{\boldsymbol{\lambda_4}}{\beta_4} \big] \cdot^{\times} \big[1 - \mathbf{p} \big]\,.$$

The p-problem: Fix $c_1\,, c_2\,, \mathbf{v}\,, \boldsymbol{\epsilon}\,, \vec{\mathbf{g}}\,, \vec{\mathbf{r}}\,, \vec{\mathbf{w}}$ and solve

$$\min_{\mathbf{p}\in\mathcal{D}} \Big\{ \mathcal{L}(\mathbf{p}) = \frac{\beta_1}{2} \sum_{l=0}^{L-1} \left\| \mathbf{r}_l - \sin\left(\frac{\pi l}{L}\right) \mathbf{D_1} \mathbf{p} - \cos\left(\frac{\pi l}{L}\right) \mathbf{p} \mathbf{D_2}^{\mathrm{T}} + \frac{\boldsymbol{\lambda_{1}}_l}{\beta_1} \right\|_{\ell_2}^2$$

$$+ \frac{\beta_4}{2} \Big\langle \big[\mathbf{f} - c_1 - \mathbf{v} - \boldsymbol{\epsilon} + \frac{\boldsymbol{\lambda_4}}{\beta_4} \big]^{\cdot 2}, \mathbf{p} \Big\rangle_{\ell_2} + \frac{\beta_4}{2} \Big\langle \big[\mathbf{f} - c_2 - \mathbf{v} - \boldsymbol{\epsilon} + \frac{\boldsymbol{\lambda_4}}{\beta_4} \big]^{\cdot 2}, 1 - \mathbf{p} \Big\rangle_{\ell_2} \Big\} \tag{28}$$

The Euler-Lagrange equation is

$$0 = \frac{\partial \mathcal{L}(\mathbf{p})}{\partial \mathbf{p}} = -\beta_1 \sum_{l=0}^{L-1} \Big[\cos\left(\frac{\pi l}{L}\right) \Big[\mathbf{r}_l - \sin\left(\frac{\pi l}{L}\right) \mathbf{D_1 p} - \cos\left(\frac{\pi l}{L}\right) \mathbf{p D_2^{\mathrm{T}}} + \frac{\boldsymbol{\lambda}_{1l}}{\beta_1} \Big] \mathbf{D_2}$$

$$+ \sin\left(\frac{\pi l}{L}\right) \mathbf{D_1^{\mathrm{T}}} \Big[\mathbf{r}_l - \sin\left(\frac{\pi l}{L}\right) \mathbf{D_1 p} - \cos\left(\frac{\pi l}{L}\right) \mathbf{p D_2^{\mathrm{T}}} + \frac{\boldsymbol{\lambda}_{1l}}{\beta_1} \Big] \Big]$$

$$+ \frac{\beta_4}{2} \Big[\mathbf{f} - c_1 - \mathbf{v} - \boldsymbol{\epsilon} + \frac{\boldsymbol{\lambda_4}}{\beta_4} \Big]^{\cdot 2} - \frac{\beta_4}{2} \Big[\mathbf{f} - c_2 - \mathbf{v} - \boldsymbol{\epsilon} + \frac{\boldsymbol{\lambda_4}}{\beta_4} \Big]^{\cdot 2} .$$

Its Fourier transform is

$$-\beta_1 \sum_{l=0}^{L-1} \Big[\sin\left(\frac{\pi l}{L}\right) (z_1^{-1} - 1) + \cos\left(\frac{\pi l}{L}\right) (z_2^{-1} - 1) \Big]$$

$$\times \Big[R_l(\boldsymbol{z}) - \big[\sin\left(\frac{\pi l}{L}\right) (z_1 - 1) + \cos\left(\frac{\pi l}{L}\right) (z_2 - 1) \big] P(\boldsymbol{z}) + \frac{\Lambda_{1l}(\boldsymbol{z})}{\beta_1} \Big]$$

$$- \beta_4 \mathcal{H}(\boldsymbol{z}) = 0$$

with the Fourier transform of $\mathcal{H}(\boldsymbol{z})$ as

$$\mathcal{H}(\boldsymbol{z}) = \mathcal{F} \left\{ -\frac{1}{2} \big[\mathbf{f} - c_1 - \mathbf{v} - \boldsymbol{\epsilon} + \frac{\boldsymbol{\lambda_4}}{\beta_4} \big]^{\cdot 2} + \frac{1}{2} \big[\mathbf{f} - c_2 - \mathbf{v} - \boldsymbol{\epsilon} + \frac{\boldsymbol{\lambda_4}}{\beta_4} \big]^{\cdot 2} \right\} (\boldsymbol{z}) .$$

Thus,

$$\beta_1 \sum_{l=0}^{L-1} \left| \sin\left(\frac{\pi l}{L}\right) (z_1 - 1) + \cos\left(\frac{\pi l}{L}\right) (z_2 - 1) \right|^2 P(\boldsymbol{z})$$

$$= \beta_1 \sum_{l=0}^{L-1} \left[\sin\left(\frac{\pi l}{L}\right) (z_1^{-1} - 1) + \cos\left(\frac{\pi l}{L}\right) (z_2^{-1} - 1) \right] \left[R_l(\boldsymbol{z}) + \frac{\Lambda_{1l}(\boldsymbol{z})}{\beta_1} \right] + \beta_4 \mathcal{H}(\boldsymbol{z})$$

To avoid the singularity, we add $\frac{\beta_4}{2} \|\mathbf{p}\|_{\ell_2}^2$ to the "**p**-problem" (28) which results in its solution as

$$\tilde{p}[\boldsymbol{k}] = \mathrm{Re} \Big[\mathcal{F}^{-1} \Big\{ \frac{\mathcal{Y}(\boldsymbol{z})}{\mathcal{X}(\boldsymbol{z})} \Big\} \Big] [\boldsymbol{k}] , \boldsymbol{k} \in \Omega$$

with

$$\mathcal{Y}(\boldsymbol{z}) = \beta_1 \sum_{l=0}^{L-1} \Big[\sin\left(\frac{\pi l}{L}\right) (z_1^{-1} - 1) + \cos\left(\frac{\pi l}{L}\right) (z_2^{-1} - 1) \Big] \Big[R_l(\boldsymbol{z}) + \frac{\Lambda_{1l}(\boldsymbol{z})}{\beta_1} \Big] + \beta_4 \mathcal{H}(\boldsymbol{z}) ,$$

$$\mathcal{X}(\boldsymbol{z}) = \beta_1 \sum_{l=0}^{L-1} \left| \sin\left(\frac{\pi l}{L}\right) (z_1 - 1) + \cos\left(\frac{\pi l}{L}\right) (z_2 - 1) \right|^2 + \beta_4 .$$

Due to $\tilde{\mathbf{p}} = \left[\tilde{p}[\boldsymbol{k}]\right]_{\boldsymbol{k}\in\Omega} \in \mathcal{D}$, we have

$$p^*[\boldsymbol{k}] = \begin{cases} 0\,, & \tilde{p}[\boldsymbol{k}] < 0 \\ 1\,, & \tilde{p}[\boldsymbol{k}] > 1 \\ \tilde{p}[\boldsymbol{k}]\,, & \tilde{p}[\boldsymbol{k}] \in [0\,,1] \end{cases}.$$

The $\boldsymbol{\epsilon}$-problem: Fix $c_1\,, c_2\,, \mathbf{p}\,, \mathbf{v}\,, \vec{\mathbf{g}}\,, \vec{\mathbf{r}}\,, \vec{\mathbf{w}}$ and given a convex set with the indicator function $G^*(\frac{\boldsymbol{\epsilon}}{\nu})$

$$\mathcal{A}(\nu) = \left\{\boldsymbol{\epsilon} \in X \;:\; \left\|\mathcal{C}\{\boldsymbol{\epsilon}\}\right\|_{\ell_\infty} \leq \nu\right\}$$

the $\boldsymbol{\epsilon}$-problem can be rewritten as

$$\min_{\boldsymbol{\epsilon}\in\mathcal{A}(\nu)} \left\{ \mathcal{L}(\boldsymbol{\epsilon}) = \frac{\beta_4}{2}\Big\langle \big[\mathbf{f} - c_1 - \mathbf{v} - \boldsymbol{\epsilon} + \frac{\boldsymbol{\lambda_4}}{\beta_4}\big]^{\cdot 2}, \mathbf{p}\Big\rangle_{\ell_2} + \frac{\beta_4}{2}\Big\langle \big[\mathbf{f} - c_2 - \mathbf{v} - \boldsymbol{\epsilon} + \frac{\boldsymbol{\lambda_4}}{\beta_4}\big]^{\cdot 2}, 1-\mathbf{p}\Big\rangle_{\ell_2} \right\}$$

The Euler-Lagrange equation is

$$0 = \frac{\partial \mathcal{L}(\boldsymbol{\epsilon})}{\partial \boldsymbol{\epsilon}} = -\beta_4\big[\mathbf{f} - c_1 - \mathbf{v} - \boldsymbol{\epsilon} + \frac{\boldsymbol{\lambda_4}}{\beta_4}\big] \cdot^{\times} \mathbf{p} - \beta_4\big[\mathbf{f} - c_2 - \mathbf{v} - \boldsymbol{\epsilon} + \frac{\boldsymbol{\lambda_4}}{\beta_4}\big] \cdot^{\times} \big[1-\mathbf{p}\big]$$

$$\Leftrightarrow \tilde{\boldsymbol{\epsilon}} = \big[\mathbf{f} - c_1 - \mathbf{v} + \frac{\boldsymbol{\lambda_4}}{\beta_4}\big] \cdot^{\times} \mathbf{p} + \big[\mathbf{f} - c_2 - \mathbf{v} + \frac{\boldsymbol{\lambda_4}}{\beta_4}\big] \cdot^{\times} \big[1-\mathbf{p}\big]\,.$$

Thus, the solution of the $\boldsymbol{\epsilon}$-problem is

$$\boldsymbol{\epsilon}^* = \mathbb{P}_{\mathcal{A}(\nu)}\big(\tilde{\boldsymbol{\epsilon}}\big) = \tilde{\boldsymbol{\epsilon}} - \mathrm{CST}\left(\tilde{\boldsymbol{\epsilon}}\,, \nu\right).$$

Update the Lagrange multipliers:

$$\boldsymbol{\lambda}_{\mathbf{1}a}^{(t)} = \boldsymbol{\lambda}_{\mathbf{1}a}^{(t-1)} + \beta_1\Big[\mathbf{r}_a - \sin\left(\frac{\pi a}{L}\right)\mathbf{D_1 p} - \cos\left(\frac{\pi a}{L}\right)\mathbf{p D_2^{\mathrm{T}}}\Big]\,,\ a = 0, \ldots, L-1$$

$$\boldsymbol{\lambda}_{\mathbf{2}a}^{(t)} = \boldsymbol{\lambda}_{\mathbf{2}a}^{(t-1)} + \beta_2\Big[\mathbf{w}_a - \mathbf{g}_a\Big]\,, a = 0, \ldots, S-1$$

$$\boldsymbol{\lambda}_{\mathbf{3}}^{(t)} = \boldsymbol{\lambda}_{\mathbf{3}}^{(t-1)} + \beta_3\Big[\mathbf{v} - \sum_{s=0}^{S-1}\big[\sin\left(\frac{\pi s}{S}\right)\mathbf{D_1 g}_s + \cos\left(\frac{\pi s}{S}\right)\mathbf{g}_s\mathbf{D_2^{\mathrm{T}}}\big]\Big]$$

$$\boldsymbol{\lambda}_{\mathbf{4}}^{(t)} = \boldsymbol{\lambda}_{\mathbf{4}}^{(t-1)} + \beta_4\Big[\big(\mathbf{f} - c_1 - \mathbf{v} - \boldsymbol{\epsilon}\big) \cdot^{\times} \mathbf{p} + \big(\mathbf{f} - c_2 - \mathbf{v} - \boldsymbol{\epsilon}\big) \cdot^{\times} (1-\mathbf{p})\Big]$$

□

Lemma 7.0.1. *The discrete directional total variation (DTV) norm* $\left\|\nabla_L^+ \mathbf{u}\right\|_{\ell_1}$ *and the discrete directional* G_L*-norm* $\|\mathbf{v}\|_{G_L}$ *are a dual pair, i.e.*

$$J_L(\mathbf{u}) = \mu\left\|\nabla_L^+ \mathbf{u}\right\|_{\ell_1} \overset{\textit{Legendre Fenchel transform}}{\longleftrightarrow} J_L^*(\frac{\mathbf{v}}{\mu}) = \begin{cases} 0\,, & \mathbf{v} \in G_L(\mu) \\ +\infty\,, & \textit{else} \end{cases} \tag{29}$$

with a convex set of G_L-norm

$$G_L(\mu)=\Big\{\mathbf{v}=div_L^-\vec{\mathbf{p}}\in X\,,\ \vec{\mathbf{p}}=\big[\mathbf{p}_l\big]_{l=0}^{L-1}\in X^L\ :\ \|\mathbf{v}\|_{G_L}=\inf_{\vec{\mathbf{p}}}\big\{\underbrace{\max_{\boldsymbol{k}\in\Omega}\sqrt{\sum_{l=0}^{L-1}p_l^2[\boldsymbol{k}]}}_{=\|\vec{\mathbf{p}}\|_{\ell_\infty}}\big\}\le\mu\Big\}.$$

Proof. **1. The discrete DTV-norm**

Given a convex set $K_L(\mu)=\big\{\mathrm{div}_L^-\vec{\mathbf{p}}\,,\ \vec{\mathbf{p}}\in X^L:\|\vec{\mathbf{p}}\|_{\ell_\infty}\le\mu\big\}$ and an adjoint operator $(\nabla_L^+)^*=-\mathrm{div}_L^-$, the discrete DTV-norm $J_L(u)$ in (29) can be rewritten as

$$J_L(\mathbf{u})=\mu\Big\|\nabla_L^+\mathbf{u}\Big\|_{\ell_1}=\max_{\vec{\mathbf{p}}\in K_L(\mu)}\big\langle\mathbf{u}\,,\mathrm{div}_L^-\vec{\mathbf{p}}\big\rangle_{\ell_2}\tag{30}$$

since

$$J_L(\mathbf{u})=\mu\sum_{\boldsymbol{k}\in\Omega}\Big|\nabla_L^+u[\boldsymbol{k}]\Big|=\max_{\vec{\mathbf{p}}\in K_L(\mu)}-\sum_{\boldsymbol{k}\in\Omega}\big\langle\nabla_L^+u[\boldsymbol{k}]\,,\vec{p}[\boldsymbol{k}]\big\rangle_{\ell_2}=\max_{\vec{\mathbf{p}}\in K_L(\mu)}\sum_{\boldsymbol{k}\in\Omega}\underbrace{\langle u[\boldsymbol{k}]\,,\mathrm{div}_L^-\vec{p}[\boldsymbol{k}]\rangle_{\ell_2}}_{=u[\boldsymbol{k}]\mathrm{div}_L^-\vec{p}[\boldsymbol{k}]}.$$

2. The Legendre-Fenchel transform (in a discrete setting) of $J_L(\mathbf{u})\,,\mathbf{u}\in X$(or $\mathbf{u}\in\ell_2(\Omega,\mathbb{R})$)

$$J_L^*(\frac{\mathbf{v}}{\mu})=\sup_{\mathbf{u}\in X}\Big\{\langle\mathbf{v},\mathbf{u}\rangle_{\ell_2(\Omega,\mathbb{R})}-\underbrace{J_L(\mathbf{u})}_{=\mu\|\nabla_L^+\mathbf{u}\|_{L_1}}\Big\}=\sup_{\mathbf{u}\in X}\Big\{\underbrace{\langle\frac{\mathbf{v}}{\mu},\mathbf{u}\rangle_{\ell_2(\Omega,\mathbb{R})}-\Big\|\nabla_L^+\mathbf{u}\Big\|_{L_1}}_{=\mathscr{H}(\mathbf{u})}\Big\},\ \mathbf{v}\in X\,.$$

Denote the dual norm of $\Big\|\nabla_L^+\mathbf{u}\Big\|_{L_1}$ as $\|\mathbf{v}\|_{\mathrm{G}_L}$. Given $\|\mathbf{v}\|_{\mathrm{G}_L}\le\mu$, the Cauchy Schwarz inequality gives

$$\frac{1}{\mu}\langle\mathbf{v}\,,\mathbf{u}\rangle_{\ell_2(\Omega,\mathbb{R})}\le\frac{1}{\mu}\|\mathbf{v}\|_{\mathrm{G}_L}\Big\|\nabla_L^+\mathbf{u}\Big\|_{\ell_1}\le\Big\|\nabla_L^+\mathbf{u}\Big\|_{\ell_1}\tag{31}$$

$$\Leftrightarrow\ \mathscr{H}(\mathbf{u})\le0\ \text{ and }\ \mathbf{v}\in\mathrm{G}_L(\mu)=\Big\{\mathbf{v}\in\ell_2(\Omega,\mathbb{R})\ :\ \|\mathbf{v}\|_{\mathrm{G}_L}\le\mu\Big\}$$

$$\Leftrightarrow\ J_L^*(\frac{\mathbf{v}}{\mu})=\sup_{\mathbf{u}\in X}\mathscr{H}(u)=\begin{cases}0\,, & \mathbf{v}\in\mathrm{G}_L(\mu)\\ +\infty\,, & \text{else}\end{cases}=\chi_{\mathrm{G}_L(\mu)}(\mathbf{v})\,.$$

We have a biconjugate form $J_L=J_L^{**}$:

$$J_L(\mathbf{u})=\Big(J_L^*\big(\frac{\mathbf{v}}{\mu}\big)\Big)^*(\mathbf{u})=\chi^*_{\mathrm{G}_L(\mu)}(\mathbf{u})=\sup_{\mathbf{v}\in X}\Big\{\langle\mathbf{u}\,,\mathbf{v}\rangle_{\ell_2(\Omega,\mathbb{R})}-\chi_{\mathrm{G}_L(\mu)}(\mathbf{v})\Big\}$$

$$=\sup_{\mathbf{v}\in\mathrm{G}_L(\mu)}\langle\mathbf{u}\,,\mathbf{v}\rangle_{\ell_2(\Omega,\mathbb{R})}\tag{32}$$

From (32) and definition of the DTV-norm (30), we have

$$\begin{cases} v[\boldsymbol{k}] & = \mathrm{div}_L^- \vec{p}[\boldsymbol{k}]\,,\ \forall \boldsymbol{k} \in \Omega \\ \mathbf{v} \in \mathrm{G}_L(\mu) & = \Big\{ \mathbf{v} \in X\ :\ \|\mathbf{v}\|_{\mathrm{G}_L} \le \mu \Big\} \\ \vec{\mathbf{p}} \in K_L(\mu) & = \Big\{ \mathrm{div}_L^- \vec{\mathbf{p}}\,,\ \vec{\mathbf{p}} \in X^L\ :\ \|\vec{\mathbf{p}}\|_{\ell_\infty} \le \mu \Big\} \end{cases}$$

$$\Leftrightarrow\ \vec{\mathbf{p}} \in K_L(\mu) = \Big\{ \mathbf{v} = \mathrm{div}_L^- \vec{\mathbf{p}} \in X\,,\ \vec{\mathbf{p}} \in X^L\ :\ \|\mathbf{v}\|_{\mathrm{G}_L} = \|\vec{\mathbf{p}}\|_{\ell_\infty} \le \mu \Big\} \equiv \mathrm{G}_L(\mu)\,.$$

Therefore, the discrete (L) DTV-norm and the discrete directional G_L-norm are a dual pair by the definition of dual space.

□

Proposition 7.2. *The DTV-ℓ_2 model is*

$$\mathbf{u}^* = \underset{\mathbf{u}\in X}{\mathrm{argmin}} \Big\{ \mathscr{F}(\mathbf{u}) = J_L(\mathbf{u}) + \frac{\mu}{2}\|\mathbf{u}-\mathbf{f}\|_{\ell_2}^2 \Big\} \tag{33}$$

$$= \mathbf{f} - \frac{1}{\mu} \underbrace{div_L^- \vec{\mathbf{p}}^*}_{=\mathbf{w}^*}$$

with $\vec{\mathbf{p}}^* \approx \vec{\mathbf{p}}^{(T)}$ *and*

$$\vec{\mathbf{p}}^{(t+1)} = \frac{\vec{\mathbf{p}}^{(t)} + \tau \nabla_L^+ \Big[div_L^- \vec{\mathbf{p}}^{(t)} - \mu \mathbf{f} \Big]}{1 + \tau \Big| \nabla_L^+ \Big[div_L^- \vec{\mathbf{p}}^{(t)} - \mu \mathbf{f} \Big] \Big|}\,,\ t = 1, \ldots, T\,.$$

Proof. The proof is extended directly from [34] for the multi-directional total variation norm $J_L(\mathbf{u})$. The Euler-Lagrange of (33) is

$$0 \in \frac{\partial \mathscr{F}(\mathbf{u})}{\partial \mathbf{u}} = \partial J_L(\mathbf{u}) + \mu(\mathbf{u}-\mathbf{f}) \quad \Leftrightarrow \quad \mathbf{u} \in \partial J_L^* \Big(\mu(\mathbf{f}-\mathbf{u}) \Big)$$

$$\Leftrightarrow \mathbf{u} - \mathbf{f} + \mathbf{f} \in \partial J_L^* \Big(\mu(\mathbf{f}-\mathbf{u}) \Big) \quad \Leftrightarrow \quad \mathbf{f} \in \partial J_L^* \Big(\mu(\mathbf{f}-\mathbf{u}) \Big) + \mathbf{f} - \mathbf{u}\,.$$

Let $\mathbf{w} = \mu(\mathbf{f}-\mathbf{u})$

$$\Leftrightarrow\ 0 \in \partial J_L^*(\mathbf{w}) + \frac{\mathbf{w}}{\mu} - \mathbf{f}$$

$$\Leftrightarrow\ \mathbf{w}^* = \underset{\mathbf{w}\in X}{\mathrm{argmin}} \left\{ J_L^*(\mathbf{w}) + \frac{\mu}{2} \left\| \frac{\mathbf{w}}{\mu} - \mathbf{f} \right\|_{\ell_2}^2 \right\}$$

$$= \underset{\mathbf{w}\in K_L(1)}{\mathrm{argmin}} \Big\{ \|\mathbf{w} - \mu\mathbf{f}\|_{\ell_2}^2 \Big\}, \quad K_L(1) = \Big\{ \mathrm{div}_L^- \vec{\mathbf{p}}\,, \vec{\mathbf{p}} = \big[\mathbf{p}_l\big]_{l=0}^{L-1} \in X^L\ :\ \big|\vec{p}[\boldsymbol{k}]\big| \le 1\,, \forall \boldsymbol{k} \in \Omega \Big\}$$

$$= \mathrm{div}_L^- \vec{\mathbf{p}}^*$$

with

$$\vec{\mathbf{p}}^{*} = \underset{\vec{\mathbf{p}} \in X^{L}}{\operatorname{argmin}} \left\{ \left\| \operatorname{div}_{L}^{-} \vec{\mathbf{p}} - \mu \mathbf{f} \right\|_{\ell_2}^{2} \quad \text{s.t.} \quad \underbrace{\sum_{l=0}^{L-1} p_l^2[\boldsymbol{k}] - 1 \leq 0 \,, \forall \boldsymbol{k} \in \Omega}_{\Leftrightarrow \left|\vec{p}[\boldsymbol{k}]\right|^2 - 1 \leq 0} \right\}.$$

Due to an inequality constraint, the KKT condition in matrix form ($\lambda[\boldsymbol{k}] > 0 \,, \forall \boldsymbol{k} \in \Omega$) is

$$\min_{\vec{\mathbf{p}} \in X^{L}} \left\{ \mathscr{L}(\vec{\mathbf{p}}) = \left\| \operatorname{div}_{L}^{-} \vec{\mathbf{p}} - \mu \mathbf{f} \right\|_{\ell_2}^{2} \; + \; \left\langle \boldsymbol{\lambda} \,, \sum_{l=0}^{L-1} \mathbf{p}_l^{\cdot 2} - 1 \right\rangle_{\ell_2} \right\}.$$

Due to its separability, we consider this problem at $l = l' \,, l' = 0, \ldots, L-1$ and its Euler-Lagrange equation is given by

$$0 = \frac{\partial \mathscr{L}(\vec{\mathbf{p}})}{\partial \mathbf{p}_{l'}} = 2 \underbrace{\frac{\partial}{\partial \mathbf{p}_{l'}} \left\{ \operatorname{div}_{L}^{-} \vec{\mathbf{p}} \right\}}_{= -\partial_{l'}^{+} \delta} \left[\operatorname{div}_{L}^{-} \vec{\mathbf{p}} - \mu \mathbf{f} \right] \; + \; 2 \boldsymbol{\lambda} \cdot^{\times} \mathbf{p}_{l'}$$

$$\Leftrightarrow - \partial_{l'}^{+} \left[\operatorname{div}_{L}^{-} \vec{\mathbf{p}} - \mu \mathbf{f} \right] \; + \; \boldsymbol{\lambda} \cdot^{\times} \mathbf{p}_{l'} = 0 \,, \; l' = 0, \ldots L-1$$

$$\Leftrightarrow - \nabla_{L}^{+} \left[\operatorname{div}_{L}^{-} \vec{\mathbf{p}} - \mu \mathbf{f} \right] \; + \; \boldsymbol{\lambda} \cdot^{\times} \vec{\mathbf{p}} = 0 \,.$$

Given $\boldsymbol{k} \in \Omega$, its element form is

$$- \nabla_{L}^{+} \left[\operatorname{div}_{L}^{-} \vec{p}[\boldsymbol{k}] - \mu f[\boldsymbol{k}] \right] \; + \; \lambda[\boldsymbol{k}] \vec{p}[\boldsymbol{k}] = 0 \tag{34}$$

$$\Leftrightarrow \; \lambda[\boldsymbol{k}] = \frac{\nabla_{L}^{+} \left[\operatorname{div}_{L}^{-} \vec{p}[\boldsymbol{k}] - \mu f[\boldsymbol{k}] \right]}{\vec{p}[\boldsymbol{k}]} := \left[\frac{\partial_{l}^{+} \left[\operatorname{div}_{L}^{-} \vec{p}[\boldsymbol{k}] - \mu f[\boldsymbol{k}] \right]}{p_l[\boldsymbol{k}]} \right]_{l=0}^{L-1}$$

$$\Leftrightarrow \; \left|\lambda[\boldsymbol{k}]\right| \overset{\lambda[\boldsymbol{k}] > 0}{=} \lambda[\boldsymbol{k}] = \frac{\left| \nabla_{L}^{+} \left[\operatorname{div}_{L}^{-} \vec{p}[\boldsymbol{k}] - \mu f[\boldsymbol{k}] \right] \right|}{\left|\vec{p}[\boldsymbol{k}]\right|} = \begin{cases} \left| \nabla_{L}^{+} \left[\operatorname{div}_{L}^{-} \vec{p}[\boldsymbol{k}] - \mu f[\boldsymbol{k}] \right] \right| \,, & \left|\vec{p}[\boldsymbol{k}]\right| = 1 \\ 0 \,, & \left|\vec{p}[\boldsymbol{k}]\right| < 1 \end{cases}$$

$$\Leftrightarrow \; \lambda[\boldsymbol{k}] = \left| \nabla_{L}^{+} \left[\operatorname{div}_{L}^{-} \vec{p}[\boldsymbol{k}] - \mu f[\boldsymbol{k}] \right] \right| .$$

Note that Lagrange multiplier is not active on an open set. We rewrite (34) as

$$- \nabla_{L}^{+} \left[\operatorname{div}_{L}^{-} \vec{p}[\boldsymbol{k}] - \mu f[\boldsymbol{k}] \right] \; + \; \left| \nabla_{L}^{+} \left[\operatorname{div}_{L}^{-} \vec{p}[\boldsymbol{k}] - \mu f[\boldsymbol{k}] \right] \right| \vec{p}[\boldsymbol{k}] = 0 \,, \; \forall \boldsymbol{k} \in \Omega \,.$$

Applying gradient descent and a fixed point algorithm (i.e. a semi-implicit gradient descent scheme), we have

$$-\nabla_L^+\Big[\mathrm{div}_L^-\vec{p}^{(t-1)}[\boldsymbol{k}]-\mu f[\boldsymbol{k}]\Big] \;+\; \Big|\nabla_L^+\Big[\mathrm{div}_L^-\vec{p}^{(t-1)}[\boldsymbol{k}]-\mu f[\boldsymbol{k}]\Big]\Big|\,\vec{p}^{(t)}[\boldsymbol{k}] = -\frac{\vec{p}^{(t)}[\boldsymbol{k}]-\vec{p}^{(t-1)}[\boldsymbol{k}]}{\tau}\,,$$

and the solution in matrix form is given by

$$\vec{\mathbf{p}}^{(t)} = \frac{\vec{\mathbf{p}}^{(t-1)}+\tau\nabla_L^+\Big[\mathrm{div}_L^-\vec{\mathbf{p}}^{(t-1)}-\mu\mathbf{f}\Big]}{1+\tau\Big|\nabla_L^+\Big[\mathrm{div}_L^-\vec{\mathbf{p}}^{(t-1)}-\mu\mathbf{f}\Big]\Big|}\,,\; t=1\,,\ldots$$

□

Proposition 7.3. *The directional $G_S-\ell_1$ model is*

$$\min_{\mathbf{v}\in X}\Big\{\mathscr{F}(\mathbf{v})=\|\mathbf{v}\|_{\ell_1}+\frac{\beta}{2}\|\mathbf{f}-\mathbf{v}\|_{\ell_2}^2 \quad s.t.\;\; \|\mathbf{v}\|_{G_S}\le\mu\Big\}\,. \tag{35}$$

For iteration t, we have

Dual variable $\vec{\mathbf{g}}=\big[\mathbf{g}_s\big]_{s=0}^{S-1}$

$$\vec{\mathbf{g}}^{(t)} = \frac{\vec{\mathbf{g}}^{(t-1)}+\tau\nabla_S^+\Big[\alpha\mu div_S^-\vec{\mathbf{g}}^{(t-1)}-\boldsymbol{\lambda}_{\mathbf{1}}^{(t-1)}-\alpha\mathbf{v}^{(t-1)}\Big]}{1+\tau\Big|\nabla_S^+\Big[\alpha\mu div_S^-\vec{\mathbf{g}}^{(t-1)}-\boldsymbol{\lambda}_{\mathbf{1}}^{(t-1)}-\alpha\mathbf{v}^{(t-1)}\Big]\Big|}\,,$$

Primal variable

$$\mathbf{v}^{(t)}=\mathrm{Shrink}\Big(\frac{\beta}{\alpha+\beta}\mathbf{f}+\frac{\alpha\mu}{\alpha+\beta}div_S^-\vec{\mathbf{g}}^{(t)}-\frac{1}{\alpha+\beta}\boldsymbol{\lambda}_{\mathbf{1}}^{(t-1)}\,,\;\frac{1}{\alpha+\beta}\Big)\,,$$

Updated Lagrange multiplier $\boldsymbol{\lambda}_{\mathbf{1}}\in X$

$$\boldsymbol{\lambda}_{\mathbf{1}}^{(t)}=\boldsymbol{\lambda}_{\mathbf{1}}^{(t-1)}+\alpha\Big[\mathbf{v}^{(t)}-\mu div_S^-\vec{\mathbf{g}}^{(t)}\Big]\,.$$

Proof. Given the directional G_S-norm [54, 55], we have the convex set

$$\mathrm{G}_S(\mu)=\Bigg\{\mathbf{v}=\mathrm{div}_S^-\vec{\mathbf{g}}\in X\,,\vec{\mathbf{g}}=\big[\mathbf{g}_s\big]_{s=0}^{S-1}\in X^S\;:\quad \underbrace{\|\mathbf{v}\|_{\mathrm{G}_S}=\Big\|\sqrt{\sum_{s=0}^{S-1}\mathbf{g}_s^{\cdot 2}}\Big\|_{\ell_\infty}\le\mu}\Bigg\}$$

$$\Leftrightarrow\big|g[\boldsymbol{k}]\big|=\sqrt{\sum_{s=0}^{S-1}g_s^2[\boldsymbol{k}]}\le\mu\,,\forall\boldsymbol{k}\in\Omega$$

Note that $\mathrm{G}_S(\mu)$ is identical to $K_S(\mu)$; see Lemma 7.0.1. The objective function of (35) can be rewritten as

$$\mathscr{F}(\mathbf{v}) = \begin{cases} \|\mathbf{v}\|_{\ell_1} + \frac{\beta}{2}\|\mathbf{f}-\mathbf{v}\|_{\ell_2}^2\,, & \mathbf{v}\in \mathrm{G}_S(\mu) \\ +\infty\,, & \text{else} \end{cases} \quad = \quad \|\mathbf{v}\|_{\ell_1} + \frac{\beta}{2}\|\mathbf{f}-\mathbf{v}\|_{\ell_2}^2 + J_S^*\left(\frac{\mathbf{v}}{\mu}\right)$$

with indicator function

$$J_S^*\left(\frac{\mathbf{v}}{\mu}\right) = \begin{cases} 0\,, & \mathbf{v}\in \mathrm{G}_S(\mu) \\ +\infty\,, & \text{else} \end{cases}\,.$$

Thus, we can rewrite (35) as

$$\min_{\mathbf{v}\in \mathrm{G}_S(\mu)} \left\{ \|\mathbf{v}\|_{\ell_1} + \frac{\beta}{2}\|\mathbf{f}-\mathbf{v}\|_{\ell_2}^2 \right\}$$

$$= \min_{\mathbf{v}\in X} \left\{ \|\mathbf{v}\|_{\ell_1} + \frac{\beta}{2}\|\mathbf{f}-\mathbf{v}\|_{\ell_2}^2\,, \mathbf{v} = \mathrm{div}_S^-\vec{\mathbf{g}}, \left|\frac{g[\boldsymbol{k}]}{\mu}\right| = \sqrt{\sum_{s=0}^{S-1}\frac{g_s^2[\boldsymbol{k}]}{\mu^2}} \le 1\,, \forall \boldsymbol{k}\in\Omega \right\}.$$

By changing variable $\vec{\mathbf{g}}'$ to $\frac{\vec{\mathbf{g}}}{\mu}$, we have

$$\min_{\mathbf{v}\in X} \left\{ \|\mathbf{v}\|_{\ell_1} + \frac{\beta}{2}\|\mathbf{f}-\mathbf{v}\|_{\ell_2}^2\,,\ \mathbf{v} = \mu\mathrm{div}_S^-\vec{\mathbf{g}},\ \sum_{s=0}^{S-1} g_s^2[\boldsymbol{k}] - 1 \le 0\,, \forall \boldsymbol{k}\in\Omega \right\}. \quad (36)$$

We then apply ALM for the equality constraint and the KKT condition (generalized Lagrange multiplier) for the inequality constraint as

$$\min_{(\mathbf{v},\vec{\mathbf{g}})\in X^{S+1}} \mathcal{L}(\mathbf{v},\vec{\mathbf{g}}\,;\ \boldsymbol{\lambda_1},\boldsymbol{\lambda_2})$$

with Lagrange function

$$\mathcal{L}(\cdot;\cdot) = \|\mathbf{v}\|_{\ell_1} + \frac{\beta}{2}\|\mathbf{f}-\mathbf{v}\|_{\ell_2}^2 + \left\langle \boldsymbol{\lambda_1}\,, \mathbf{v}-\mu\mathrm{div}_S^-\vec{\mathbf{g}} \right\rangle_{\ell_2} + \frac{\alpha}{2}\left\| \mathbf{v}-\mu\mathrm{div}_S^-\vec{\mathbf{g}} \right\|_{\ell_2}^2 + \left\langle \boldsymbol{\lambda_2}\,, \sum_{s=0}^{S-1}\mathbf{g}_s^{\cdot 2} - 1 \right\rangle_{\ell_2}.$$

Note that $\lambda_2[\boldsymbol{k}] > 0\,, \forall \boldsymbol{k}\in\Omega$. In a sequential fashion, we consider the primal, dual problems and then update the Lagrange multiplier $\boldsymbol{\lambda_1}$ as:

The primal v-problem: fix $\vec{\mathbf{g}}$ and solve

$$\min_{\mathbf{v}\in X} \left\{ \mathcal{L}(\mathbf{v}) = \|\mathbf{v}\|_{\ell_1} + \frac{\beta}{2}\|\mathbf{f}-\mathbf{v}\|_{\ell_2}^2 + \left\langle \boldsymbol{\lambda_1}\,, \mathbf{v}-\mu\mathrm{div}_S^-\vec{\mathbf{g}} \right\rangle_{\ell_2} + \frac{\alpha}{2}\left\| \mathbf{v}-\mu\mathrm{div}_S^-\vec{\mathbf{g}} \right\|_{\ell_2}^2 \right\}$$

The Euler-Lagrange equation is given by

$$0 = \frac{\partial \mathcal{L}(\mathbf{v})}{\partial \mathbf{v}} = \frac{\mathbf{v}}{|\mathbf{v}|} + \beta(\mathbf{v} - \mathbf{f}) + \boldsymbol{\lambda_1} + \alpha\Big[\mathbf{v} - \mu \mathrm{div}_S^- \vec{\mathbf{g}}\Big]$$

$$\Leftrightarrow \ \mathbf{v}^* = \frac{\beta}{\alpha+\beta}\mathbf{f} + \frac{\alpha\mu}{\alpha+\beta}\mathrm{div}_S^- \vec{\mathbf{g}} - \frac{1}{\alpha+\beta}\boldsymbol{\lambda_1} - \frac{1}{\alpha+\beta}\frac{\mathbf{v}}{|\mathbf{v}|}$$

$$:= \mathrm{Shrink}\left(\frac{\beta}{\alpha+\beta}\mathbf{f} + \frac{\alpha\mu}{\alpha+\beta}\mathrm{div}_S^- \vec{\mathbf{g}} - \frac{1}{\alpha+\beta}\boldsymbol{\lambda_1}\,,\ \frac{1}{\alpha+\beta}\right).$$

The dual $\vec{\mathbf{g}} = \big[\mathbf{g}_s\big]_{s=0}^{S-1}$-problem: Fix $\mathbf{v}$ and solve

$$\min_{\vec{\mathbf{g}} \in X^S} \left\{ \mathcal{L}(\vec{\mathbf{g}}) = \Big\langle \boldsymbol{\lambda_1}\,, \mathbf{v} - \mu \mathrm{div}_S^- \vec{\mathbf{g}} \Big\rangle_{\ell_2} + \frac{\alpha}{2}\Big\| \mathbf{v} - \mu \mathrm{div}_S^- \vec{\mathbf{g}} \Big\|_{\ell_2}^2 + \Big\langle \boldsymbol{\lambda_2}\,, \sum_{s=0}^{S-1} \mathbf{g}_s^{\cdot 2} - 1 \Big\rangle_{\ell_2} \right\}$$

Due to its separability, we evaluate the dual $\vec{\mathbf{g}}$ problem at $s = s'\,, s' = 0, \ldots, S-1$ and its Euler-Lagrange equation is given by

$$0 = \frac{\partial \mathcal{L}(\vec{\mathbf{g}})}{\partial \mathbf{g}_{s'}} = -\mu \underbrace{\Big\langle \boldsymbol{\lambda_1}\,, \overbrace{\frac{\partial\big\{\mathrm{div}_S^- \vec{\mathbf{g}}\big\}}{\partial \mathbf{g}_{s'}}}^{=-\partial_{s'}^+ \delta} \Big\rangle_{\ell_2}}_{=-\partial_{s'}^+ \boldsymbol{\lambda_1}} - \alpha\mu \underbrace{\frac{\partial\big\{\mathrm{div}_S^- \vec{\mathbf{g}}\big\}}{\partial \mathbf{g}_{s'}}}_{=-\partial_{s'}^+ \delta} \Big[\mathbf{v} - \mu \mathrm{div}_S^- \vec{\mathbf{g}}\Big] + 2\boldsymbol{\lambda_2} \cdot^{\times} \mathbf{g}_{s'}$$

$$\Leftrightarrow \ -\mu\partial_{s'}^+ \Big[\alpha\mu \mathrm{div}_S^- \vec{\mathbf{g}} - \boldsymbol{\lambda_1} - \alpha\mathbf{v}\Big] + 2\boldsymbol{\lambda_2} \cdot^{\times} \mathbf{g}_{s'} = 0\,,\ s' = 0, \ldots, S-1$$

$$\Leftrightarrow \ -\mu\nabla_S^+ \Big[\alpha\mu \mathrm{div}_S^- \vec{\mathbf{g}} - \boldsymbol{\lambda_1} - \alpha\mathbf{v}\Big] + 2\boldsymbol{\lambda_2} \cdot^{\times} \vec{\mathbf{g}} = 0\,.$$

As in (34), with $\lambda_2[\boldsymbol{k}] > 0\,, \boldsymbol{k} \in \Omega$, its element form is

$$-\mu\nabla_S^+ \Big[\alpha\mu \mathrm{div}_S^- \vec{g}[\boldsymbol{k}] - \lambda_1[\boldsymbol{k}] - \alpha v[\boldsymbol{k}]\Big] + 2\lambda_2[\boldsymbol{k}]\vec{g}[\boldsymbol{k}] = 0 \qquad (37)$$

$$\Leftrightarrow \ \lambda_2[\boldsymbol{k}] = \frac{\mu}{2}\Big|\nabla_S^+ \Big[\alpha\mu \mathrm{div}_S^- \vec{g}[\boldsymbol{k}] - \lambda_1[\boldsymbol{k}] - \alpha v[\boldsymbol{k}]\Big]\Big|\,.$$

Thus, we rewrite (37) with $\boldsymbol{k} \in \Omega$ as

$$-\nabla_S^+ \Big[\alpha\mu \mathrm{div}_S^- \vec{g}[\boldsymbol{k}] - \lambda_1[\boldsymbol{k}] - \alpha v[\boldsymbol{k}]\Big] + \Big|\nabla_S^+ \Big[\alpha\mu \mathrm{div}_S^- \vec{g}[\boldsymbol{k}] - \lambda_1[\boldsymbol{k}] - \alpha v[\boldsymbol{k}]\Big]\Big| \vec{g}[\boldsymbol{k}] = 0\,.$$

Applying gradient descent and the fixed point algorithm, we have

$$-\nabla_S^+ \Big[\alpha\mu \mathrm{div}_S^- \vec{g}^{(t-1)}[\boldsymbol{k}] - \lambda_1[\boldsymbol{k}] - \alpha v[\boldsymbol{k}]\Big] + \Big|\nabla_S^+ \Big[\alpha\mu \mathrm{div}_S^- \vec{g}^{(t-1)}[\boldsymbol{k}] - \lambda_1[\boldsymbol{k}] - \alpha v[\boldsymbol{k}]\Big]\Big| \vec{g}^{(t)}[\boldsymbol{k}]$$

$$= -\frac{\vec{g}^{(t)}[\boldsymbol{k}] - \vec{g}^{(t-1)}[\boldsymbol{k}]}{\tau}\,,$$

the solution of the $\vec{\mathbf{g}}$-problem in matrix form is

$$\vec{\mathbf{g}}^{(t)} = \frac{\vec{\mathbf{g}}^{(t-1)} + \tau\nabla_S^+\left[\alpha\mu\mathrm{div}_S^-\vec{\mathbf{g}}^{(t-1)} - \boldsymbol{\lambda_1} - \alpha\mathbf{v}\right]}{1+\tau\left|\nabla_S^+\left[\alpha\mu\mathrm{div}_S^-\vec{\mathbf{g}}^{(t-1)} - \boldsymbol{\lambda_1} - \alpha\mathbf{v}\right]\right|}\,,\ t=1,\ldots.$$

Update the Lagrange multiplier $\boldsymbol{\lambda_1} \in X$:

$$\boldsymbol{\lambda_1}^{(t)} = \boldsymbol{\lambda_1}^{(t-1)} + \alpha\left[\mathbf{v} - \mu\mathrm{div}_S^-\vec{\mathbf{g}}\right].$$

□

Proposition 7.4. *The $\vec{\mathbf{p}}$-problem in the SHT model is*

$$\min_{\vec{\mathbf{p}}\in X^N}\left\{\mu_3\sum_{n=1}^N\left\|\nabla_M^+\mathbf{p}_n\right\|_{\ell_1} + \frac{\mu_4}{2}\left\|\mathbf{u} - \sum_{n=1}^N c_n\mathbf{p}_n\right\|_{\ell_2}^2 \quad s.t.\ \sum_{n=1}^N \mathbf{p}_n = 1, p_n[\boldsymbol{k}] > 0, n=1,\ldots,N, \boldsymbol{k}\in\Omega\right\}.$$

At iteration t, we have

The primal variable:

$$\mathbf{p}_n^{(t)} = \frac{\exp\left\{-\frac{1}{\xi}\left[div_M^-\vec{\mathbf{q}}_n^{(t-1)} + \frac{\mu_4}{2\mu_3}\left(\mathbf{u}-c_n\right)^{\cdot 2}\right]\right\}}{\sum_{i=1}^N\exp\left\{-\frac{1}{\xi}\left[div_M^-\vec{\mathbf{q}}_i^{(t-1)} + \frac{\mu_4}{2\mu_3}\left(\mathbf{u}-c_i\right)^{\cdot 2}\right]\right\}}$$

$$= \frac{\exp\left\{-\frac{1}{\xi}\Big[-\sum_{m=0}^{M-1}\Big[\cos\left(\frac{\pi m}{M}\right)\mathbf{q}_{nm}^{(t-1)}\mathbf{D_2} + \sin\left(\frac{\pi m}{M}\right)\mathbf{D_1}^T\mathbf{q}_{nm}^{(t-1)}\Big] + \frac{\mu_4}{2\mu_3}\left(\mathbf{u}-c_n\right)^{\cdot 2}\Big]\right\}}{\sum_{i=1}^N\exp\left\{-\frac{1}{\xi}\Big[-\sum_{m=0}^{M-1}\Big[\cos\left(\frac{\pi m}{M}\right)\mathbf{q}_{im}^{(t-1)}\mathbf{D_2} + \sin\left(\frac{\pi m}{M}\right)\mathbf{D_1}^T\mathbf{q}_{im}^{(t-1)}\Big] + \frac{\mu_4}{2\mu_3}\left(\mathbf{u}-c_i\right)^{\cdot 2}\Big]\right\}},\ n=1,\ldots,N$$

The dual variable:

$$\vec{\mathbf{q}}_n^{(t)} = \frac{\vec{\mathbf{q}}_n^{(t-1)} + \tau\nabla_M^+\mathbf{p}_n^{(t)}}{1+\tau\left|\nabla_M^+\mathbf{p}_n^{(t)}\right|}\,,\quad a=1,\ldots,N\,,$$

or

$$\mathbf{q}_{nm}^{(t)} = \frac{\mathbf{q}_{nm}^{(t-1)} + \tau\left[\cos\left(\frac{\pi m}{M}\right)\mathbf{p}_n^{(t)}\mathbf{D_2}^T + \sin\left(\frac{\pi m}{M}\right)\mathbf{D_1}\mathbf{p}_n^{(t)}\right]}{1+\tau\left[\sum_{m=0}^{M-1}\left[\cos\left(\frac{\pi m}{M}\right)\mathbf{p}_n^{(t)}\mathbf{D_2}^T + \sin\left(\frac{\pi m}{M}\right)\mathbf{D_1}\mathbf{p}_n^{(t)}\right]^{\cdot 2}\right]^{\cdot\frac{1}{2}}},\quad n=1,\ldots,N\,,\ m=0,\ldots,M-1$$

Proof. This subproblem is solved by a smoothed primal-dual model [42] and Chambolle's projection [34] for the dual variable (gradient descent of the Euler Lagrange equation and fixed point algorithm). In order to make the paper self-contained, the extension of [42] to the multi-directional case is provided here by introducing a primal model, a primal-dual model, a dual model and then a smoothed dual model and a smoothed primal-dual model.

The primal model:

Given the relaxed version on the binary set, the "$\vec{\mathbf{p}}$-problem" can be rewritten as the convex minimization

$$\min_{\vec{\mathbf{p}}\in\mathcal{Q}_+}\left\{\mathcal{L}^{\mathrm{P}}(\vec{\mathbf{p}})=\sum_{n=1}^{N}\left\|\nabla_M^+\mathbf{p}_n\right\|_{\ell_1}+\frac{\mu_4}{2\mu_3}\underbrace{\sum_{n=1}^{N}\left\langle\left(\mathbf{u}-c_n\right)^{\cdot 2},\mathbf{p}_i\right\rangle_{\ell_2}}_{=\left\|\mathbf{u}-\sum_{n=1}^{N}c_n\mathbf{p}_n\right\|_{\ell_2}^2}\right\} \tag{38}$$

with the convex set

$$\mathcal{Q}_+=\left\{\vec{\mathbf{p}}=\left[\mathbf{p}_n\right]_{n=1}^{N}\in X^N\ :\ \sum_{n=1}^{N}\mathbf{p}_n=1\,,p_n[\boldsymbol{k}]>0\,,n=1,\ldots,N\,,\boldsymbol{k}\in\Omega\right\}.$$

The primal-dual model:

From Lemma 7.0.1, given a convex set of the DTV-norm

$$K_M(1)=\left\{\vec{\mathbf{q}}_n=\left[\mathbf{q}_{nm}\right]_{m=0}^{M-1}\in X^M\ :\ |\vec{\mathbf{q}}_n|=\sqrt{\sum_{m=0}^{M-1}\mathbf{q}_{nm}^{\cdot 2}}\leq 1\right\}$$

with the notation $\vec{\mathbf{q}}=\left[\vec{\mathbf{q}}_n\right]_{n=1}^{N}=\left[\mathbf{q}_{nm}\right]_{n=[1,N]}^{m=[0,M-1]}\in X^{NM}$, the primal-dual model of (38) (a separable problem) can be written as

$$\begin{aligned}\mathcal{L}^{\mathrm{P}}(\vec{\mathbf{p}})&=\sum_{n=1}^{N}\max_{\vec{\mathbf{q}}_n\in K_M(1)}\left\langle\mathbf{p}_n\,,\mathrm{div}_M^-\vec{\mathbf{q}}_n\right\rangle_{\ell_2}+\frac{\mu_4}{2\mu_3}\sum_{n=1}^{N}\left\langle\mathbf{p}_n\,,\left(\mathbf{u}-c_n\right)^{\cdot 2}\right\rangle_{\ell_2}\\&=\max_{\vec{\mathbf{q}}\in\left[K_M(1)\right]^N}\left\{\sum_{n=1}^{N}\left\langle\mathbf{p}_n\,,\mathrm{div}_M^-\vec{\mathbf{q}}_n+\frac{\mu_4}{2\mu_3}\left(\mathbf{u}-c_n\right)^{\cdot 2}\right\rangle_{\ell_2}\right\}.\end{aligned}$$

From (38) and the Min-Max theorem, the primal ($\vec{\mathbf{p}}$) - dual ($\vec{\mathbf{q}}$) model is

$$\max_{\vec{\mathbf{q}}\in\left[K_M(1)\right]^N}\min_{\vec{\mathbf{p}}\in\mathcal{Q}_+}\left\{\mathcal{L}^{\mathrm{PD}}(\vec{\mathbf{q}},\vec{\mathbf{p}})=\sum_{n=1}^{N}\left\langle\mathbf{p}_n\,,\mathrm{div}_M^-\vec{\mathbf{q}}_n+\frac{\mu_4}{2\mu_3}\left(\mathbf{u}-c_n\right)^{\cdot 2}\right\rangle_{\ell_2}\right\}. \tag{39}$$

The dual model: We first recall a result from [42]:

Lemma 7.0.2. *Given a convex set*

$$\Delta_+ = \Big\{ \big(v_1(x), \ldots, v_N(x)\big) \Big\} \ : \ \sum_{n=1}^{N} v_n(x) = 1\,, v_n(x) \geq 0\,, n = 1, \ldots, N\,, \boldsymbol{k} \in \Omega \Big\}\,,$$

we have

$$\min_{(v_1,\ldots,v_N)\in\Delta_+} \sum_{n=1}^{N} v_n q_n = \min\big(q_1, \ldots, q_N\big)\,.$$

Since the pixels are assumed to be independent, the primal-dual model (39) can be rewritten as

$$\max_{\vec{\mathbf{q}}\in\left[K_M(1)\right]^N} \min_{\vec{\mathbf{p}}\in\mathcal{Q}_+} \Big\{ \mathcal{L}^{\mathrm{PD}}(\vec{\mathbf{q}}, \vec{\mathbf{p}}) = \sum_{\boldsymbol{k}\in\Omega} \sum_{n=1}^{N} p_n[\boldsymbol{k}] \Big[\mathrm{div}_M^- \vec{q}_n[\boldsymbol{k}] + \frac{\mu_4}{2\mu_3} \big(u[\boldsymbol{k}] - c_n\big)^2 \Big] \Big\}$$

$$= \max_{\vec{\mathbf{q}}\in\left[K_M(1)\right]^N} \sum_{\boldsymbol{k}\in\Omega} \quad \underbrace{\min_{\vec{p}[\boldsymbol{k}]\in\mathcal{Q}_{+\boldsymbol{k}}} \Big\{ \mathcal{L}^{\mathrm{PD}}(\vec{q}[\boldsymbol{k}], \vec{p}[\boldsymbol{k}]) = \sum_{n=1}^{N} p_n[\boldsymbol{k}] \Big[\mathrm{div}_M^- \vec{q}_n[\boldsymbol{k}] + \frac{\mu_4}{2\mu_3} \big(u[\boldsymbol{k}] - c_n\big)^2 \Big] \Big\}}$$

$$= \min_{1\leq n\leq N} \Big\{ \mathrm{div}_M^- \vec{q}_1[\boldsymbol{k}] + \frac{\mu_4}{2\mu_3} \big(u[\boldsymbol{k}] - c_1\big)^2, \ldots, \mathrm{div}_M^- \vec{q}_N[\boldsymbol{k}] + \frac{\mu_4}{2\mu_3} \big(u[\boldsymbol{k}] - c_N\big)^2 \Big\}$$

with an element version at a pixel $\boldsymbol{k}$ of a convex set Q_+

$$Q_{+\boldsymbol{k}} = \Big\{ \vec{p}[\boldsymbol{k}] = \big[p_n[\boldsymbol{k}]\big]_{n=1}^{N} \in \mathbb{R}^N \ : \ \sum_{n=1}^{N} p_n[\boldsymbol{k}] = 1\,, p_n[\boldsymbol{k}] > 0\,, n = 1, \ldots, N\,, \boldsymbol{k} \in \Omega \Big\}\,. \tag{40}$$

Thus, the dual problem is

$$\max_{\vec{\mathbf{q}}\in\left[K_M(1)\right]^N} \Big\{ \mathcal{L}^{\mathrm{D}}(\vec{\mathbf{q}}) = \sum_{\boldsymbol{k}\in\Omega} \min_{1\leq n\leq N} \Big\{ \mathrm{div}_M^- \vec{q}_1[\boldsymbol{k}] + \frac{\mu_4}{2\mu_3} \big(u[\boldsymbol{k}] - c_1\big)^2, \ldots, \mathrm{div}_M^- \vec{q}_N[\boldsymbol{k}] + \frac{\mu_4}{2\mu_3} \big(u[\boldsymbol{k}] - c_N\big)^2 \Big\} \Big\}\,. \tag{41}$$

The smoothed dual model:

Lemma 7.0.3. *Given $\vec{u} = \big[u_n\big]_{n=1}^{N}$, the non-smooth function $\max_{1\leq n\leq N} u_i$ is defined as the asympototic function of a proper convex function $g(\vec{u}) = \log\Big[\sum_{n=1}^{N} e^{u_n}\Big]$ as*

$$\max_{1\leq n\leq N} u_n = \lim_{\xi\to 0^+} \xi g\big(\frac{\vec{u}}{\xi}\big) = \lim_{\xi\to 0^+} \xi \log\Big[\sum_{n=1}^{N} e^{\frac{u_n}{\xi}}\Big]$$

$$\approx \ \xi \log\Big[\sum_{n=1}^{N} e^{\frac{u_n}{\xi}}\Big]$$

for some small constant $\xi > 0$.

From (41), we have

$$\mathcal{L}^{\mathrm{D}}(\vec{\mathbf{q}}) = -\sum_{\boldsymbol{k}\in\Omega} \max_{1\le n\le N} \Big\{ -\operatorname{div}_M^- \vec{q}_1[\boldsymbol{k}] - \frac{\mu_4}{2\mu_3}\big(u[\boldsymbol{k}]-c_1\big)^2, \dots, -\operatorname{div}_M^- \vec{q}_N[\boldsymbol{k}] - \frac{\mu_4}{2\mu_3}\big(u[\boldsymbol{k}]-c_N\big)^2 \Big\}$$

$$\approx -\xi \sum_{\boldsymbol{k}\in\Omega} \log\Big[\sum_{n=1}^{N} \exp\Big\{ \frac{1}{\xi}\Big[-\operatorname{div}_M^- \vec{q}_n[\boldsymbol{k}] - \frac{\mu_4}{2\mu_3}\big(u[\boldsymbol{k}]-c_n\big)^2 \Big\}\Big] \;:=\; \mathcal{L}^{\mathrm{D}}_{\xi>0}(\vec{\mathbf{q}})\,.$$

Thus, a smoothed dual model is

$$\max_{\vec{\mathbf{q}}\in\left[K_M(1)\right]^N} \Big\{ \mathcal{L}^{\mathrm{D}}_{\xi>0}(\vec{\mathbf{q}}) = -\xi \sum_{\boldsymbol{k}\in\Omega} \log\Big[\sum_{n=1}^{N} \exp\Big\{ -\frac{1}{\xi}\Big[\operatorname{div}_M^- \vec{q}_n[\boldsymbol{k}] + \frac{\mu_4}{2\mu_3}\big(u[\boldsymbol{k}]-c_n\big)^2 \Big]\Big\}\Big]\Big\}. \tag{42}$$

The smoothed primal-dual model:

Lemma 7.0.4. *For any given* $\mathbf{u}\in\mathcal{Q}_+$ *and* $h\in\mathbb{R}^N$

$$\log\sum_{n=1}^{N}\mu_n e^{h_n} = \max_{u\in\mathcal{Q}_+}\Big\{ \langle u,h\rangle_{\ell_2} - \sum_{n=1}^{N} u_n \log\frac{u_n}{\mu_n}\Big\}\,.$$

Given the convex set $Q_{+\boldsymbol{k}}$ in (40) and because the pixels are assumed to be independent, the energy function of a smoothed dual model (42) can be rewritten as

$$\mathcal{L}^{\mathrm{D}}_{\xi>0}(\vec{\mathbf{q}}) = -\xi \sum_{\boldsymbol{k}\in\Omega} \max_{\vec{p}_N[\boldsymbol{k}]\in\mathcal{Q}_{+\boldsymbol{k}}} \Big\{ -\frac{1}{\xi}\Big\langle \vec{p}_N[\boldsymbol{k}]\,, \operatorname{div}_M^- \vec{q}[\boldsymbol{k}] + \frac{\mu_4}{2\mu_3}\big(u[\boldsymbol{k}]-\vec{c}\big)^2\Big\rangle_{\ell_2} - \sum_{n=1}^{N} p_n[\boldsymbol{k}]\log p_n[\boldsymbol{k}] \Big\}$$

$$= \min_{\vec{\mathbf{p}}\in\mathcal{Q}_+} \Big\{ \sum_{n=1}^{N} \underbrace{\sum_{\boldsymbol{k}\in\Omega} p_n[\boldsymbol{k}]\Big[\operatorname{div}_M^- \vec{q}_n[\boldsymbol{k}] + \frac{\mu_4}{2\mu_3}\big(u[\boldsymbol{k}]-c_n\big)^2\Big]}_{=\left\langle \mathbf{p}_n\,, \operatorname{div}_M^-\vec{\mathbf{q}}_n + \frac{\mu_4}{2\mu_3}(\mathbf{u}-c_n)^{\cdot 2}\right\rangle_{\ell_2}} + \xi \sum_{n=1}^{N} \underbrace{\sum_{\boldsymbol{k}\in\Omega} p_n[\boldsymbol{k}]\log p_n[\boldsymbol{k}]}_{=\left\langle \mathbf{p}_n\,, \log \mathbf{p}_n\right\rangle_{\ell_2}} \Big\}.$$

From (42), we have the smoothed primal-dual model

$$\max_{\vec{\mathbf{q}}\in\left[K_M(1)\right]^N} \underbrace{\min_{\vec{\mathbf{p}}\in\mathcal{Q}_+} \Big\{ \mathcal{L}^{\mathrm{PD}}_{\xi>0}(\vec{\mathbf{q}},\vec{\mathbf{p}}) = \sum_{n=1}^{N} \Big\langle \mathbf{p}_n\,, \operatorname{div}_M^-\vec{\mathbf{q}}_n + \frac{\mu_4}{2\mu_3}\big(\mathbf{u}-c_n\big)^{\cdot 2}\Big\rangle_{\ell_2} + \xi\sum_{n=1}^{N}\big\langle \mathbf{p}_n\,, \log\mathbf{p}_n\big\rangle_{\ell_2}\Big\}}$$

$$= \mathcal{L}^{\mathrm{D}}_{\xi>0}(\vec{\mathbf{q}}) := -\xi\sum_{\boldsymbol{k}\in\Omega}\log\left[\sum_{n=1}^{N}\exp\left\{-\frac{1}{\xi}\Big[\operatorname{div}_M^-\vec{q}_n[\boldsymbol{k}] + \frac{\mu_4}{2\mu_3}\big(u[\boldsymbol{k}]-c_n\big)^2\Big]\right\}\right] \tag{43}$$

a) Primal $(\vec{\mathbf{p}})$-problem: The primal problem of (43) over a convex set $\mathcal{Q}_+ = \Big\{\vec{\mathbf{p}} = \big[\mathbf{p}_n\big]_{n=1}^N \in X^N \ : \ \sum_{n=1}^N \mathbf{p}_n = 1\,, p_n[\boldsymbol{k}] \geq 0\,, n = 1,\ldots,N\,, \boldsymbol{k} \in \Omega\Big\}$ is

$$\min_{\vec{\mathbf{p}} \in \mathcal{Q}_+} \mathcal{L}^{\mathrm{PD}}_{\xi>0}(\vec{\mathbf{p}})\,.$$

Applying ALM for the equality constraint, the primal $(\vec{\mathbf{p}})$-problem can be rewritten as

$$\min_{0<\vec{\mathbf{p}} \in X^N} \max_{\boldsymbol{\lambda} \in X} \Bigg\{ \mathcal{L}^{\mathrm{PD}}_{\xi>0}(\vec{\mathbf{p}}\,;\boldsymbol{\lambda}) = \sum_{n=1}^N \big\langle \mathbf{p}_n\,, \mathrm{div}_M^- \vec{\mathbf{q}}_n + \frac{\mu_4}{2\mu_3}\big(\mathbf{u} - c_n\big)^{\cdot 2} \big\rangle_{\ell_2} + \xi \sum_{n=1}^N \big\langle \mathbf{p}_n\,, \log \mathbf{p}_n \big\rangle_{\ell_2}$$
$$+ \big\langle \boldsymbol{\lambda}\,, \sum_{n=1}^N \mathbf{p}_n - 1 \big\rangle_{\ell_2} + \frac{\gamma}{2} \Bigg\| \sum_{n=1}^N \mathbf{p}_n - 1 \Bigg\|_{\ell_2}^2 \Bigg\}\,.$$

Due to its separability, we consider the problem at $n = a\,, a = 1,\ldots,N$. The Euler-Lagrange equation is

$$\begin{cases} 0 = \dfrac{\partial \mathcal{L}^{\mathrm{PD}}_{\xi>0}(\vec{\mathbf{p}}\,,\boldsymbol{\lambda})}{\partial \boldsymbol{\lambda}} = \displaystyle\sum_{n=1}^N \mathbf{p}_n - 1 & \text{(a)} \\ 0 = \dfrac{\partial \mathcal{L}^{\mathrm{PD}}_{\xi>0}(\vec{\mathbf{p}}\,,\boldsymbol{\lambda})}{\partial \mathbf{p}_a} = \mathrm{div}_M^- \vec{\mathbf{q}}_a + \dfrac{\mu_4}{2\mu_3}\big(\mathbf{u} - c_a\big)^{\cdot 2} + \xi(1 + \log \mathbf{p}_a) + \boldsymbol{\lambda} + \gamma \underbrace{\Big[\displaystyle\sum_{n=1}^N \mathbf{p}_n - 1\Big]}_{=0} & \text{(b)} \end{cases}$$

$$\text{(b)} \ \Leftrightarrow \ \mathbf{p}_a = \frac{1}{e^{\frac{\boldsymbol{\lambda}}{\xi}} + 1} \exp\Big\{ -\frac{1}{\xi}\Big[\mathrm{div}_M^- \vec{\mathbf{q}}_a + \frac{\mu_4}{2\mu_3}\big(\mathbf{u} - c_a\big)^{\cdot 2}\Big]\Big\}\ , \ a = 1,\ldots,N$$

$$\text{(a)} \ \Leftrightarrow \ \sum_{n=1}^N \exp\Big\{ -\frac{1}{\xi}\Big[\mathrm{div}_M^- \vec{\mathbf{q}}_n + \frac{\mu_4}{2\mu_3}\big(\mathbf{u} - c_n\big)^{\cdot 2}\Big]\Big\} = e^{\frac{\boldsymbol{\lambda}}{\xi}+1}\,.$$

Thus, the primal variable is

$$\mathbf{p}_a = \frac{\exp\Big\{ -\dfrac{1}{\xi}\Big[\mathrm{div}_M^- \vec{\mathbf{q}}_a + \dfrac{\mu_4}{2\mu_3}\big(\mathbf{u} - c_a\big)^{\cdot 2}\Big]\Big\}}{\displaystyle\sum_{n=1}^N \exp\Big\{ -\frac{1}{\xi}\Big[\mathrm{div}_M^- \vec{\mathbf{q}}_n + \frac{\mu_4}{2\mu_3}\big(\mathbf{u} - c_n\big)^{\cdot 2}\Big]\Big\}}\ , \ a = 1,\ldots,N\,.$$

b) The Dual $(\vec{\mathbf{q}})$-problem: Given the convex set $K_M(1) = \Big\{\vec{\mathbf{q}}_n = \big[\mathbf{q}_{nm}\big]_{m=0}^{M-1} \in X^M \ : \ |\vec{\mathbf{q}}_n| = \sqrt{\sum_{m=0}^{M-1} \mathbf{q}_{nm}^{\cdot 2}} \leq 1\Big\}$, the dual problem of (43) is

$$\max_{\vec{\mathbf{q}} \in \big[K_M(1)\big]^N} \Bigg\{ \mathcal{L}^{\mathrm{D}}_{\xi>0}(\vec{\mathbf{q}}) = -\xi \sum_{\boldsymbol{k} \in \Omega} \log\Big[\sum_{n=1}^N \exp\Big\{ -\frac{1}{\xi}\Big[\mathrm{div}_M^- \vec{q}_n[\boldsymbol{k}] + \frac{\mu_4}{2\mu_3}\big(u[\boldsymbol{k}] - c_n\big)^2\Big]\Big\}\Big]\Bigg\}\,.$$

Due to the pixel independence, we consider the problem at $\boldsymbol{k} = \boldsymbol{x} \in \Omega\,, n = a, a = 1, \ldots, N$ and with the KKT condition (with the Lagrange multiplier $\lambda[\boldsymbol{k}] > 0$) for the inequality constraint, we have

$$\frac{\partial \mathcal{L}^{\mathrm{D}}_{\xi>0}(\vec{\mathbf{q}})}{\partial \vec{q}_a[\boldsymbol{x}]} + \lambda[\boldsymbol{x}] \underbrace{\frac{\partial}{\partial \vec{q}_a[\boldsymbol{x}]} \Big\{ \big|\vec{q}_a[\boldsymbol{x}]\big|^2 - 1 \Big\}}_{=2\vec{q}_a[\boldsymbol{x}]} = 0\,,\ a = 1, \ldots, N\,, \boldsymbol{x} \in \Omega \tag{44}$$

with

$$\begin{aligned}
\frac{\partial \mathcal{L}^{\mathrm{D}}_{\xi>0}(\vec{\mathbf{q}})}{\partial \vec{q}_a[\boldsymbol{x}]} &= -\xi \frac{\partial}{\partial \vec{q}_a[\boldsymbol{x}]} \Big\{ \log \Big[\sum_{n=1}^{N} \exp \Big\{ -\frac{1}{\xi} \Big[\mathrm{div}^-_M \vec{q}_n[\boldsymbol{x}] + \frac{\mu_4}{2\mu_3} \big(u[\boldsymbol{x}] - c_n\big)^2 \Big] \Big\} \Big] \Big\} \\
&= -\xi(-\frac{1}{\xi}) \underbrace{\frac{\partial}{\partial \vec{q}_a[\boldsymbol{x}]} \Big\{ \mathrm{div}^-_M \vec{q}_a[\boldsymbol{x}] \Big\}}_{=(\mathrm{div}^-_M)^* \frac{\partial \vec{q}_a[\boldsymbol{x}]}{\partial \vec{q}_a[\boldsymbol{x}]} = (-\nabla^+_M)\delta[\boldsymbol{x}]} \underbrace{\frac{\exp \Big\{ -\frac{1}{\xi} \Big[\mathrm{div}^-_M \vec{q}_a[\boldsymbol{x}] + \frac{\mu_4}{2\mu_3} \big(u[\boldsymbol{x}] - c_a\big)^2 \Big] \Big\}}{\sum_{n=1}^{N} \exp \Big\{ -\frac{1}{\xi} \Big[\mathrm{div}^-_M \vec{q}_n[\boldsymbol{x}] + \frac{\mu_4}{2\mu_3} \big(u[\boldsymbol{x}] - c_n\big)^2 \Big] \Big\}}}_{=p_a[\boldsymbol{x}]} \\
&= -\nabla^+_M p_a[\boldsymbol{x}]\,.
\end{aligned}$$

As in (34), given $a = 1, \ldots, N\,, \boldsymbol{x} \in \Omega$, we rewrite the KKT condition (44) in vector form as

$$-\nabla^+_M p_a[\boldsymbol{x}] + 2\lambda[\boldsymbol{x}] \vec{q}_a[\boldsymbol{x}] = 0 \ \Leftrightarrow\ \lambda[\boldsymbol{x}] = \frac{1}{2} \Big| \nabla^+_M p_a[\boldsymbol{x}] \Big|$$

and thus

$$-\nabla^+_M p_a[\boldsymbol{x}] \ + \ \Big| \nabla^+_M p_a[\boldsymbol{x}] \Big| \, \vec{q}_a[\boldsymbol{x}] \ = \ 0\,.$$

Applying gradient descent and the fixed point algorithm with $t = 1, \ldots$, we have

$$-\nabla^+_M p_a[\boldsymbol{x}] \ + \ \Big| \nabla^+_M p_a[\boldsymbol{x}] \Big| \, \vec{q}^{\,(t)}_a[\boldsymbol{x}] \ = \ -\frac{\vec{q}^{\,(t)}_a[\boldsymbol{x}] - \vec{q}^{\,(t-1)}_a[\boldsymbol{x}]}{\tau}\,,$$

and the solution in matrix form with $\vec{\mathbf{q}}_a = \big[\mathbf{q}_{am}\big]_{m=0}^{M-1}$ and $\nabla^+_M \mathbf{p}_a = \big[\partial^+_m \mathbf{p}_a\big]_{m=0}^{M-1}$ is given by

$$\vec{\mathbf{q}}^{\,(t)}_a = \frac{\vec{\mathbf{q}}^{\,(t-1)}_a + \tau \nabla^+_M \mathbf{p}_a}{1 + \tau \Big| \nabla^+_M \mathbf{p}_a \Big|}\,, \quad a = 1, \ldots, N\,. \tag{45}$$

□

Proposition 7.5. *Given a primal-dual model (23) in the bilevel-SHT, a smoothed primal-dual model is defined as*

$$\max_{\vec{\mathbf{q}}\in\left[K_M(1)\right]^N} \underbrace{\min_{\vec{\mathbf{p}}\in\mathcal{Q}_+} \left\{ \mathcal{L}^{PD}_{\xi>0}(\vec{\mathbf{p}};\vec{\mathbf{q}}) = \sum_{n=1}^{N} \Big\langle \mathbf{p}_n \,,\, \frac{\mu_3}{2}\big(\mathbf{u}-c_n\big)^{.2} + div_M^- \vec{\mathbf{q}}_n \Big\rangle_{\ell_2} + \xi \sum_{n=1}^{N} \Big\langle \mathbf{p}_n \,,\, \log \mathbf{p}_n \Big\rangle_{\ell_2} \right\}}$$

$$= \mathcal{L}^{D}_{\xi>0}(\vec{\mathbf{q}}) := -\xi \sum_{\boldsymbol{k}\in\Omega} \log\Big[\sum_{n=1}^{N} \exp\Big\{ -\frac{1}{\xi}\Big[\frac{\mu_3}{2}(u[\boldsymbol{k}]-c_n)^2 + div_M^- \vec{q}_n[\boldsymbol{k}]\Big]\Big\}\Big] \tag{46}$$

At iteration t, the primal and dual solutions are given by

$$\mathbf{p}_n^{(t)} = \frac{\exp\left[-\frac{1}{\xi}\left[\frac{\mu_3}{2}\big(\mathbf{u}-c_n\big)^{.2} + div_M^- \vec{\mathbf{q}}_n^{(t-1)}\right]\right]}{\sum_{i=1}^{N} \exp\Big[-\frac{1}{\xi}\Big[\frac{\mu_3}{2}\big(\mathbf{u}-c_i\big)^{.2} + div_M^- \vec{\mathbf{q}}_i^{(t-1)}\Big]\Big]}$$

$$= \frac{\exp\left[-\frac{1}{\xi}\left[\frac{\mu_3}{2}\big(\mathbf{u}-c_n\big)^{.2} - \sum_{m=0}^{M-1}\left[\cos\left(\frac{\pi m}{M}\right)\mathbf{q}_{nm}^{(t-1)}\mathbf{D_2} + \sin\left(\frac{\pi m}{M}\right)\mathbf{D}_\mathbf{1}^T\mathbf{q}_{nm}^{(t-1)}\right]\right]\right]}{\sum_{i=1}^{N}\exp\left[-\frac{1}{\xi}\left[\frac{\mu_3}{2}\big(\mathbf{u}-c_i\big)^{.2} - \sum_{m=0}^{M-1}\left[\cos\left(\frac{\pi m}{M}\right)\mathbf{q}_{im}^{(t-1)}\mathbf{D_2} + \sin\left(\frac{\pi m}{M}\right)\mathbf{D}_\mathbf{1}^T\mathbf{q}_{im}^{(t-1)}\right]\right]\right]}, \quad n=1,\ldots,N,$$

and

$$\vec{\mathbf{q}}_n^{(t)} = \frac{\vec{\mathbf{q}}_n^{(t-1)} + \tau\nabla_M^+\mathbf{p}_n^{(t)}}{1+\tau\left|\nabla_M^+\mathbf{p}_n^{(t)}\right|}, \quad n=1,\ldots,N,$$

or

$$\mathbf{q}_{nm}^{(t)} = \frac{\mathbf{q}_{nm}^{(t-1)} + \tau\left[\cos\left(\frac{\pi m}{M}\right)\mathbf{p}_n^{(t)}\mathbf{D}_\mathbf{2}^T + \sin\left(\frac{\pi m}{M}\right)\mathbf{D_1}\mathbf{p}_n^{(t)}\right]}{1+\tau\left[\sum_{m=0}^{M-1}\left[\cos\left(\frac{\pi m}{M}\right)\mathbf{p}_n^{(t)}\mathbf{D}_\mathbf{2}^T + \sin\left(\frac{\pi m}{M}\right)\mathbf{D_1}\mathbf{p}_n^{(t)}\right]^{.2}\right]^{.\frac{1}{2}}}, \quad n=1,\ldots,N,\ m=0,\ldots,M-1.$$

Proof. As in Section 3.1, with $\vec{\mathbf{p}} \in \mathcal{Q}_+$, a dual-primal model (23) is recast as the dual model

$$\max_{\vec{\mathbf{q}}\in\left[K_M(1)\right]^N} \left\{ \mathcal{L}^{\mathrm{D}}(\vec{\mathbf{q}}) = \sum_{\boldsymbol{k}\in\Omega} \min\left\{ \frac{\mu_3}{2}\big(u[\boldsymbol{k}]-c_1\big)^2 + \mathrm{div}_M^-\vec{q}_1[\boldsymbol{k}], \ldots, \frac{\mu_3}{2}\big(u[\boldsymbol{k}]-c_N\big)^2 + \mathrm{div}_M^-\vec{q}_N[\boldsymbol{k}]\right\}\right\}. \tag{47}$$

Due to the min operator in the energy function $\mathcal{L}_{\mathrm{D}}(\cdot)$, the minimization in (47) is a non-smooth dual model whose smoothed version (called a smoothed dual model) is defined as

$$\max_{\vec{\mathbf{q}}\in\left[K_M(1)\right]^N}\left\{\mathcal{L}^{\mathrm{D}}_{\xi>0}(\vec{\mathbf{q}})=-\xi\sum_{\boldsymbol{k}\in\Omega}\log\left[\sum_{n=1}^{N}\exp\left\{\frac{-\frac{\mu_3}{2}\big(u[\boldsymbol{k}]-c_n\big)^2-\mathrm{div}_M^-\vec{q}_n[\boldsymbol{k}]}{\xi}\right\}\right]\right\}. \tag{48}$$

Note that $\mathcal{L}^{\mathrm{D}}(\vec{\mathbf{q}})\approx\mathcal{L}^{\mathrm{D}}_{\xi>0}(\vec{\mathbf{q}})$. By the smooth log-sum function in convex analysis [68] and the pixel independence, a smoothed dual energy function in (48) can be rewritten as

$$\begin{aligned}\mathcal{L}^{\mathrm{D}}_{\xi>0}(\vec{\mathbf{q}})&=-\xi\sum_{\boldsymbol{k}\in\Omega}\max_{\vec{p}[\boldsymbol{k}]\in\mathcal{Q}_{+\boldsymbol{k}}}\Big\{-\frac{1}{\xi}\Big\langle\vec{p}[\boldsymbol{k}]\,,\frac{\mu_3}{2}\big(u[\boldsymbol{k}]-\vec{c}\big)^2+\mathrm{div}_M^-\vec{q}[\boldsymbol{k}]\Big\rangle_{\ell_2}-\sum_{n=1}^{N}p_n[\boldsymbol{k}]\log p_n[\boldsymbol{k}]\Big\}\\&=\min_{\vec{\mathbf{p}}\in\mathcal{Q}_+}\Big\{\sum_{n=1}^{N}\underbrace{\sum_{\boldsymbol{k}\in\Omega}p_n[\boldsymbol{k}]\Big[\frac{\mu_3}{2}\big(u[\boldsymbol{k}]-c_n\big)^2+\mathrm{div}_M^-\vec{q}_n[\boldsymbol{k}]\Big]}_{=\left\langle\mathbf{p}_n\,,\frac{\mu_3}{2}(\mathbf{u}-c_n)\cdot^2+\mathrm{div}_M^-\vec{\mathbf{q}}_n\right\rangle_{\ell_2}}+\xi\sum_{n=1}^{N}\underbrace{\sum_{\boldsymbol{k}\in\Omega}p_n[\boldsymbol{k}]\log p_n[\boldsymbol{k}]}_{=\left\langle\mathbf{p}_n\,,\log\mathbf{p}_n\right\rangle_{\ell_2}}\Big\}.\end{aligned}$$

Thus, we rewrite (48) as a smoothed primal-dual model

$$\max_{\vec{\mathbf{q}}\in\left[K_M(1)\right]^N}\left\{\mathcal{L}^{\mathrm{D}}_{\xi>0}(\vec{\mathbf{q}})=\min_{\vec{\mathbf{p}}\in\mathcal{Q}_+}\left\{\mathcal{L}^{\mathrm{PD}}_{\xi>0}(\vec{\mathbf{p}};\vec{\mathbf{q}})=\sum_{n=1}^{N}\Big\langle\mathbf{p}_n\,,\frac{\mu_3}{2}(\mathbf{u}-c_n)^{\cdot 2}+\mathrm{div}_M^-\vec{\mathbf{q}}_n\Big\rangle_{\ell_2}+\xi\sum_{n=1}^{N}\Big\langle\mathbf{p}_n\,,\log\mathbf{p}_n\Big\rangle_{\ell_2}\right\}\right\}. \tag{49}$$

The primal $\vec{\mathbf{p}}$-problem: We apply ALM for the equality constraint $\sum_{n=1}^{N}\mathbf{p}_n=1$ in a set $\mathcal{Q}_+$ to the primal $\vec{\mathbf{p}}$ problem of (49) as

$$\begin{aligned}\min_{0<\vec{\mathbf{p}}\in X^N}\max_{\boldsymbol{\lambda}\in X}\Big\{\mathcal{L}^{\mathrm{PD}}_{\xi>0}(\vec{\mathbf{p}};\boldsymbol{\lambda})&=\sum_{n=1}^{N}\Big\langle\mathbf{p}_n\,,\frac{\mu_3}{2}\big(\mathbf{u}-c_n\big)^{\cdot 2}+\mathrm{div}_M^-\vec{\mathbf{q}}_n\Big\rangle_{\ell_2}+\xi\sum_{n=1}^{N}\Big\langle\mathbf{p}_n\,,\log\mathbf{p}_n\Big\rangle_{\ell_2}\\&\quad+\Big\langle\boldsymbol{\lambda}\,,\sum_{n=1}^{N}\mathbf{p}_n-1\Big\rangle_{\ell_2}+\frac{\gamma}{2}\Big\|\sum_{n=1}^{N}\mathbf{p}_n-1\Big\|^2_{\ell_2}\Big\}\end{aligned} \tag{50}$$

Due to the separability in $\vec{\mathbf{p}}$ and $\boldsymbol{\lambda}$, the Euler Lagrange equations of the minimization problem (50) w.r.t. a primal variable $\mathbf{p}_n\,|_{n=a}\,, a=1,\ldots,N$ and the

Lagrange multiplier $\boldsymbol{\lambda}$ are

$$\begin{cases} 0 = \dfrac{\partial \mathcal{L}^{\mathrm{PD}}_{\xi>0}(\vec{\mathbf{p}};\boldsymbol{\lambda})}{\partial \boldsymbol{\lambda}} = \displaystyle\sum_{n=1}^{N} \mathbf{p}_n - 1 \\ 0 = \dfrac{\partial \mathcal{L}^{\mathrm{PD}}_{\xi>0}(\vec{\mathbf{p}};\boldsymbol{\lambda})}{\partial \mathbf{p}_a} = \dfrac{\mu_3}{2}\big(\mathbf{u}-c_a\big)^{\cdot 2} + \mathrm{div}_L^- \vec{\mathbf{q}}_a + \xi(1+\log \mathbf{p}_a) + \boldsymbol{\lambda} + \gamma\Big[\underbrace{\displaystyle\sum_{n=1}^{N} \mathbf{p}_n - 1}_{=0}\Big] \end{cases}$$

$$\Leftrightarrow\ \mathbf{p}_a^* = \frac{\exp\Big[-\dfrac{1}{\xi}\Big[\dfrac{\mu_3}{2}\big(\mathbf{u}-c_a\big)^{\cdot 2} + \mathrm{div}_M^- \vec{\mathbf{q}}_a\Big]\Big]}{\displaystyle\sum_{n=1}^{N} \exp\Big[-\frac{1}{\xi}\Big[\frac{\mu_3}{2}\big(\mathbf{u}-c_n\big)^{\cdot 2} + \mathrm{div}_M^- \vec{\mathbf{q}}_n\Big]\Big]},\ a=1,\dots,N. \tag{51}$$

We observe that $\vec{\mathbf{p}} = \big[\mathbf{p}_a\big]_{a=1}^N > 0$, i.e. $p_a[\boldsymbol{k}] > 0, \forall \boldsymbol{k} \in \Omega\,,\ a=1,\dots,N.$

The dual $\vec{\mathbf{q}}$-problem: Due to the inequality constraint in a convex set $K_M(1)$, the KKT condition of the minimization in (48) (or in a smoothed primal-dual model (49)), with given a Lagrange multiplier $\lambda[\boldsymbol{x}] > 0\,, \forall \boldsymbol{x} \in \Omega$ yields

$$\frac{\partial \mathcal{L}^D_{\xi>0}(\vec{\mathbf{q}})}{\partial \vec{q}_a[\boldsymbol{x}]} \ +\ \lambda[\boldsymbol{x}] \underbrace{\frac{\partial}{\partial \vec{q}_a[\boldsymbol{x}]}\Big\{\big|\vec{q}_a[\boldsymbol{x}]\big|^2 - 1\Big\}}_{=2\vec{q}_a[\boldsymbol{x}]} \ =\ 0\,,\quad a=1,\dots,N\,, \boldsymbol{x} \in \Omega\,. \tag{52}$$

Because of the pixel independence $\boldsymbol{k} \in \Omega$, in order to calculate $\frac{\partial \mathcal{L}^D_{s>0}(\vec{\mathbf{q}})}{\partial \vec{\mathbf{q}}_a}$ (in matrix form), we consider this derivative in element form at $\boldsymbol{k} = \boldsymbol{x} \in \Omega$ and $n = a\,, a = 1,\dots,N$:

$$\frac{\partial \mathcal{L}^D_{\xi>0}(\vec{\mathbf{q}})}{\partial \vec{q}_a[\boldsymbol{x}]} = -\xi(-\frac{1}{\xi}) \underbrace{\frac{\partial}{\partial \vec{q}_a[\boldsymbol{x}]}\Big\{\mathrm{div}_M^- \vec{q}_a[\boldsymbol{x}]\Big\}}_{=\left(-\nabla_M^+\right)\delta[\boldsymbol{x}]} \frac{\exp\Big\{\frac{-\frac{\mu_3}{2}\left(u[\boldsymbol{x}]-c_a\right)^2 - \mathrm{div}_M^- \vec{q}_a[\boldsymbol{x}]}{\xi}\Big\}}{\displaystyle\sum_{n=1}^{N} \exp\Big\{\frac{-\frac{\mu_3}{2}\left(u[\boldsymbol{x}]-c_n\right)^2 - \mathrm{div}_M^- \vec{q}_n[\boldsymbol{x}]}{\xi}\Big\}}$$

$$= -\nabla_M^+ \left\{ \frac{\exp\Big[-\dfrac{1}{\xi}\Big[\dfrac{\mu_3}{2}\big(u[\boldsymbol{x}]-c_a\big)^2 + \mathrm{div}_M^- \vec{q}_a[\boldsymbol{x}]\Big]\Big]}{\displaystyle\sum_{n=1}^{N} \exp\Big[-\frac{1}{\xi}\Big[\frac{\mu_3}{2}\big(u[\boldsymbol{x}]-c_n\big)^2 + \mathrm{div}_M^- \vec{q}_n[\boldsymbol{x}]\Big]\Big]} \right\}$$

$$\overset{(51)}{=} -\nabla_M^+ p_a[\boldsymbol{x}]\,.$$

As in Section 3.1 and [34], the KKT condition (52) (in vector form with $\vec{\mathbf{q}}_a =$

$\left[\mathbf{q}_{am}\right]_{m=1}^{M}$) can be rewritten as

$$-\nabla_M^+ p_a[\boldsymbol{x}] \;+\; \left|\nabla_M^+ p_a[\boldsymbol{x}]\right| \vec{q}_a[\boldsymbol{x}] \;=\; 0\,, \quad a = 1, \ldots, N$$

for $\boldsymbol{x} \in \Omega$. Applying gradient descent and the fixed point algorithm, we have

$$-\nabla_M^+ p_a[\boldsymbol{x}] \;+\; \left|\nabla_M^+ p_a[\boldsymbol{x}]\right| \vec{q}_a^{(t)}[\boldsymbol{x}] \;=\; -\,\frac{\vec{q}_a^{(t)}[\boldsymbol{x}] - \vec{q}_a^{(t-1)}[\boldsymbol{x}]}{\tau}\,,$$

and the solution in matrix form with $\vec{\mathbf{q}}_a = \left[\mathbf{q}_{am}\right]_{m=0}^{M-1}$ and $\nabla_M^+ \mathbf{p}_a = \left[\partial_m^+ \mathbf{p}_a\right]_{m=0}^{M-1}$ is given by

$$\vec{\mathbf{q}}_a^{(t)} = \frac{\vec{\mathbf{q}}_a^{(t-1)} + \tau \nabla_M^+ \mathbf{p}_a}{1 + \tau \left|\nabla_M^+ \mathbf{p}_a\right|}\,, \quad a = 1, \ldots, N\,.$$

□

Algorithm 5 A two-phase piecewise constant & texture segmentation

I. Compute $\Big(\big[\mathbf{r}_b^{(t)}\big]_{b=0}^{L-1}, \big[\mathbf{w}_a^{(t)}\big]_{a=0}^{S-1}, \big[\mathbf{g}_a^{(t)}\big]_{a=0}^{S-1}, \mathbf{v}^{(t)}, \mathbf{u}^{(t)}, \boldsymbol{\epsilon}^{(t)}\Big) \in X^{L+2S+3}$:

1. $c_1^{(t)} = \dfrac{\sum_{\boldsymbol{k}\in\Omega}\big[f[\boldsymbol{k}] - v^{(t-1)}[\boldsymbol{k}] - \epsilon^{(t-1)}[\boldsymbol{k}] + \frac{\lambda_4^{(t-1)}[\boldsymbol{k}]}{\beta_4}\big]p^{(t-1)}[\boldsymbol{k}]}{\sum_{\boldsymbol{k}\in\Omega} p^{(t-1)}[\boldsymbol{k}]}$

2. $c_2^{(t)} = \dfrac{\sum_{\boldsymbol{k}\in\Omega}\big[f[\boldsymbol{k}] - v^{(t-1)}[\boldsymbol{k}] - \epsilon^{(t-1)}[\boldsymbol{k}] + \frac{\lambda_4^{(t-1)}[\boldsymbol{k}]}{\beta_4}\big]\big[1 - p^{(t-1)}[\boldsymbol{k}]\big]}{\sum_{\boldsymbol{k}\in\Omega}(1 - p^{(t-1)}[\boldsymbol{k}])}$

3. $\mathbf{r}_a^{(t)} = \text{Shrink}\left(\sin\left(\dfrac{\pi a}{L}\right)\mathbf{D_1}\mathbf{p}^{(t-1)} + \cos\left(\dfrac{\pi a}{L}\right)\mathbf{p}^{(t-1)}\mathbf{D_2}^{\mathrm{T}} - \dfrac{\boldsymbol{\lambda}_{\mathbf{1}a}^{(t-1)}}{\beta_1}, \dfrac{1}{\beta_1}\right), \quad a = 0, \ldots, L-1$

4. $\mathbf{w}_a^{(t)} = \text{Shrink}\left(\mathbf{g}_a^{(t-1)} - \dfrac{\boldsymbol{\lambda}_{\mathbf{2}a}^{(t-1)}}{\beta_2}, \dfrac{\mu_1}{\beta_2}\right), a = 0, \ldots, S-1$

5. $\mathbf{g}_a^{(t)} = \text{Re}\left[\mathcal{F}^{-1}\left\{\dfrac{\mathcal{B}_a^{(t)}(\boldsymbol{z})}{\mathcal{A}_a^{(t)}(\boldsymbol{z})}\right\}\right][\boldsymbol{k}]\Big|_{\boldsymbol{k}\in\Omega}, a = 0, \ldots, S-1$

$$\mathcal{A}_a^{(t)}(\boldsymbol{z}) = \beta_2 + \beta_3\left|\sin\left(\frac{\pi a}{S}\right)(z_1 - 1) + \cos\left(\frac{\pi a}{S}\right)(z_2 - 1)\right|^2$$

$$\mathcal{B}_a^{(t)}(\boldsymbol{z}) = \beta_2\Big[W_a^{(t)}(\boldsymbol{z}) + \frac{\Lambda_{2a}^{(t-1)}(\boldsymbol{z})}{\beta_2}\Big] + \beta_3\Big[\sin\left(\frac{\pi a}{S}\right)(z_1^{-1} - 1) + \cos\left(\frac{\pi a}{S}\right)(z_2^{-1} - 1)\Big]\times$$

$$\Big[V^{(t-1)}(\boldsymbol{z}) - \sum_{s=[0,S-1]\setminus\{a\}}\big[\sin\left(\frac{\pi s}{S}\right)(z_1 - 1) + \cos\left(\frac{\pi s}{S}\right)(z_2 - 1)\big]G_s^{(t-1)}(\boldsymbol{z}) + \frac{\Lambda_3^{(t-1)}(\boldsymbol{z})}{\beta_3}\Big]$$

6. $\mathbf{v}^{(t)} = \text{Shrink}\left(\mathcal{J}^{(t)}, \dfrac{\mu_2}{\beta_3 + \beta_4}\right)$

$$\mathcal{J}^{(t)} = \frac{\beta_3}{\beta_3 + \beta_4}\Big[\sum_{s=0}^{S-1}\big[\sin\left(\frac{\pi s}{S}\right)\mathbf{D_1}\mathbf{g}_s^{(t)} + \cos\left(\frac{\pi s}{S}\right)\mathbf{g}_s^{(t)}\mathbf{D_2}^{\mathrm{T}}\big] - \frac{\boldsymbol{\lambda}_{\mathbf{3}}^{(t-1)}}{\beta_3}\Big]$$

$$+ \frac{\beta_4}{\beta_3 + \beta_4}\big[\mathbf{f} - c_1^{(t)} - \boldsymbol{\epsilon}^{(t-1)} + \frac{\boldsymbol{\lambda}_{\mathbf{4}}^{(t-1)}}{\beta_4}\big] \cdot^{\times} \mathbf{p}^{(t-1)} + \frac{\beta_4}{\beta_3 + \beta_4}\big[\mathbf{f} - c_2^{(t)} - \boldsymbol{\epsilon}^{(t-1)} + \frac{\boldsymbol{\lambda}_{\mathbf{4}}^{(t-1)}}{\beta_4}\big] \cdot^{\times} \big[1 - \mathbf{p}^{(t-1)}\big]$$

(continued Algorithm 5)

7. $p^{(t)}[\boldsymbol{k}] = \begin{cases} 0\,, & \tilde{p}^{(t)}[\boldsymbol{k}] < 0 \\ 1\,, & \tilde{p}^{(t)}[\boldsymbol{k}] > 1 \\ \tilde{p}^{(t)}[\boldsymbol{k}]\,, & \tilde{p}^{(t)}[\boldsymbol{k}] \in [0\,,1] \end{cases}\,,\quad \tilde{p}^{(t)}[\boldsymbol{k}] = \operatorname{Re}\Big[\mathcal{F}^{-1}\Big\{\frac{\mathcal{Y}^{(t)}(\boldsymbol{z})}{\mathcal{X}^{(t)}(\boldsymbol{z})}\Big\}\Big][\boldsymbol{k}]\,,\ \boldsymbol{k} \in \Omega$

$$\mathcal{X}^{(t)}(\boldsymbol{z}) = \beta_1 \sum_{l=0}^{L-1} \left| \sin\left(\frac{\pi l}{L}\right)(z_1 - 1) + \cos\left(\frac{\pi l}{L}\right)(z_2 - 1) \right|^2 + \beta_4$$

$$\mathcal{Y}^{(t)}(\boldsymbol{z}) = \beta_1 \sum_{l=0}^{L-1} \left[\sin\left(\frac{\pi l}{L}\right)(z_1^{-1} - 1) + \cos\left(\frac{\pi l}{L}\right)(z_2^{-1} - 1) \right] \left[R_l^{(t)}(\boldsymbol{z}) + \frac{\Lambda_{1l}^{(t-1)}(\boldsymbol{z})}{\beta_1} \right] + \beta_4 \mathcal{H}^{(t)}(\boldsymbol{z})$$

$$\mathcal{H}^{(t)}(\boldsymbol{z}) = \mathcal{F}\left\{ -\frac{1}{2}\left[\mathbf{f} - c_1^{(t)} - \mathbf{v}^{(t)} - \boldsymbol{\epsilon}^{(t-1)} + \frac{\boldsymbol{\lambda_4}^{(t-1)}}{\beta_4} \right]^{\cdot 2} + \frac{1}{2}\left[\mathbf{f} - c_2^{(t)} - \mathbf{v}^{(t)} - \boldsymbol{\epsilon}^{(t-1)} + \frac{\boldsymbol{\lambda_4}^{(t-1)}}{\beta_4} \right]^{\cdot 2} \right\}(\boldsymbol{z})$$

8. $\boldsymbol{\epsilon}^{(t)} = \tilde{\boldsymbol{\epsilon}}^{(t)} - \operatorname{CST}\left(\tilde{\boldsymbol{\epsilon}}^{(t)}, \nu\right)$

$$\tilde{\boldsymbol{\epsilon}}^{(t)} = \left[\mathbf{f} - c_1^{(t)} - \mathbf{v}^{(t)} + \frac{\boldsymbol{\lambda_4}^{(t-1)}}{\beta_4} \right] \cdot^{\times} \mathbf{p}^{(t)} + \left[\mathbf{f} - c_2^{(t)} - \mathbf{v}^{(t)} + \frac{\boldsymbol{\lambda_4}^{(t-1)}}{\beta_4} \right] \cdot^{\times} \left[1 - \mathbf{p}^{(t)} \right]$$

II. Update $\left(\left[\boldsymbol{\lambda}_{\mathbf{1}b}^{(t)}\right]_{b=0}^{L-1}, \left[\boldsymbol{\lambda}_{\mathbf{2}a}^{(t)}\right]_{a=0}^{S-1}, \boldsymbol{\lambda}_{\mathbf{3}}^{(t)}, \boldsymbol{\lambda}_{\mathbf{4}}^{(t)} \right) \in X^{L+S+2}$:

$$\boldsymbol{\lambda}_{\mathbf{1}a}^{(t)} = \boldsymbol{\lambda}_{\mathbf{1}a}^{(t-1)} + \beta_1 \left[\mathbf{r}_a^{(t)} - \sin\left(\frac{\pi a}{L}\right) \mathbf{D_1} \mathbf{p}^{(t)} - \cos\left(\frac{\pi a}{L}\right) \mathbf{p}^{(t)} \mathbf{D}_{\mathbf{2}}^{\mathrm{T}} \right],\ a = 0, \ldots, L-1$$

$$\boldsymbol{\lambda}_{\mathbf{2}a}^{(t)} = \boldsymbol{\lambda}_{\mathbf{2}a}^{(t-1)} + \beta_2 \left[\mathbf{w}_a^{(t)} - \mathbf{g}_a^{(t)} \right],\ a = 0, \ldots, S-1$$

$$\boldsymbol{\lambda}_{\mathbf{3}}^{(t)} = \boldsymbol{\lambda}_{\mathbf{3}}^{(t-1)} + \beta_3 \left[\mathbf{v}^{(t)} - \sum_{s=0}^{S-1} \left[\sin\left(\frac{\pi s}{S}\right) \mathbf{D_1} \mathbf{g}_s^{(t)} + \cos\left(\frac{\pi s}{S}\right) \mathbf{g}_s^{(t)} \mathbf{D}_{\mathbf{2}}^{\mathrm{T}} \right] \right]$$

$$\boldsymbol{\lambda}_{\mathbf{4}}^{(t)} = \boldsymbol{\lambda}_{\mathbf{4}}^{(t-1)} + \beta_4 \left[\left(\mathbf{f} - c_1^{(t)} - \mathbf{v}^{(t)} - \boldsymbol{\epsilon}^{(t)} \right) \cdot^{\times} \mathbf{p}^{(t)} + \left(\mathbf{f} - c_2^{(t)} - \mathbf{v}^{(t)} - \boldsymbol{\epsilon}^{(t)} \right) \cdot^{\times} \left(1 - \mathbf{p}^{(t)} \right) \right]$$